UNIVERSIDADE DE LISBOA
FACULDADE DE CIÊNCIAS
DEPARTAMENTO DE QUÍMICA E BIOQUÍMICA

Mimetics of donepezil as potential hybrid drugs against Alzheimer's disease – synthesis and biochemical evaluation

Daniel Renato Tomás Teixeira

Mestrado em Bioquímica
Bioquímica Médica

Dissertação orientada por:
Professora Doutora Maria Amélia Loureiro dos Santos Seabra (CQE/IST)
Professora Doutora Maria Luísa Mourato de Oliveira Marques Serralheiro (BioIsi/FCUL)

2017

AGRADECIMENTOS

Agradeço à professora Amélia Santos por ter aceite ser minha orientadora. Esta tese não teria sido possível sem esse voto de confiança. Agradeço todos os ensinamentos, apoio e amizade dados ao longo da realização desta tese. Nunca me vou esquecer que "*Time is our biggest enemy*".

À professora Sílvia Chaves por ter sido uma orientadora extra durante a realização desta tese. Agradeço toda a ajuda e incentivos dados ao longo deste trabalho, principalmente na parte mais analítica do mesmo.

À professora Luísa Serralheiro, com quem apesar de não ter trabalhado diretamente, sempre teve uma palavra amiga e principalmente sempre esteve disponível para me ajudar com todas as burocracias da tese.

Thanks to both Luca and Asha for being my lab seniors. I learned a lot from you! Also, thanks to Sara, Rajeshwari, Gaia and Simone for the friendship and good moments spend together during work hours.

Aos restantes membros do CQE IV – BIOIN por sempre me terem ajudado quando precisei.

Ao DQB e todos os membros (passados e presentes) que me acolherem quando vim para Lisboa. Sem dúvida, são anos que nunca esquecerei.

À minha família e amigos por estarem sempre do meu lado, no bem e no mal. A minha vida seria muito mais triste sem a presença de todos!

À minha tia Belita, por me ter permitido viver todos estes anos em Lisboa com ela. Todo este percurso teria sido mais difícil sem essa ajuda.

À minha irmã Rute, que mesmo na China faz a minha vida ter mais sentido!

Por fim, e mais importante, agradeço à minha mãe. Agradeço todos os sacrifícios feitos até hoje. Nada disto faria sentido sem ela, e espero que seja apenas o início de um futuro repleto de coisas boas para nós.

A todos os envolvidos na minha vida durante a realização deste trabalho, o meu sincero obrigado! Daqui em diante trabalharei duro e darei sempre o meu melhor para ser um Daniel Tomás que só dá orgulhos e felicidades!

ABSTRACT

Alzheimer's disease (AD) is a neurodegenerative disorder and the biggest cause of senile dementia, among the elderly population. Currently, almost all the drugs approved by the Food and Drug Administration (FDA) for AD treatment function as acetylcholinesterase inhibitors (AChEI), due to low levels of acetylcholine found in AD patients' brains. However, these drugs can only improve the symptoms of the disease, but don't interfere with its progress and don't have any role in the disease cure. AD has proven to have a pathology with several different hallmarks associated with complex biochemical mechanisms, which difficult the understanding of the cause of the disease.

Even though, efforts are being made worldwide for the development of potential therapeutic drug candidates for AD treatment. The aim of this thesis is to contribute to the development of drug candidates based on a multi-target approach, involving the design, synthesis and biochemical evaluation of the compounds. The compounds were designed based on the conjugation of donepezil (an AChEI) derivatives and benzimidazole or benzofuran derivatives, to obtain molecules with two different moieties and, consequently, non-toxic multifunctional compounds.

Following this approach, six compounds were fully synthesized and studied for their AChE inhibition, antioxidant activity and Aβ aggregation inhibition, with moderate results. Some of the compounds containing a phenol group, were also studied for their *in vitro* metal chelation capacity. Specifically, hydroxyphenylbenzimidazole derivatives demonstrated good copper(II) and moderate zinc(II) chelating ability. Pharmacokinetic properties were also calculated in view of their possible administration as drugs.

Overall, these results provide a set of information that, in association with the molecular modulation study, can give an insight on the capacity of these donepezil mimetics as potential multi-targeting anti-AD agents and also on future suggestion for structural modifications to improve important properties, namely the AChE inhibition and Aβ aggregation. Moreover, two analogue compounds with chelation power towards copper(II) and zinc(II) are in the final stage of synthesis development.

Keywords: Alzheimer's disease; Donepezil; Multifunctionality; Acetylcholinesterase inhibitors; Metal chelators.

RESUMO

A doença de Alzheimer (AD) é uma doença neurodegenerativa progressiva caraterizada pela perda de neurónios no córtex cerebral e regiões subcorticais. É a forma mais comum de demência na população idosa, sendo que os primeiros sintomas podem mesmo ser confundidos com características de idade avançada, como o esquecimento de eventos recentes. Com o avançar da doença, a memória a longo prazo também começa a ficar afetada, e outros fenómenos, tais como alterações de humor e dificuldades com a linguagem, começam a aparecer. Num estádio final, a doença é fatal para o paciente.

Num contexto molecular, a AD ainda não é 100% compreensível devido ao envolvimento de diferentes mecanismos bioquímicos. De entre as diferentes caraterísticas da doença podem-se realçar os baixos níveis de acetilcolina, a presença de depósitos extracelulares de placas amiloides, um aumento do stress oxidativo e uma disrupção da homeostase de metais de transição, como o cobre, o ferro e o zinco. Diferentes hipóteses foram propostas para a causa da doença, mas nenhuma com aceitação universal, sendo que as hipóteses com maior apoio são a hipótese colinérgica e a hipótese da cascata amiloide. A primeira admite que a principal causa da perda da função cognitiva está associada a uma degeneração dos neurónios colinérgicos e da sua neurotransmissão, enquanto a segunda assenta na premissa de que a acumulação de proteínas β-amiloides (Aβ) é a principal caraterística da patologia.

Atualmente, os fármacos aprovados pela FDA atuam essencialmente com base na hipótese colinérgica, funcionando enquanto inibidores do acetilcolinesterase (AChEI), de forma a bloquear a hidrólise de acetilcolina. No entanto, estes fármacos apenas permitem melhorar os sintomas da doença, permanecendo a doença como incurável. Todos estes fatores levaram à criação de uma nova abordagem para o combate da doença baseada no desenvolvimento de compostos multifuncionais. Em geral, estes compostos são desenvolvidos a partir de uma estrutura já conhecida, de um dos fármacos que atuam como AChEI, os quais são conjugados com diferentes motivos que acrescentem propriedades favoráveis para os pacientes de AD.

Com base nesses conhecimentos, o objetivo desta tese foi o desenvolvimento de novas moléculas multifuncionais que pudessem atuar como potencias fármacos para o tratamento de AD. Em particular, foram desenvolvidos compostos a partir da estrutura base do donepezilo, comercializado como Aricept®, um dos fármacos aprovados pela FDA. O donepezilo apresenta na sua constituição uma benzil piperidina que foi usada para o design de novas moléculas, tal como um isóstero benzil piperazina. Estes derivados de donepezilo, foram por sua vez conjugados com derivados de dois tipos de heterociclos, benzimidazol e benzofurano, que por sua vez já são estruturas privilegiadas em química medicinal.

O primeiro passo do trabalho foi o design dos compostos que são agrupados em duas séries, uma com um fragmento derivado da piperidina e outra com um derivado de piperazina. Foram sintetizados seis compostos (três por série), com dois compostos para os quais ainda é necessária uma otimização do esquema reacional (apesar de ter sido possível sintetizar um deles, mas em muita baixa quantidade). Os compostos sintetizados foram caraterizados por técnicas de análise elementar, como espectroscopia de ressonância magnética nuclear e espectrometria de massa, posteriormente avaliadas as suas propriedades, com o objetivo de testar a sua potencial utilização para o tratamento de pacientes com AD. Foram feitos estudos de inibição enzimática do acetilcolinesterase, de atividade antioxidante e de inibição da agregação Aβ. Os estudos de inibição enzimática mostraram uma inibição a um nível micromolar, apresentando o composto PZ3 o melhor valor de inibição (4.0 μM), enquanto o composto PP2 apresentou o valor mais baixo (30.0 μM). Apesar destes valores demonstrarem que os compostos de ambas as séries possuem capacidade inibitória, em comparação com os fármacos de referência, a tacrina e o donepezilo, que inibem a um nível nanomolar, os novos compostos são inibidores mais fracos do enzima. Estes resultados foram racionalizados por modulação molecular, em que a nova molécula é

sobreposta sobre um ligando, no centro ativo do enzima. No caso, foi escolhida a estrutura 1EVE da base de dados PDB, uma vez que esta apresenta a molécula de donepezilo enquanto ligando. A conjugação de ambos os dados, esclarece em relação à interação dupla das moléculas, com o centro catalítico e periférico do enzima, mas também permite observar futuras modificações que podem vir a ser benéficas no desenvolvimento deste género de compostos. Uma dessas modificações seria a adição de mais um grupo metileno na série PP, de modo a que as moléculas possam ter um comprimento ideal para uma interação bimodal mais forte.

Os estudos de atividade antioxidante não tiveram o mesmo sucesso, uma vez que apenas um dos compostos apresentou atividade, enquanto um dos restantes não pode ser testado devido a problemas de solubilidade. O composto PZ1 apresentou um valor de 594.4 μM, representando uma atividade num nível moderado-baixo, apesar de ser um resultado positivo, dado que a estrutura original do donepezilo não apresenta atividade. Os compostos com derivados de benzofurano não apresentaram atividade antioxidante, mas a síntese de compostos com um grupo hidroxilo na posição de substituição poderá ser um passo para uma estrutura com maior poder antioxidante.

Os estudos de inibição da agregação Aβ também apresentaram valores que podem ser considerados moderados-baixos (14.4 – 36.3%), sendo que as moléculas com o hidroxifenilbenzimidazol apresentam melhor capacidade do que as moléculas com os benzofuranos não substituídos (PZ4 sendo uma exceção). Os compostos PZ1 e PZ4 foram também analisados para a inibição da agregação Aβ induzida pelo cobre, dado a presença de uma unidade quelante na sua estrutura. Ambos os compostos apresentaram resultados positivos, com percentagens de inibição superiores à inibição na ausência do metal. Estes estudos foram feitos por técnicas de fluorescência, sendo que a técnica de microscopia de transmissão eletrónica, foi também realizada, enquanto técnica imagiológica, para uma racionalização dos resultados.

Como reportado anteriormente, o fragmento molecular hidroxifenilo associado ao grupo amina do benzimidazole, tem potencial para funcionar como quelante. Assim, os compostos que o incluem (PP1 e PZ1) foram também avaliados para a sua capacidade quelante para o cobre e o zinco por titulação potenciométrica. Apesar do composto PP1 não se ter demonstrado solúvel na mistura H_2O/DMSO em toda a gama de pH da titulação, o composto PZ1 demonstrou ter um bom potencial quelante para o cobre (pCu = 16.3) e um razoável para o zinco (pZn = 6.4). Por fim, através do programa QikProp, foram calculados alguns parâmetros farmacocinéticos, com especial atenção para potenciais violações da regra de Lipinski, regra esta que indica se determinado composto tem propriedades para ser ativo por administração oral. Nenhum dos compostos estudados apresentou violações a esta regra, representando o seu potencial enquanto possíveis fármacos para administração oral.

Apesar de provada a multifuncionalidade dos compostos estudados, os mesmos não se podem considerar excecionais em nenhuma das propriedades individuais. Contudo, estes compostos não deverão ser tóxicos, esperando-se que possa haver efeitos sinergéticos associados ao conjunto das suas propriedades avaliadas. Deste trabalho podem ainda ser inferidas orientações positivas para o desenvolvimento de novos candidatos a fármacos anti-AD. Concretamente, a adição de um grupo metileno na série com piperidina pode vir a ser chave para o estabelecimento de interações mais fortes com o acetilcolinesterase, com consequência obtenção de uma melhor inibição do enzima, enquanto a substituição no benzofurano por um grupo hidroxilo pode vir a originar um composto com boa atividade antioxidante, e também potencial atividade quelante.

Palavras-chave: Doença de Alzheimer; Donepezilo; Multifuncionalidade; Inibidores de acetilcolinesterase; Quelantes de metais.

TABLE OF CONTENTS

LIST OF FIGURES

LIST OF TABLES

LIST OF SCHEMES

ABBREVIATIONS

Å	ångström;
AA	antioxidant activity;
Aβ	β-amyloid;
$A\beta_{1-40}$	β-amyloid with 40 amino acids;
$A\beta_{1-42}$	β-amyloid with 42 amino acids;
ACh	acetylcholine;
AChE	acetylcholinesterase;
AChEI	acetylcholinesterase inhibitors;
AChI	acetylthiocholine iodide;
AD	Alzheimer's disease;
APP	amyloid precursor protein;
A_{DPPH}	absorbance of the DPPH solution against the blank solution;
A_{sol}	absorbance of the sample against the blank solution;
bs	broad singlet;
^{13}C NMR	carbon-13 nuclear magnetic resonance;
^{o}C	Celsius degree;
CAS	catalytic anionic site;
C_L	ligand concentration;
clog *P*	calculated partition-coefficient (octanol/water);
C_M	metal concentration;
CNS	central nervous system;
CTF	C-terminal fragment;
CYP	cytochrome P450;
d	doublet;
DCC	*N*,*N*'-dicyclohexylcarbodiimide;
DCM	dichloromethane;
DCU	dicyclohexylurea;
dd	doublet of doublets;
δ	chemical shift;
DMF	dimethylformamide;
DMSO	dimethyl sulfoxide;
DPPH	2,2-diphenyl-1-picrylhydrazyl;
DPPH-H	diphenylpicrylhydrazine;
DTNB	5,5'-dithiobis-(2-nitrobenzoic acid);
EC_{50}	half maximal effective concentration;

eq	equivalents;
ESI-MS	ionization electrospray mass spectrometry;
η	percentage of yield;
FDA	Food and Drug Administration;
Glu	glutamate;
h	hour;
^{1}H NMR	proton nuclear magnetic resonance;
HEPES	4-(2-hydroxyethyl)-1-piperazineethanesulfonic acid;
HFIP	1,1,1,3,3,3-hexafluoro-2-propanol;
His	histidine;
HPLC-HRMS	high-performance liquid chromatography – high resolution mass spectrometry;
HSAB	Hard and Soft Acids and Bases theory;
Hz	hertz;
%I	percentage of inhibition of enzymatic activity;
IC_{50}	half maximal inhibitory concentration;
J	coupling constant;
k_{cat}	turnover number;
K_d	dissociation constant;
λ_{em}	emission wavelength;
λ_{exc}	excitation wavelength;
log BB	passive blood-brain partitioning;
M	molar;
m	multiplet;
MAO	monoamine oxidase;
MeOH	methanol;
MHz	megahertz;
min	minute;
mL	milliliter;
mM	millimolar;
µL	microliter;
µM	micromolar;
m/z	mass to charge ratio;
N	normal;
NHS	*N*-hydroxysuccinimide;
nm	nanometer;
nM	nanomolar;
NMDAr	*N*-methyl-D-aspartate receptor;

NMM	*N*-methylmorpholine;
NMR	nuclear magnetic resonance;
PAS	peripheral anionic site;
PDB	Protein Data Bank;
Phe	phenylalanine;
ppm	parts-per-million;
ROS	reactive oxygen species;
rt	room temperature;
s	second;
SD	standard deviation;
Ser	serine;
sg	singlet;
τ	tau;
t	triplet;
T3P	propylphosphonic anhydride solution;
TBAI	tetrabutylammonium iodide;
TEM	transmission electron microscopy;
THF	tetrahydrofuran;
ThT	thioflavin T;
TLC	thin-layer chromatography;
t_R	retention time;
TRIS	tris(hydroxymethyl)aminomethane;
Trp	tryptophan;
Tyr	tyrosine;
U	enzyme unit;
USA	United States of America;
UV-vis	ultraviolet-visible;
v_i	initial velocity in the presence of inhibitor;
$v_{control}$	initial velocity of the control reaction.

I. INTRODUCTION

I.1 Alzheimer's disease

Alzheimer's disease (AD) is a neurodegenerative disorder characterized by the progressive deterioration of memory and cognition, being the most common cause of senile dementia in the elderly population. The disease affects millions of people worldwide, while, specifically in the USA alone, the disease affects 5.5 million individuals[1], being also the most common neurodegenerative disorder related to age (50-70% of the cases)[2].

Since the Greco-Roman period, dementia is a recognized condition, although it was dismissed as a feature of aging[3]. Only in the 19th century, with the systematized classification of mental disorders[3,4], senile dementia started to be differentiated from other dementias, being established as a mental disorder. In 1906, AD was first identified by Alois Alzheimer, a German psychiatrist and neuropathologist. An autopsy of the brain of one of his diseased patients showed histological features nowadays associated with AD: a loss of neurons and the presence of amyloid plaques and neurofibrillary tangles[4].

AD is a disease that affects the central nervous system (CNS), causing damage or destruction of neurons in regions of the brain involved in cognitive functions. This destruction will eventually lead to damage of other neurons with basic surviving function, such as swallowing, and in the last instance will be fatal. The first symptoms are short-term memory loss and an occasional forget about things, that will progress to a poor ability to think and speaking problems[1]. The neocortex and hippocampus are the most affected regions of the brain by the characteristic pathology of AD[5].

The aetiology of AD is still unknown, but there are characteristic hallmarks of the disease, such as, deposits of β-amyloid protein plaques, neurofibrillary tangles of hyperphosphorilated τ protein, low levels of acetylcholine, oxidative stress in the CNS and metal dyshomeostasis[6,7]. With these different hallmarks involved, a new therapy based on multifunctional drugs is still a new way to prevent the progress of this disease. Even so, the lack of knowledge of the biochemical mechanisms behind it, represent a challenge in the design of these new compounds[2,7,8].

I.2 Hypothesis for AD cause

The causes of AD are still mostly unknown, with the exceptions of 1-5% of cases, which are caused by genetic differences[9]. Several hypotheses have been proposed, competing for the explanation of the disease cause, however none with universal acceptance. Between these hypotheses, the cholinergic and amyloid cascade are the most acknowledged ones, with other hypotheses including factors such as τ protein phosphorylation regulation, oxidative stress, metallobiology or calcium levels[10].

I.2.1 Cholinergic hypothesis

The oldest hypothesis for AD cause is the cholinergic hypothesis. This hypothesis proposes that the cognitive loss of function is associated with a degeneration of cholinergic neurons in the basal forebrain (the major cholinergic output of the CNS) and the loss of cholinergic neurotransmission in the cerebral cortex[11,12].

The biggest argument for this hypothesis is the reduced levels of acetylcholine (ACh), an important neurotransmitter involved in both memory and learning[11]. Other cholinergic effects are associated with the initiation of aggregation of amyloids, eventually leading to a general neuroinflammation[13].

Among the five available drugs in the market, four of them act by inhibiting acetylcholinesterase (AChE), increasing the levels of ACh in the synaptic cleft[13,14]. There are four inhibitors of AChE drugs approved by the Food and Drug Administration (FDA): tacrine, donepezil, rivastigmine and galantamine (**Figure I.1**). These drugs show an impact in the life of patients with AD, by improvement of the cognitive symptoms, but only for a short period of time (6-12 months), leading to loss of support for this hypothesis[8].

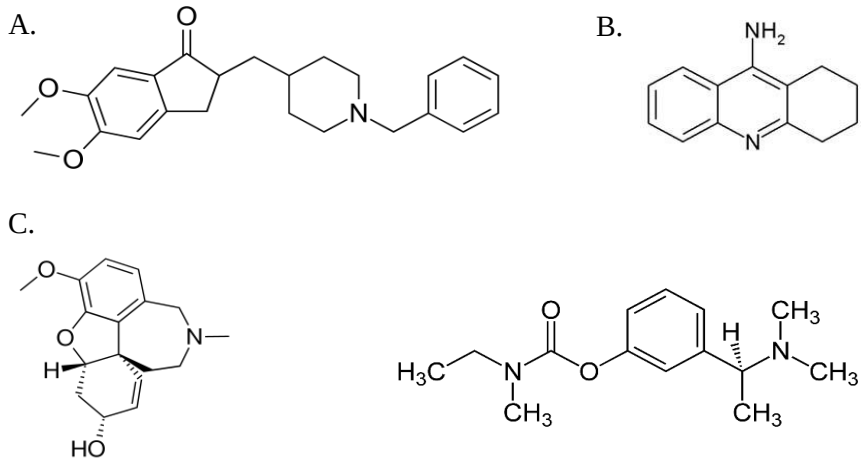

Figure I.1 – FDA approved AChE inhibitors: A. Donepezil; B. Tacrine; C. Galantamine; D. Rivastigmine.

I.2.2 Amyloid cascade hypothesis

The amyloid cascade hypothesis was developed on the premise that β-amyloid protein (Aβ) accumulation is the primary event in AD pathogenesis, with β-amyloid plaques being the main neurotoxic species due to oxidative stress and cell membrane perturbation[15,16]. Aβ species are produced from the APP protein by proteolytic cleavage (by β- and γ-secretases). These amyloid species can aggregate into plaques that promote cellular stress and phosphorylation of τ-protein.

APP is a type-1 membrane protein expressed in various tissues, including high levels in the CNS. Its true physiological function is still not well understood, but it can give rise to Aβ-peptide. The majority of the protein forms an extracellular domain, followed by a transmembrane domain and an intracellular domain, with about 50 amino acids[7]. APP is proteolytically processed by 3 proteases: α-, β- and γ-secretases; both α- and β-secretase hydrolyse the protein extracellularly, near the transmembrane domain. The generated C-terminal fragment (CTF) CTFα is rapidly degraded, while CTFβ remains anchored in the membrane. γ-secretase cuts the substrate in different positions, forming the Aβ group of peptides, that can differ in length at the C-terminus, from 36 to 43 amino acids (**Figure I.2**)[17].

There are two principal forms of Aβ in the brain tissue of AD patients: $A\beta_{1-40}$ (the dominant species) and $A\beta_{1-42}$; the former one is responsible for the initial self-aggregation of Aβ. Compared to $A\beta_{1-40}$, $A\beta_{1-42}$ is more insoluble, leading to a better facility for aggregation and neurotoxicity[18]. The aggregation is accompanied by a conformation transition from α-helix to β-sheet[7], with the result β-amyloid oligomers and fibrils being neurotoxic. However, Aβ peptide monomers are not toxic at physiological concentration[7,17].

It is still unclear how Aβ interacts with τ protein, but it is been reported a synergistic effect between them[19]. τ protein is a microtubule stabilizer, abundant in the neurons. Its structure presents different phosphorylation sites, enzymatically regulated by kinases and phosphatases. A disequilibrium in their

regulation can lead to a hyperphosphorylation of the protein, that associated to an altered solubility generates the neurofibrillary tangles present in the brains of AD patients[19].

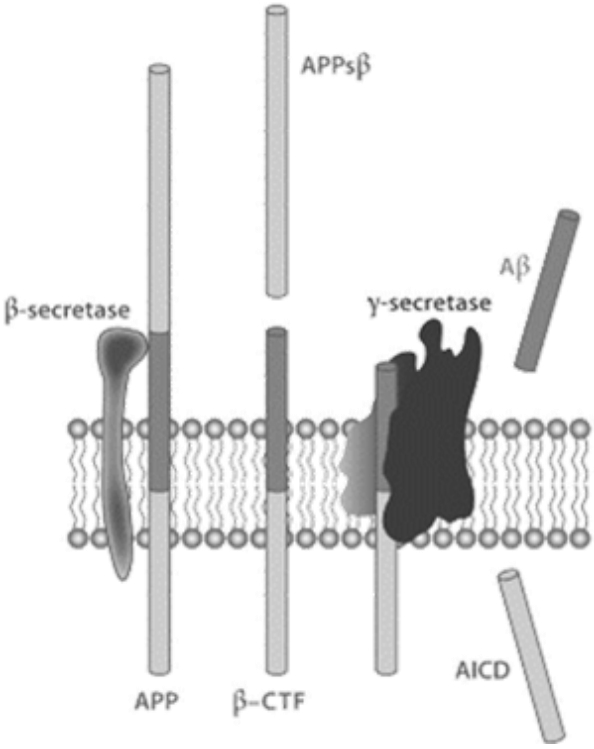

Figure I.2 – Processing of APP by β- and γ-secretase, adapted from [17].

It is still unclear how Aβ interacts with τ protein, but it is been reported a synergistic effect between them[19]. τ protein is a microtubule stabilizer, abundant in the neurons. Its structure presents different phosphorylation sites, enzymatically regulated by kinases and phosphatases. A disequilibrium in their regulation can lead to a hyperphosphorylation of the protein, that associated to an altered solubility generates the neurofibrillary tangles present in the brains of AD patients[19].

Despite nowadays the amyloid cascade being the most accepted hypothesis for AD cause, it is not by any means established as the correct hypothesis, with some reports of oligomeric Aβ assemblies as the primary neurotoxic basis for cognitive decline in AD[20,21].

I.2.3 Metal dyshomeostasis

Essential trace elements, like iron, copper and zinc, exist in the brain and have crucial roles in normal brain functions, such as myelination, neurotransmitter synthesis and/or neural information. It was observed an imbalance of the levels of these metals in the brains of AD patients, correlated with adverse effects on CNS functions, especially learning and memory[22]. Both free ionic zinc and copper are released into the synaptic cleft which are central nodes of neural networks[23].

The imbalance of metals in the brain can be responsible for some important hallmarks of the neurodegenerative process. Both Cu(II) and Fe(III) can promote Fenton reaction with the formation of reactive oxygen species (ROS), which can oxidize biomolecules and induce severe damage on neuronal cells[15,16]. This oxidative stress is especially dangerous in patients with neurodegenerative diseases, since there is a high concentration of O_2 in the brain, compared with other body tissues. Production of ROS from H_2O_2, lipid peroxidation and autoxidation of physiological and xenobiotic compounds, are some

of the consequences of the oxidative stress[24]. Other metallic ions, such as Zn(II), can interact in the protein folding, leading to abnormal aggregation and formation of β-amyloid deposits[18].

Aβ contains metal binding sites, with copper and zinc been found in high concentrations in Aβ plaques, while iron can interact with Aβ through proteins, such as ferritin. These metals can affect the morphology of Aβ aggregates, accelerate Aβ fibrillation and increase Aβ cytotoxicity[8,15]. Both copper and zinc can bind to the same amino acid residues in Aβ[25], but since zinc is an inert redox species, copper is considered as the most pertinent biological target. However, in micromolar concentrations, zinc inhibits Aβ-induced toxicity and can compete with copper for binding to Aβ, preventing Cu(II)-Aβ induced formation of hydrogen peroxide and free radicals[26,27]. These adverse effects, due to high concentrations of metals in the brains of AD patients, have led to chelation therapy as an adjuvant option for therapeutic action against AD.

Chelation therapy is the procedure used to reduce the toxicity of metal ions in the organism. This therapy has two main mechanisms of action: the removal of the complexed metal ion from the organism, or the dislocation to tissues where it doesn't exert toxic action. Nevertheless, potential serious side effects are present, since the homeostasis of essential metal ions is hard to control and its imbalance can lead to serious damage, as reported. Chelation therapy is approved for some metal toxicity problems, such as systematic iron overload and lead poisoning[28].

I.3 Acetylcholinesterase

AChE (EC 3.1.1.7) belongs to the α/β hydrolase superfamily[29], with the principal physiological function of hydrolysing ACh for termination of nerve impulse (**Scheme I.1**), in the synapse and neuromuscular junction[30,31]. This enzyme exhibits a high specific activity, with a high value of k_{cat}, functioning at a rate approaching that of a diffusion-controlled reaction[32].

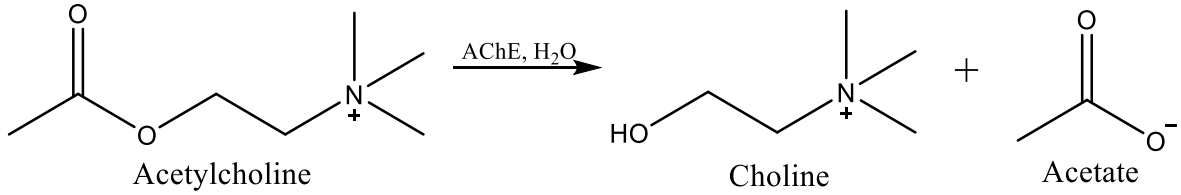

Scheme I.1 – Enzymatic hydrolysis of ACh, adapted from [32].

The crystal structure of AChE from different species showed conservation of the active site gorge, with structures from different electric fish proved to be structurally similar to those of vertebrate nerves and muscles[32]. The gorge spread about 20 Å lined by 14 aromatic residues, through more than half of the enzymatic structure[33]. In particular, pacific electric ray *Torpedo californica* shows more than 50% of identity of sequence to that of human AChE, with similar active site structure. Because of that, this organism is usually used as a model for both docking and new compounds design. The deep and narrow AChE gorge consists in two subsites: at the gorge entrance the peripheral anionic site (PAS), and at the bottom of the gorge the catalytic anionic side (CAS), which contains the catalytic triad[31–33] (**Figure I.3**).

The catalytic triad is formed by Ser200, Glu327 and His440 in a form of a planar matrix, being a highly conserved region of proteins of the α/β hydrolase superfamily[32]. It is located at the base of the gorge, where the hydrolysis of the ester bond of ACh happens. Besides the catalytic triad, CAS also presents another two important residues, Trp84 and Phe330. The first is a significant residue for the interaction between the quaternary ammonium group of ACh and the indole group of the residue,

through a cation-π interaction, while Phe330 can change its conformation depending on the type of ligand complexed with the enzyme (possibly controlling the entry or exit in the gorge)[34].

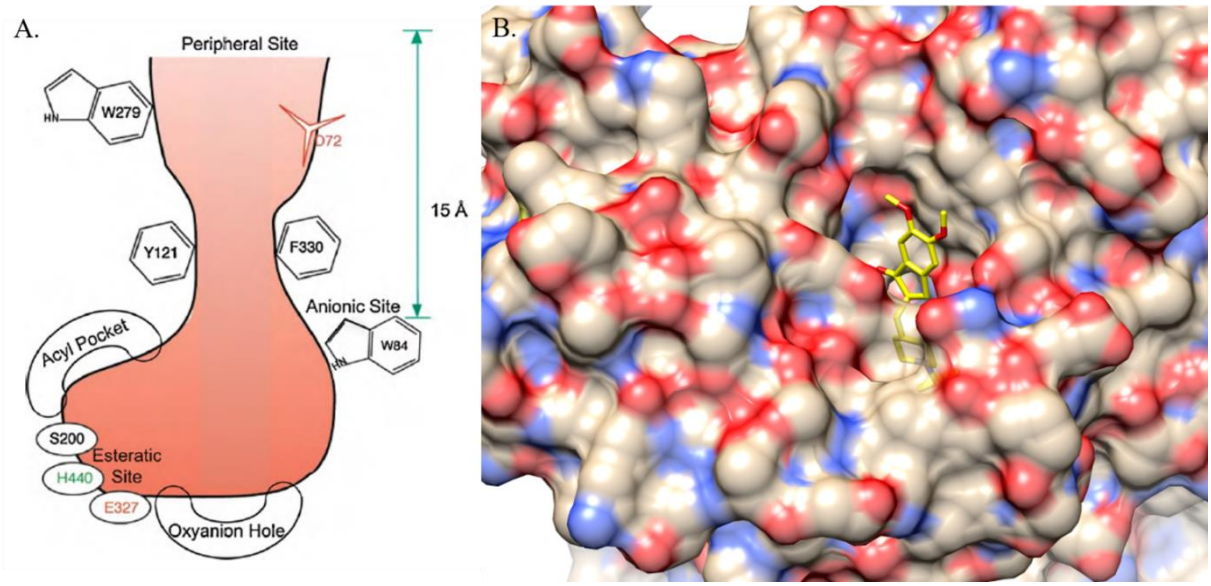

Figure I.3 – **A.** Illustration of the AChE active site, with some important amino acid residues highlighted (adapted from [32]); **B.** View of the enzyme gorge complexed with a ligand (yellow) (PDB code 1EVE), transparency 45%.

The PAS is a not-well defined area at the entrance of the gorge, at 15 Å of distance from the active centre. It binds to substrate transiently enhancing catalytic efficiency in the catalytic pathway, while the ligand interaction can modify the active centre conformation. PAS presents two important amino acid residues, Tyr70 and Trp279, which are responsible for the adhesion functions of the enzyme[31]. It is also proposed that this subsite can bind to non-amyloidogenic Aβ, promoting a change in conformation to their amyloidogenic form, and consequently their fibril aggregation[22].

Due to this double interaction action, a therapeutic approach is being used by scientists worldwide: the design of compounds with double interaction, both on CAS and PAS. Thus, both the ACh hydrolysis and the β-amyloid aggregation will be inhibited. It is also noteworthy that different ligands in the enzyme gorge can interact with different amino acid residues and not only with the ones reported.

A different cholinesterase is present in the blood plasma and presents some similarities with AChE, known as butyrylcholinesterase (EC 3.1.1.8). Both catalyse the hydrolysis of ACh and can be differentiated by their tissue distribution and inhibitor sensitivity, with some of the drugs used for AD treatment also affecting butyrylcholinesterase[30,31].

I.4 Drugs in AD

Up to now, AD persists as an incurable disease, mostly due to its multi-aetiology. As reported before, almost all the approved drugs by FDA are acetylcholinesterase inhibitors (AChEI) (**Figure I.1**) that act by inhibiting AChE. Even so, these drugs only showed an improvement of symptoms for a short period of time, delaying the progress of the pathology[6,35]. AChEI inhibit AChE reversibly, increasing the ACh available in cholinergic synapses, consequently increasing the cholinergic transmission[36].

AChEI are also used in the treatment of glaucoma, neuromuscular block in surgery anaesthesia and myasthenia gravis[31]. Another drug used by AD patients is memantine (commercialized as Axura® or

Ebixa®), a *N*-methyl-D-aspartate receptor (NMDAr) antagonist, which restores the calcium imbalance induced by Aβ and the decrease of neuronal death[22]. In some countries, it is also marketed Namzaric®, a drug composed of a mixture of donepezil and memantine.

I.4.1 Tacrine

Tacrine (1,2,3,4-tetrahydroacridin-9-amine, Cognex®) was the first drug approved for treatment of AD by the FDA, in 1993. It is a non-competitive AChEI, with a high protein binding. Besides its cholinergic activity, tacrine also has additional pharmacological activity with monoamines and ionic channels. It is metabolized by cytochrome P450 isoenzyme CYP1A2, in three metabolites, with 1-hydroxytacrine being the active metabolite. Despite cognitive improvements, tacrine exhibits hepatoxicity, which led to its discontinuity. Nevertheless, tacrine is still one of the drugs used for the design of multifunctional molecules with therapeutic action against AD[22,37].

I.4.2 Donepezil

Donepezil (2-((1-benzylpiperidin-4-yl)methyl-5,6-dimethoxy-2,3-dihydro-1*H*-inden-1-one, Aricept®) is an hydrochloride salt of piperidine, approved by FDA in 1997. It is a reversible, non-competitive AChEI, with a high protein binding. It is metabolized by cytochrome P450 isoenzymes CYP2D6 and CYP3A4, being the major metabolite 6-*O*-demethyl-donepezil, showing equal pharmacological effect as donepezil. It is a more selective drug between cholinesterases, when compared with tacrine, and shows the adverse effects associated with cholinergic drugs such as nauseas, diarrhoea and vomiting, but unlike tacrine doesn't show hepatoxicity[22,38].

I.4.3 Rivastigmine

Rivastigmine (3-(1-dimethylamino)ethyl)phenyl ethyl(methyl)carbamate, Exelon®) is an AChEI approved by FDA in 2000. It shows a "pseudo irreversible" AChEI activity, since the effect produced persists for more time than the drug in the plasma. It is hydrolysed by the enzyme, with minimum involvement of the cytochrome P450. This hydrolysis leads to the formation of a phenolic derivative that is excreted by the kidneys. Rivastigmine is also used to treat dementia in Parkinson's disease, another neurodegenerative disorder[22,39].

I.4.4 Galantamine

Galantamine ((8As)-3-methoxy-11-methyl-4a,5,9,10,11,12-hexahydro-6H-benzo[2,3]benzofuro [4,3-cd]azepin-6-ol, Razadine®, Reminyl®) is a reversible and competitive AChEI, approved by FDA in 2000. Besides activity as AChEI, it is also an allosteric modulator of nicotinic ACh receptors, showing double cholinergic action. It is metabolized in the liver by the isoenzymes of cytochrome P450, CYP2D6 and CYP3A4[22,40].

I.4.5 Double-interaction drugs

Drugs with only one target are inadequate for the treatment of diseases such as neurodegenerative disorders, diabetes, cardiovascular diseases, or cancer, which involve several pathogenic hallmarks. In these cases, various therapies are used, like the combination therapy (famously known as "the cocktail") where a patient takes different drugs or the multiple-compound medication where different drugs are incorporated in the same formulation[35]. A new strategy assumes that the same compound can act in a multi-target way: multi-target directed ligands (MTDL). These drugs can interfere with two or more causes of the disease simultaneously and complementary, achieving better therapeutic results[16].

From a design standpoint, since the drugs available used by AD patients are AChEI, a multifunctional drug can be designed, where one of the moieties will have AChEI property, while the

other moieties can have other properties such as, anti Aβ aggregation, scavenging of ROS, modulation of active redox metals and/or inhibition of the monoamine oxidase (MAO) activity[22].

I.5 Benzimidazole and benzofuran

Benzimidazole structure is a fusion between an aromatic imidazole ring system and a benzene in the positions 4 and 5 of the imidazole ring. These rings present both acidic and basic characteristics, named due to the -NH group. Also, unsubstituted -NH groups exhibit fast prototropic tautomerism, which leads to equilibrium mixtures of asymmetrically substituted compounds[41]. Benzimidazole motif is one of the bioactive heterocyclic compounds that exhibits a wide range of biological activities; also the fact that it is a structural isostere of nucleotides (adenine and guanine) allows it to interact easily with biomolecules in living organisms[42,43]. Optimization of benzimidazole-based structure has resulted in various drugs currently in the market, such as omeprazole, pimobendane and mebendazole, also being a constituent of vitamin B12. Benzimidazole and its derivatives also showed anthelmintic, antimicrobial and anticancer activity[43].

Benzofuran is a different heterocyclic compound resulting from the fusion of a benzene with a furan ring. It is found in many plants, being widespread in nature[44]. Some substituted benzofuran are psychoactive drugs, being classified as stimulants, hallucinogens and empathogens, like 5-APB and 6-APB. Benzofuran scaffolds display a wide spectrum of potent biological activities such as anti-viral, anti-inflammatory and anticancer[45].

These set of characteristics of both heterocycles have led to their recognition as privileged structures for the drug development in medicinal chemistry.

I.6 Multifunctionality of donepezil hybrids – literature examples

Since the recognized importance of developing multifunctional compounds for new anti-AD therapy, a lot has been done, especially using tacrine as a starting material. New compounds with AChEI properties, antioxidant activity and inhibition of Aβ aggregation have been studied as tacrine hybrids with caffeic acid[46], benzothiazole[47] or cinnamic acid derivatives[6], as examples. Donepezil has also been considered as a pharmacological target for the design of new multifunctional compounds, but due to its more complex structure, the development of its derivatives has been based in modification in both its benzylpiperidine or dimethoxy-indanone moiety[22].

Donepezil-feruloyl conjugates were studied for their properties as potential drug candidates for AD. **Figure I.4 A** shows one example of these hybrids, which presented a good AChE inhibitory capacity (IC_{50} = 0.46 μM), antioxidant activity (49.41 μM), *in vivo* anti-inflammatory activity (for mice paw oedema, pleurisy and formalin-induced hyperalgesia models), and *in vitro* chelation activity of Fe(II) and Cu(II)[48]. Another example of donepezil derivatives involved the conjugation of benzylpiperidine with indolyl-aminopropargyl derivatives, resulting in potent inhibitors of both AChE and MAO. The compound in **Figure I.4 B**, presented an inhibition for AChE of 0.19 μM, an inhibition of MAO A of 5.50 nM, and an inhibition of MAO B of 0.15 μM, proving also to be a selective compound for MAO variants inhibition[49].

A continuous work for finding new multifunctional drugs is being done worldwide, as shown by the frequent release of articles regarding this line of work[22]. One last interesting example involving a combination of a tacrine and a donepezil derivative (isoindolinedione), a tacrine-donepezil hybrid, has

been reported[50], as a potential drug candidate, namely because of the excellent AChE inhibition attributed to its binding to both CAS and PAS binding. Compound **Figure I.4 C** showed a strong AChE inhibitory capacity, with IC_{50} value (2.4 nM) quite lower than the values presented for both tacrine and donepezil (167 nM and 19 nM, respectively), thus being a promising candidate for further disease-modifying drugs.

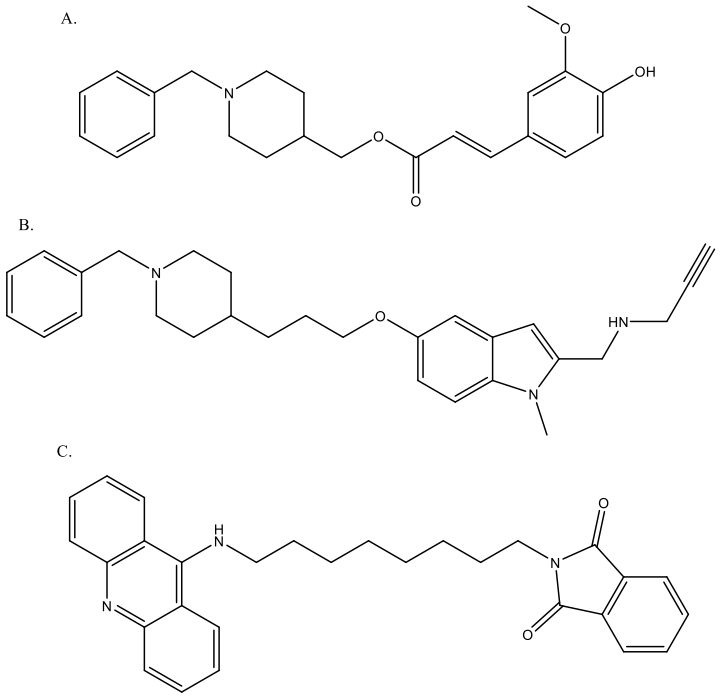

Figure I.4 - Examples of donepezil hybrids present in literature.

I.7 Thesis objective

Based on several of the aspects described in the present introduction, the benefits regarding the use of multifunctional drugs in terms of pharmacological efficiency are greater than those of drugs based solely on AChE inhibition. This thesis objective was to obtain new multifunctional compounds with potential ability to target different hallmarks of AD, namely by conjugating both the cholinergic and amyloid hypotheses. These new compounds are hybrids of donepezil derivatives and benzimidazole or benzofuran derivatives.

The drug development process starts with the design of the compounds, based on previous knowledge of structure-activity relationship of some molecular fragments, and making adequate conjugates, specifically based on docking simulations aimed to predict and optimize their interaction within the CAS and PAS of AChE. The most promising compounds are selected and follow for the synthesis and the study of different biochemical properties: AChE inhibition, antioxidant activity and inhibition of $A\beta_{1-42}$ aggregation. For the compounds enclosing chelating groups, their chelating capacity towards copper(II) and zinc(II) is also studied.

II. RESULTS AND DISCUSSION

II.1 Design and synthesis of the compounds

The design strategy for the new compounds was based on the coupling of two different chemical moieties, a donepezil derivative and a benzimidazole or benzofuran derivative. For donepezil derivatives, two moieties were chosen: one composed of a piperidine ring (the original ring of donepezil), resulting in the so-called **PP** series, and another with a piperazine ring, resulting in the **PZ** series (with an extra methylene group). A hydroxyphenylbenzimidazole was used as benzimidazole derivative (motif **1**) to provide a metal chelating group (aminophenol); also, different substituted benzofurans were also used (unsubstituted, a methoxyl-substituted and hydroxyl-substituted, corresponding to moieties **2**, **3** and **4**, respectively) (**Figure II.1**).

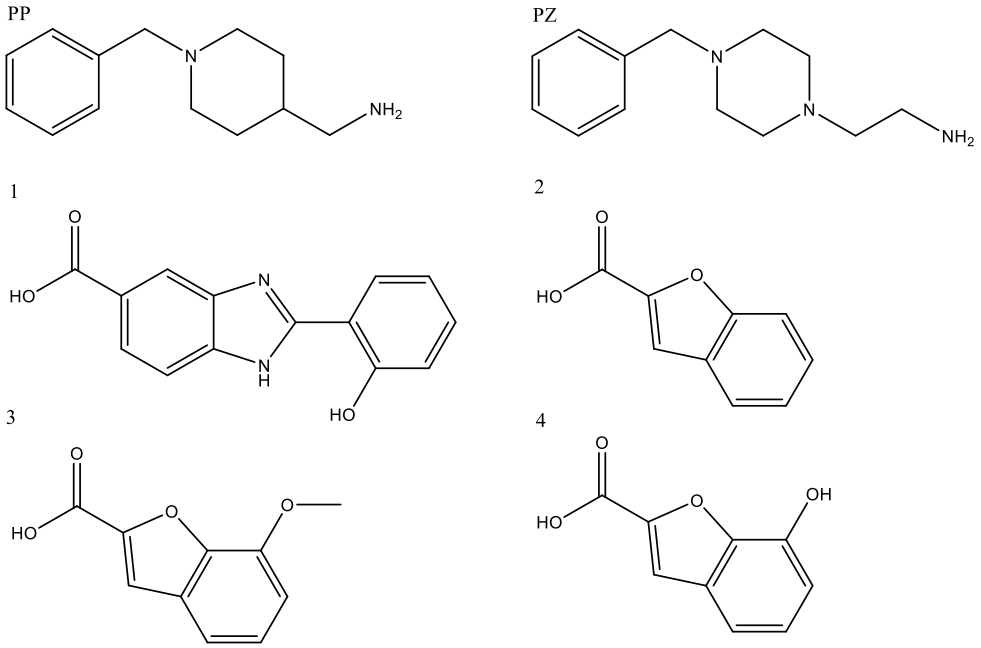

Figure II.1 – Moieties used in the design and synthesis of the final compounds: PP and PZ were used as donepezil derivatives, 1 as benzimidazole derivative and 2,3 and 4 as benzofuran derivatives.

The different functional groups present in each motif will allow a diversity of properties for each final compound. The final products were obtained by a coupling reaction between the primary amine of the donepezil derivatives and the carboxylic acid of the other moieties. This conjugation will provide a final molecule with an adequate lipo-hydrophilic balance and large enough to interact with both the binding sites, CAS and PAS, within the AChE active site, while being able to cross the blood-brain barrier.

II.1.1 Synthesis of donepezil derivatives

For the synthesis of the donepezil derivative moieties (**PP** and **PZ**), both the corresponding starting material (aminoalkyl-piperidine **AP** and aminoalkyl-piperazine **AZ**, respectively) were acquired commercially. The main objective in the synthesis process is the benzylation of the *N*-ring atom of these compounds. However, since they presented both one primary aminoalkyl group as ring substituent, a selective orthogonal protection for primary amine was necessary, to obtain compounds in good yields. For this purpose, a solvent-free procedure using phthalic anhydride as the protective group[51] was used, leading to the corresponding phthalimidic derivatives (**protAP** and **protAZ**) (**Scheme II.1**).

Following the protection of the primary amine, it was possible to benzylate on the secondary amine[52] of the ring. For that, a standard nucleophilic substitution was carried out with benzyl chloride, in the presence of sodium carbonate and triethylamine to counterbalance the formation of HCl. The back deprotection of the primary amine was obtained by hydrazinolysis of the phthalimide, according to reported procedure[53], leading to the formation of the primary amine and phthalazine-dione as a secondary product of the reaction (**Scheme II.1**). This last step is common on other synthetic mechanisms, like the Gabriel synthesis, that use potassium phthalimide for the preparation of primary amines.

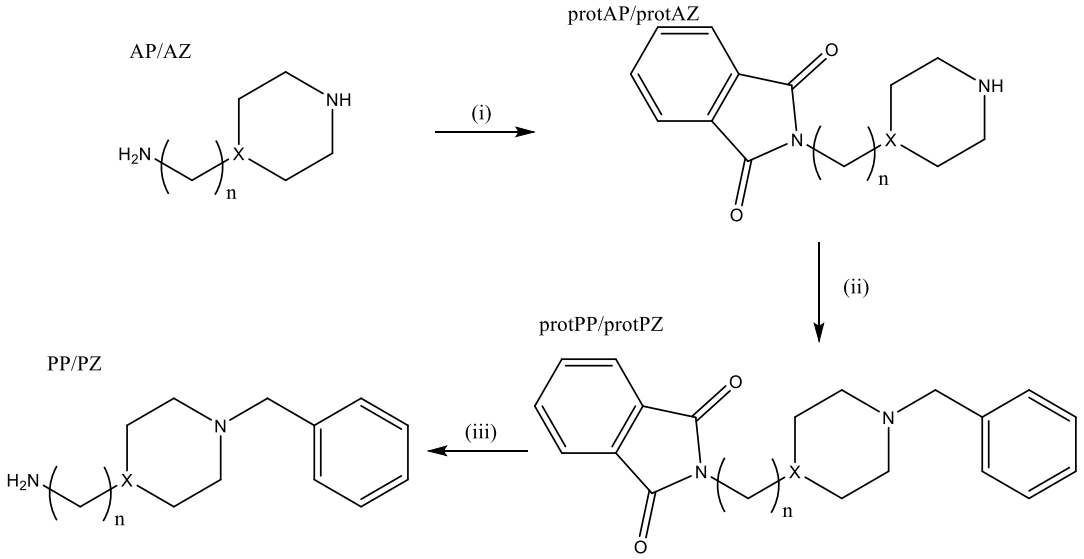

Scheme II.1 – Synthesis of PP (X = CH, n = 1) and PZ (X = N, n = 2). Reagents and conditions: (i) phthalic acid anhydride, 160 ºC, 4 h; (ii) benzyl chloride, K_2CO_3, triethylamine, acetonitrile, reflux, 50 ºC, 3 h; (iii) $N_2H_4.H_2O$, absolute ethanol, reflux, 60 ºC, 3 h.

II.1.2 Synthesis of benzimidazole derivative

The benzimidazole carboxylic derivate (motif **1**) was prepared by condensation of salicylaldehyde with 3,4-diaminobenzoic acid in the presence of sodium metabisulfite, an oxidizing agent, following literature procedure[42] (**Scheme II.2**).

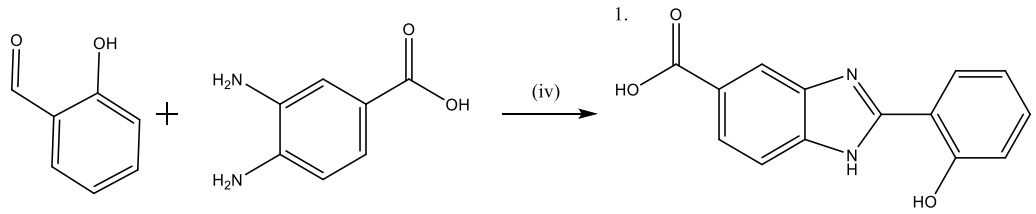

Scheme II.2 – Synthesis of the benzimidazole carboxylic derivative (motif 1). Reagents and conditions: (iv) $Na_2S_2O_5$, dimethylacetamide, reflux, 100 ºC, 12 h.

II.1.3 Synthesis of the benzofuran derivatives

Benzofuran derivatives were synthesized from the condensation between the corresponding salicylaldehyde (**a2** and **a3**) with ethyl chloroacetate, in basic conditions (to counterbalance the production of HCl). Then the ester formed (**b2**/**b3**), was heated at high temperature to promote cyclization, through an intramolecular rearrangement. The last reaction step involved a water hydrolysis of the ester (**c2**/**c3**) to afford the corresponding benzofuran acid moieties **2** and **3** (**Scheme II.3**).

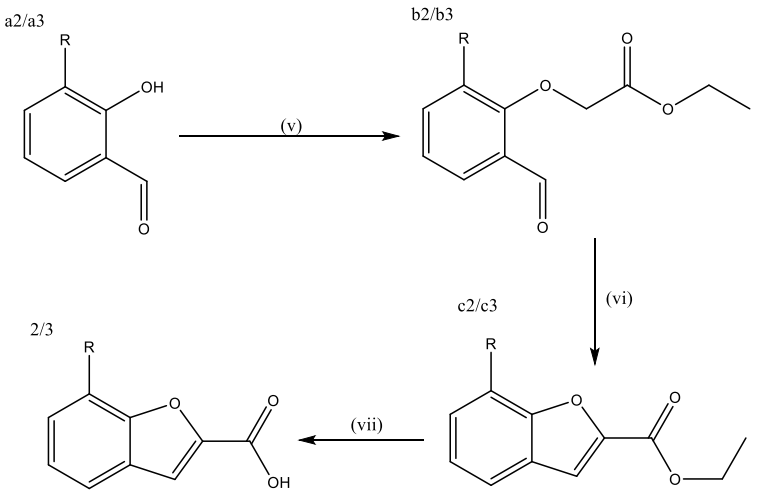

Scheme II.3 – Synthesis of unsubstituted (R = H) and methoxy (R = OMe) benzofuran derivatives (moieties 2 and 3). Reagents and conditions: (v) ethyl chloroacetate, K_2CO_3, DMF, reflux, 110 ºC, 1,5 h; (vi) reflux, 150 ºC, 4 h; (vii) H_2O, reflux, 150 ºC, 1,5 h.

The hydroxy-benzofuran carboxylic acid was obtained from the corresponding methoxy derivative by demethylation using boron trichloride as a Lewis acid and tetrabutylammonium iodide (TBAI) (**Scheme II.4**). By itself, BCl_3 does not remove the methyl group at low temperature, but, in the presence of TBAI, its reactivity is highly enhanced[54].

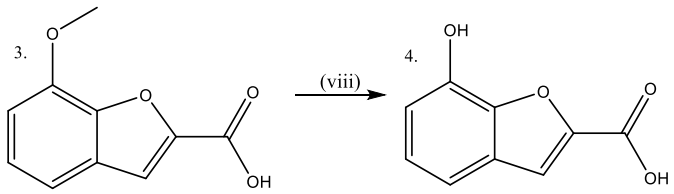

Scheme II.4 – Synthesis of motif 4. Reagents and conditions: (viii) BCl_3, TBAI, dry DCM, -78 ºC→rt, 3 h→overnight.

II.1.4 Synthesis of final conjugated products

The final products were synthesized through a coupling reaction between the amine group from the donepezil motif and the carboxylic group from the benzimidazole/benzofuran-carboxyl derivatives. The direct reaction between an amine and a carboxylic acid *via* conversion to an amide is difficult due to the hydroxyl group of the carboxylic group being a bad leaving group. So, before the nucleophilic attack to the carbonyl it is necessary to use a coupling agent to activate the carboxylic group (transforming the OH group into another one with good capacity as a leaving group). Propylphophonic anhydride (T3P) is a non-toxic and very efficient coupling agent for the preparation of amides[6,47]. Furthermore, T3P has the advantage of producing sub products that can be easily eliminated by an aqueous extraction and so it was chosen for this reaction. It requires a base for the activation of the carboxylic acid, *N*-methylmorpholine (NMM) being the base chosen.

In this reaction, the base deprotonates the carboxylic acid, resulting a carboxylate that will attack T3P. Then, the amine group will attack the now active carboxylic acid intermediate, while a second equivalent of base picks up the excess proton, providing the amide bond[47,55] (**Scheme II.5 A**).

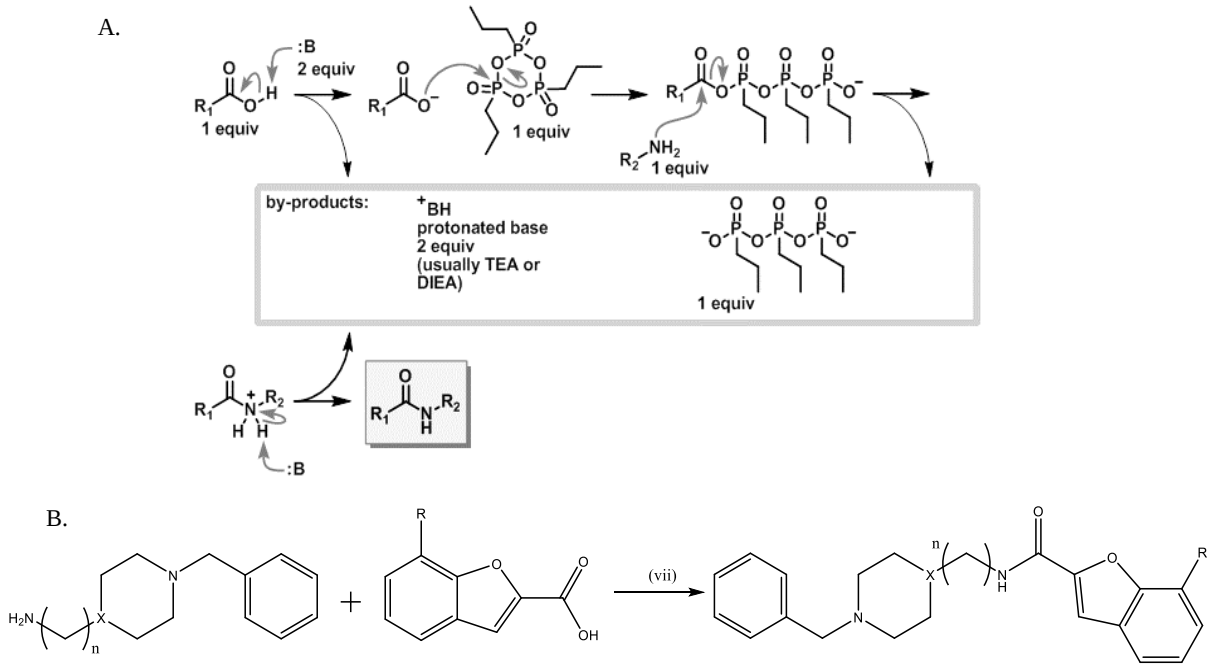

Scheme II.5 - **A**. T3P mechanism, adapted from [55]; **B**. Synthesis of PP2 (X = CH, n = 1, R = H), PP3 (X = CH, n = 1, R = OCH_3), PZ2 (X = N, n = 2, R = H) and PZ3 (X = N, n = 2, R = OCH_3). Reagents and conditions: (vii) T3P, NMM, DCM, rt, overnight.

Final products **PP2**, **PP3**, **PZ2** and **PZ3** were obtained following this coupling method, but the same proved unsuccessful for the coupling between the donepezil derivatives and the hydroxyphenylbenzimidazole and hydroxybenzofuran moieties. The reason is not yet understood, but the presence of that hydroxyl (phenol) group in those benzimidazole/benzofuran-carboxyl derivatives may account for inactivating the role of T3P in its reaction with the carboxylic group. Therefore, in those cases a different coupling agent *N*,*N*'-dicyclohexycarbodiimide (DCC) was used for the amine-carboxylic conjugation.

In this reaction, the carboxylic acid adds to DCC, forming a good leaving group that will be displaced by the amine through nucleophilic substitution. DCC and the carboxylic acid can form an *O*-acyl-isourea intermediate (ester 1). Because this intermediate is unstable, we have used a coadjuvant coupling agent, *N*-hydroxysuccinimide (NHS), which is added to the carboxylic acid together with the carbodiimide. NHS attacks the electrophilic carbon of the carbonyl group to form dicyclohexylurea (DCU) and the NHS-ester (ester 2), which is a much more stable compound that remains reactive with amines. Upon the final addition of the amine, the final desired coupling product, an amide, is formed by displacement of the NHS, with a proton transfer to the activating reagent (**Scheme II.6**).

This change in the coupling strategy allowed the synthesis of the final compounds with hydroxyphenylbenzimidazole motif (**PP1** and **PZ1**), while the other compounds (benzofuran derivatives) with hydroxyl substitution still presented some difficulties with this coupling mechanism. Compound **PZ4** was obtained in a small yield, while compound **PP4** was not obtained, thus being the only compound from the designed series that was not synthesized under the time-window of this Master thesis (**Scheme II.7**). The presence of abundant secondary products makes the purification of the intended products a difficult task, which compared with T3P reaction turns out to consist in a huge disadvantage for this one.

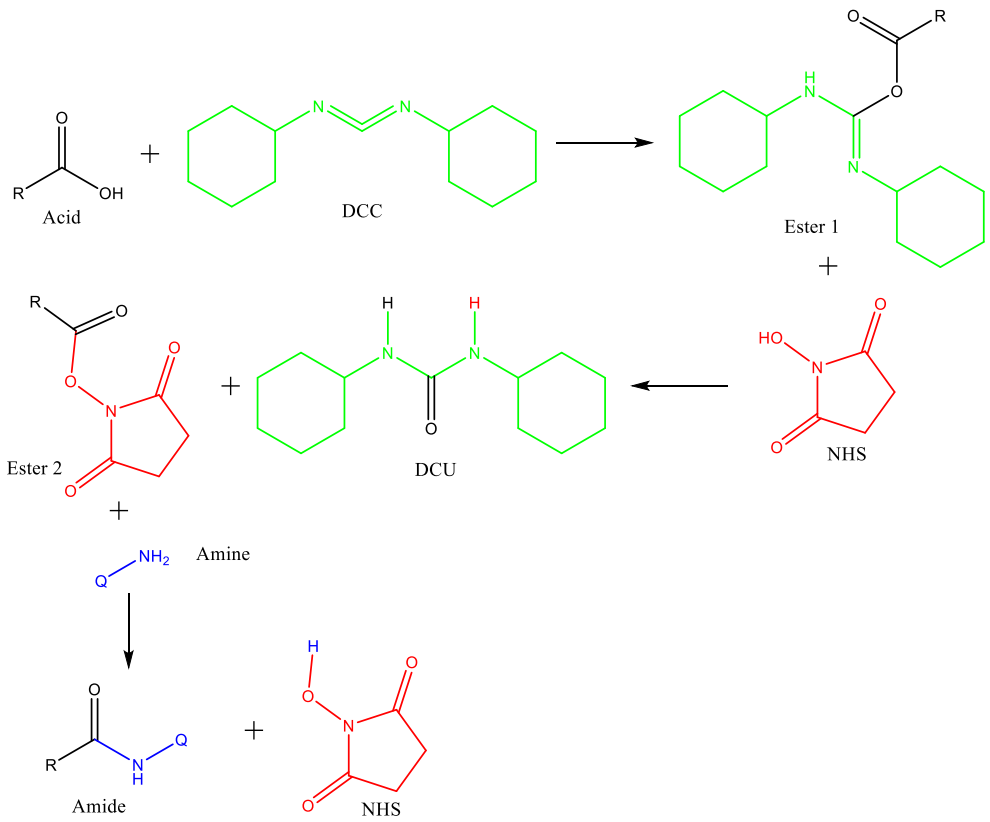

Scheme II.6 – Mechanism of DCC-induced amide bond synthesis.

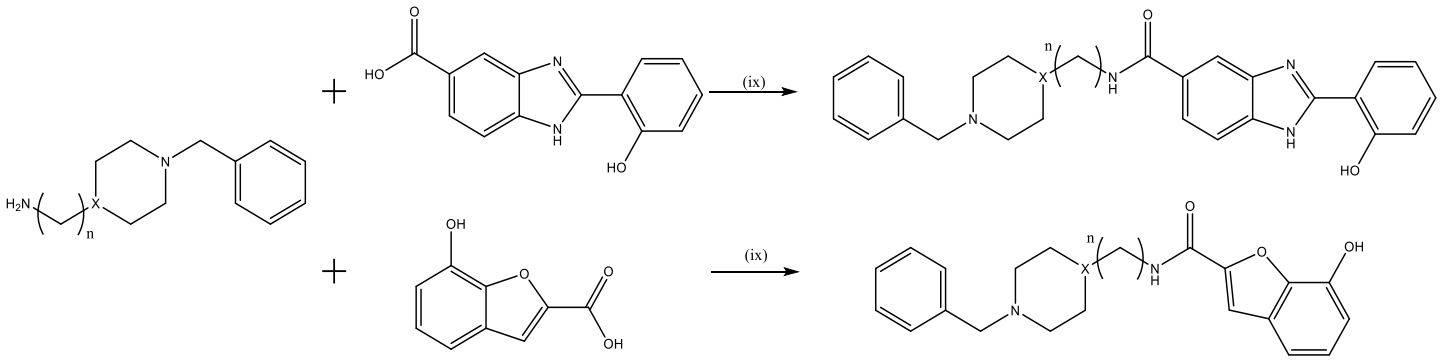

Scheme II.7 – Synthesis of PP1 and PP4 (X = CH, n = 1) up and PZ1 and PZ4 (X = N, n = 2) down. Reagents and conditions: (ix) DCC, NHS, DMF, rt, 40 h.

All these reactional steps led to the final compounds used in molecular modulation and all the biochemical studies described in the respective sections of this thesis (**Figure II.2**). Regarding compounds with motif **4**, a different approach is in progress, in which the demethylation of the methoxy group, leading to the corresponding hydroxyl derivatives is proposed to be made after the final amine-carboxylic coupling reaction (e.g. from the final product **PP3** and **PZ3**), instead of making it before that coupling reaction, as it is presented in **Scheme II.4**.

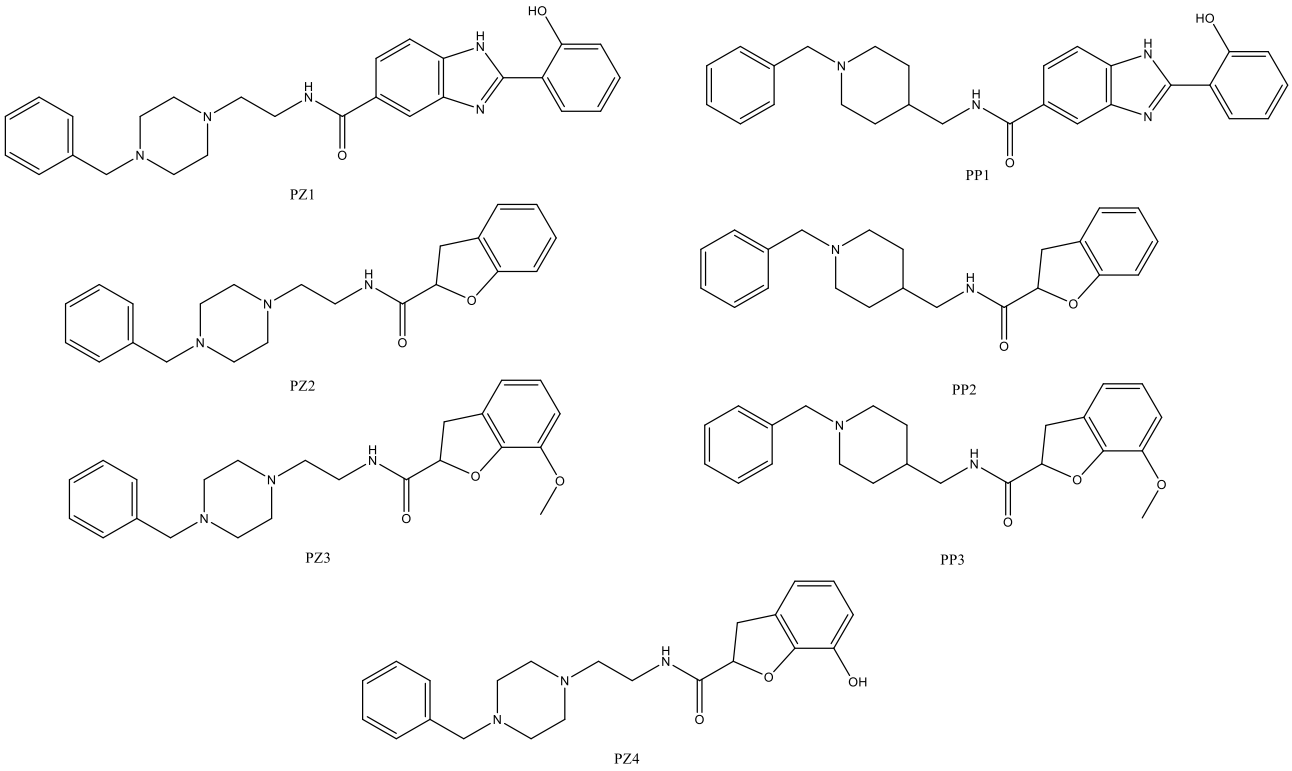

Figure II.2 – Final products synthesized.

II.2 Molecular modulation

Molecular modulation and docking techniques are indispensable tools in different scientific areas, presenting a niche as powerful tools in the design of new drugs in medicinal chemistry. These studies allow the predictions of interactions between the newly designed compounds and potential biomolecules for different purposes. In the specific case of AD, docking studies constitute a huge source of information, since they allow getting a good insight on the understanding of how the new compounds can interact with AChE.

Molecular modulation studies were performed with software GOLD version 5.1[56], which has already proven successful as a docking tool regarding our line of studies[6,47]. Docking simulation with this program enables the prediction of the most stable conformations of our ligand in the AChE active centre, as well as the determination of the most probable interaction between molecules. The three-dimensional structure of the enzyme was obtained from the Protein Data Bank (PDB) database, with the code 1EVE, the x-ray structure of the complex AChE with E2020, Aricept® (donepezil). The choice is based on the resemblance between our newly designed ligands and donepezil, implying a potential similarity in the way followed by both compounds in their interaction with AChE. The protein in this model belongs to the specie *Torpedo californica*, which active site presents an important resemblance with the active centre of human AChE, as prior reported[32].

Donepezil presents three distinct interactions with AChE that are responsible for its strong binding with the enzyme (**Figure II.3**). In the bottom of the gorge, the benzyl motif performs parallel π-π stacking with the indole group from Trp84 while, in the middle of the gorge, the charged nitrogen can establish a cation-π binding interaction with the phenyl group of Phe330. At the entrance of the gorge, the indanone ring of donepezil and the indole ring of Trp279 also interact through π-π stacking[57]. It is

also reported that the carbonyl group interacts via van der Waals forces with the aromatic ring of Phe331 and Phe290, but that the lack of this carbonyl group leads to inactive compounds[58], thus being hypothesized that this group could be responsible for a favourable orientation of the indanone ring for the π-π stacking.

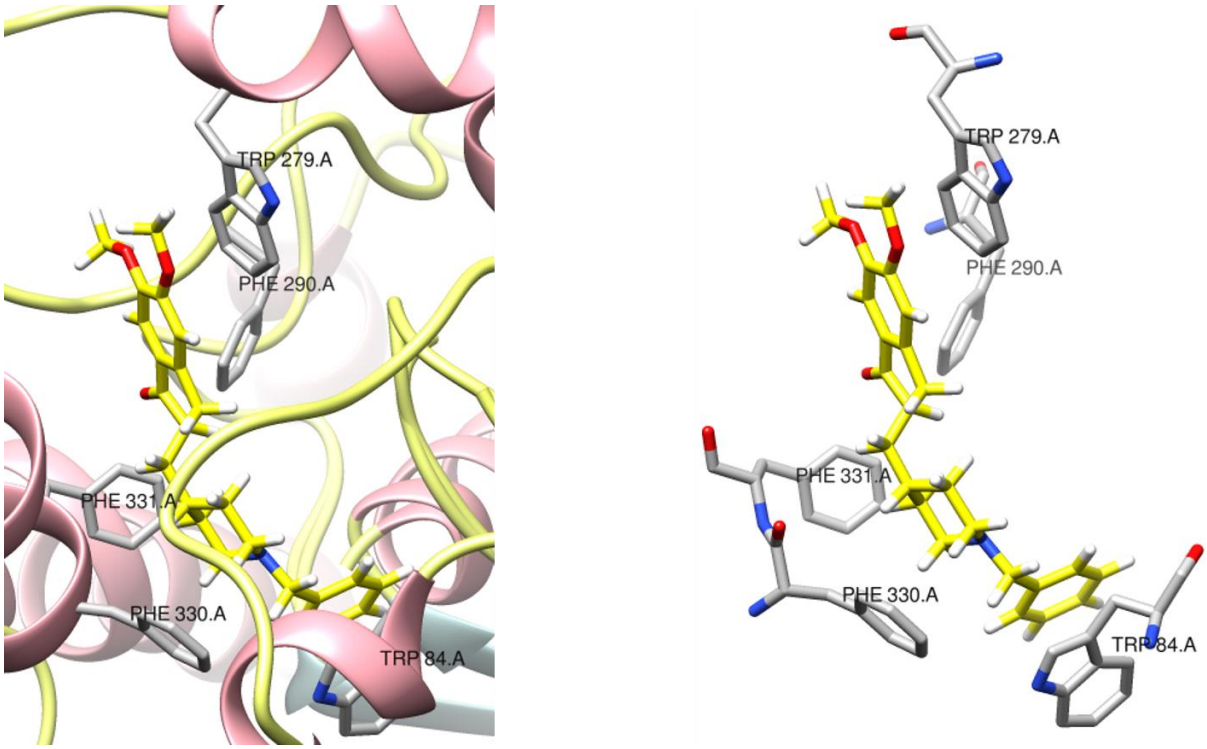

Figure II.3 – Donepezil (yellow) in AChE active centre (PDB code 1EVE), with and without secondary structure.

Docking studies have shown that some of the aromatic interactions established between donepezil and AChE are maintained in the new series of compounds designed, especially the coincident position of the donepezil motif at the CAS. All newly designed compounds present a similar position in the gorge of the enzyme, with donepezil moieties in CAS and benzimidazole/benzofuran moieties in PAS. Interactions at the level of benzyl group are predicted to be maintained, namely the π-π stacking with Trp84, while most of the cation-π interaction with Phe330 are also maintained. On the other hand, the change of a piperidine ring to a piperazine ring is expected to lower the affinity of the resulting analogues, which, according to reported in literature, can decrease around 19-fold[57]. In PAS, both benzimidazole and benzofuran could also lead to π-π interaction with the indole group from Trp279, but the absence of the carbonyl group could lead to a less favourable orientation of the compound.

However, some differences are worthy of notice, both inter and intra-series. **PP1** and **PZ1** present an excellent superimposition in CAS, regarding their comparison with the original ligand donepezil (**Figure II.4**), but in PAS, it becomes a bit lost. The presence of an extra methylene group in **PZ1** leads to the accommodation of the benzimidazole ring closer of the indole ring of Trp279, than that of **PP1** and donepezil. This can allow the hydroxyphenyl motif to present different conformation at the entrance of the gorge, therefore modifying the interaction of the molecule in PAS. Both compounds also present a conformation length bigger than that of donepezil, mostly due to the presence of the hydroxyphenyl molecular fragment (**Figure II.5**).

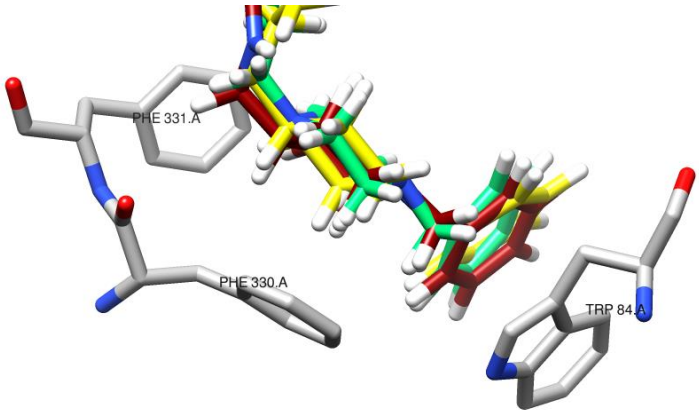

Figure II.4 – Superimposition of PP1 (dark red), PZ1 (green) and the original ligand E2020 (yellow), from PDB code 1EVE.

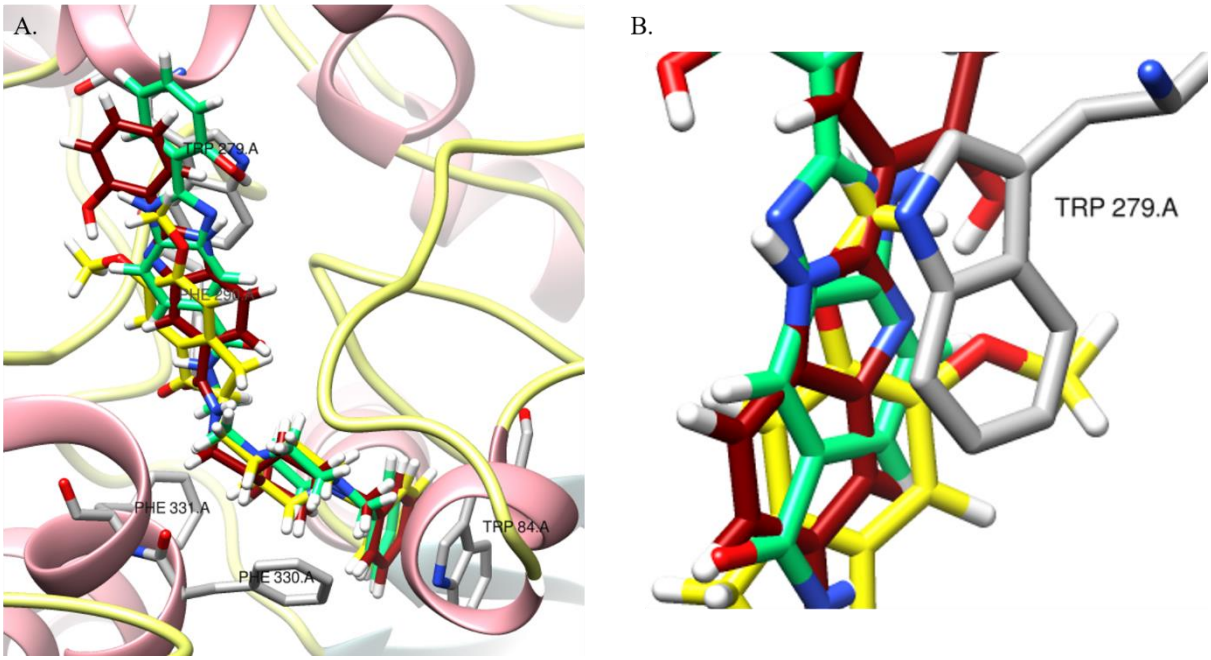

Figure II.5 – **A**. Superimposition of donepezil (yellow), PP1 (dark red) and PZ1 (green) in the active centre of AChE (PDB code 1EVE); **B**. Close-up of the superimposition of the same structures near Trp279.

Comparing both **PP2** with **PZ2** and **PP3** with **PZ3** a good fitting in the gorge of the enzyme is observed, with good overlap with the original ligand. However, in both **PP2** and **PP3** the piperidine unit presents a minimalist difference in the overlap, while the compounds with piperazine present an identical superimposition to that of donepezil, which is a particular difference, since donepezil present a piperidine ring in its structure. This could be due to the chain length chain of the compounds: since **PZ** series compounds present an extra methylene group, there is an easier approach for the docking calculi to fit the structure to the original ligand, while the lack of this group could lead to a "stretch" of the **PP** series compounds for a better fitting in the gorge (**Figure II.6**).

Comparison inside each series (**PP2** with **PP3** and **PZ2** with **PZ3**), didn't show much difference, with exception of the extra methoxy group that by itself doesn't appear to present any extra interaction with the AChE active centre. Despite that, the methoxy group could work as the carbonyl group in donepezil and define a better orientation for the molecule in the enzyme active site.

These docking results will be further discussed in the next sub-chapter regarding the rationalization of the values obtained in the enzymatic inhibition studies, in particular on the effect of different

substitution between them. In future studies, there will also be interesting to evaluate the effect of these compounds towards butyrylcholinesterase: will they be selective or will they inhibit both enzymes in the same order of magnitude?

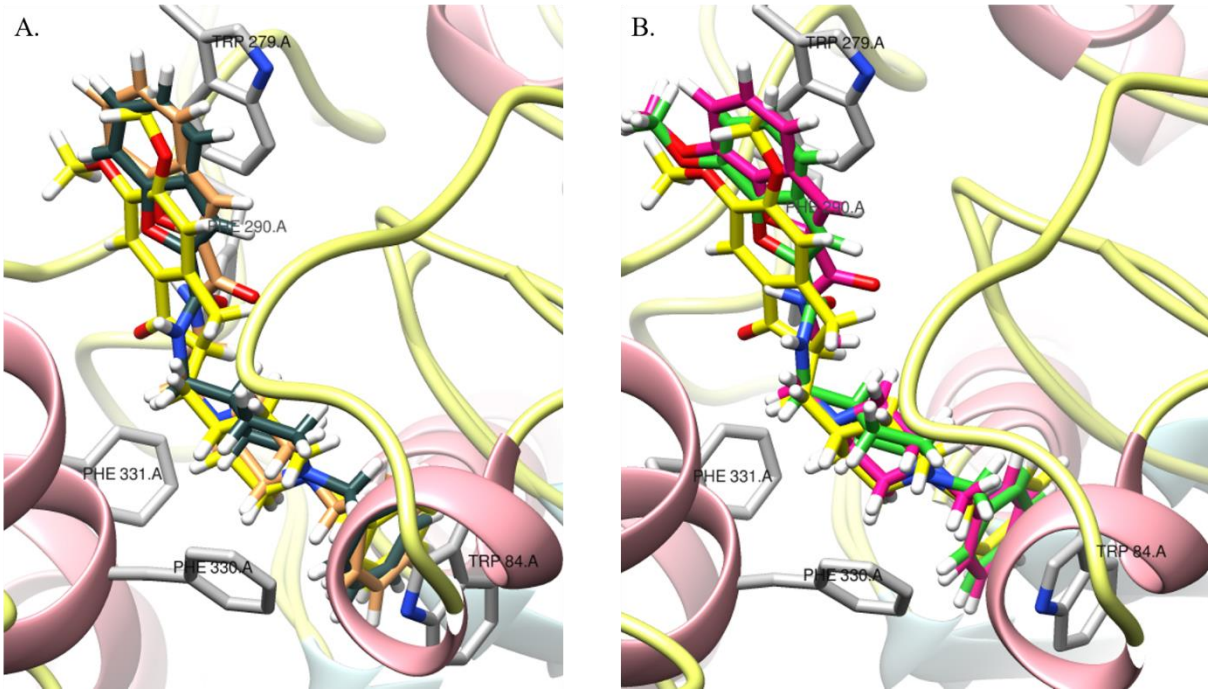

Figure II.6 – **A**. Superimpostion of donepezil (yellow), PP2 (brown) and PZ2 (dark blue) in AChE active centre (PDB code 1EVE); **B**. Superimpostion of donepezil (yellow), PP3 (green) and PZ3 (pink) in AChE active centre (PDB code 1EVE).

II.3 Enzyme inhibition

Inhibition studies of AChE were made through an adaptation of Ellman's method[59], a photometric method for determining AChE activity. This method follows the progress of substrate hydrolysis by the measurement of product formation (**Scheme II.8**).

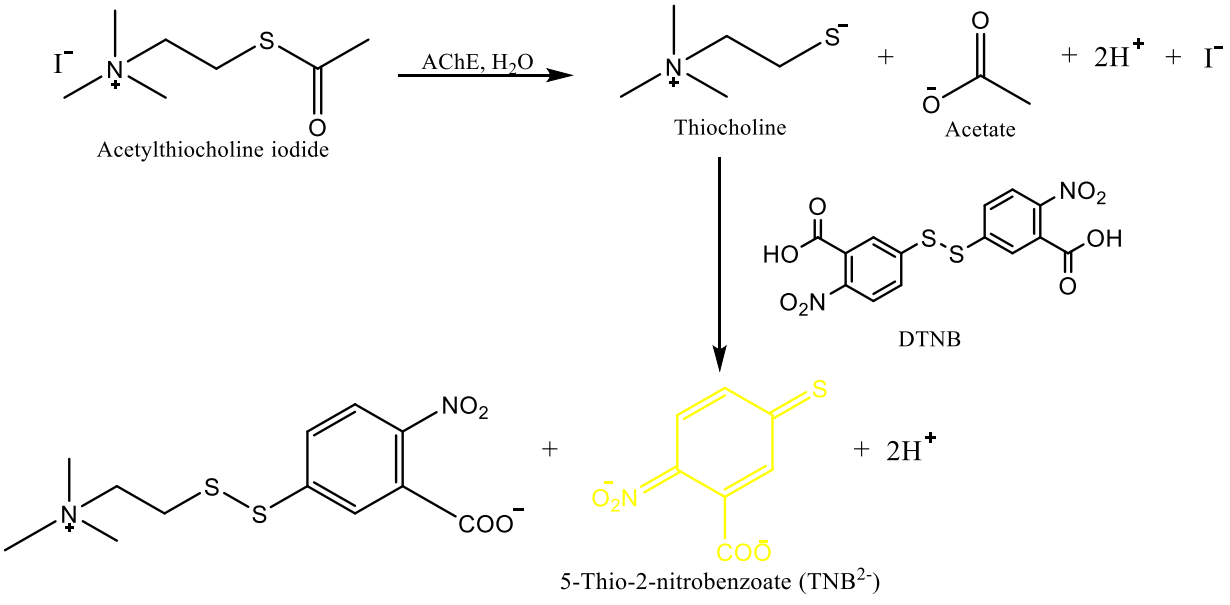

Scheme II.8 – Ellman's method for AChE activity determination.

Ellman's method involves a two-step successive mechanism. The first step is the hydrolysis of acetylthiocholine iodide (AChI) by AChE, originating thiocholine and acetate. Thiocholine will react with 5-5'-dithiobis-(2-nitrobenzoic acid) (DTNB), also known as Ellman's reagent, forming TNB^{2-}. TNB^{2-} presents a yellow colour that can be further detected spectrophotometrically by the absorbance measurement at 405 nm (wavelength that corresponds to maximum absorption). This second reaction is rapid, not rate limiting the measurement of the enzyme[59,60].

Ellman's method is the most used assay for AChE activity determination due to its simplicity, speed, and sensibility. However, since reproducibility is important in biological assays, it is needed to take into account the initial velocity of AChI hydrolysis, studying a range where the reaction velocity is linear and TNB^{2-} formation is proportional to AChI hydrolysis[60]. It is also reported that the data obtained from AChI is like that of using acetylcholine as a substrate[59].

The initial velocity of substrate hydrolysis by AChE is obtained in the beginning of the assay. Enzymatic velocity was calculated from the relation between the slope of the absorbance curve in function of time, at 405 nm. This relation is only valid until 5 min, where it is observed the linearity of the absorbance curve[59,60]. The graphical representation of enzyme activity in the presence of different inhibitor concentrations is compared to that of the activity in the absence of inhibitor, allowing the calculation of the IC_{50} for each compound. This way, the new compounds were evaluated by their capacity of inhibition of AChE, in comparison with reference drugs (tacrine and donepezil). This last drug is between the most potent AChE inhibitors, inhibiting in the nanomolar range.

Table II.1 – IC_{50} values for each compound, referring to inhibition of AChE.

Compound	IC_{50}(μM) ± SD[a]
PP1	4.2 ± 0.8
PP2	30.0 ± 1.9
PP3	19.9 ± 3.0
PZ1	6.9 ± 0.7
PZ2	18.5 ± 0.9
PZ3	4.0 ± 0.4
PZ4	20.0 ± 1.8
Tacrine	0.15 ± 0.02
Donepezil	(26 nM)[22]

[a]values are a mean of two independent experiments ± SD

Analysis of **Table II.1** illustrates that the newly synthesized compounds possess an inhibition capacity in a low micromolar magnitude. Comparing with reference drugs, such as tacrine and donepezil, the herein determined values don't show the same good inhibition. Particularly, comparing these values with donepezil, since they present a motif similar to a fragment of this compound, the differences between the values are huge. This difference could be explained by the lack of the dimethoxy indanone group and it π-π stacking with the indole ring of Trp279, showing the importance of this group in the full structure of donepezil. Also, as reported in the previous sub-chapter, is hypothesized that the carbonyl group is responsible for the favourable orientation in PAS, namely for the interaction with the indole ring of Trp279[58].

The small differences found on the magnitude of the capacity of the compounds for AChE inhibition may be explained based on their different structures. For the rationalization of their structure-activity relationship, the docking results previously obtained appeared as a potentially important extra source of

information. **PZ3** shows the lowest IC_{50} value (best inhibitory capacity), while **PP2** presents the worst value, being considered the worst AChE inhibitor in the series.

Starting with compounds presenting benzimidazole motif, **PP1** showed to be the best inhibitor, although not with a big difference from its counterpart **PZ1**. Since the docking results showed a good overlap of both structures in CAS (**Figure II.4**), the difference could be explained by the presence of an extra methylene group in chain length and its effect on PAS. As explained in the molecular modulation sub-chapter, this different chain length, leads to a closer distance between the benzimidazole ring of **PZ1** and the indole ring of Trp279, comparing to **PP1** and donepezil. This proximity could be a cause for the difference between the IC_{50} values. However, the big difference comparing both compounds with donepezil could also relate to the hydroxyphenyl group that, as referred before, is outside the enzymatic gorge, and doesn't interact with PAS. This is observed by the molecular simulation results, where the group is better accommodated outside the enzyme gorge, which could account for a worst interaction between the compounds and AChE (**Figure II.7**).

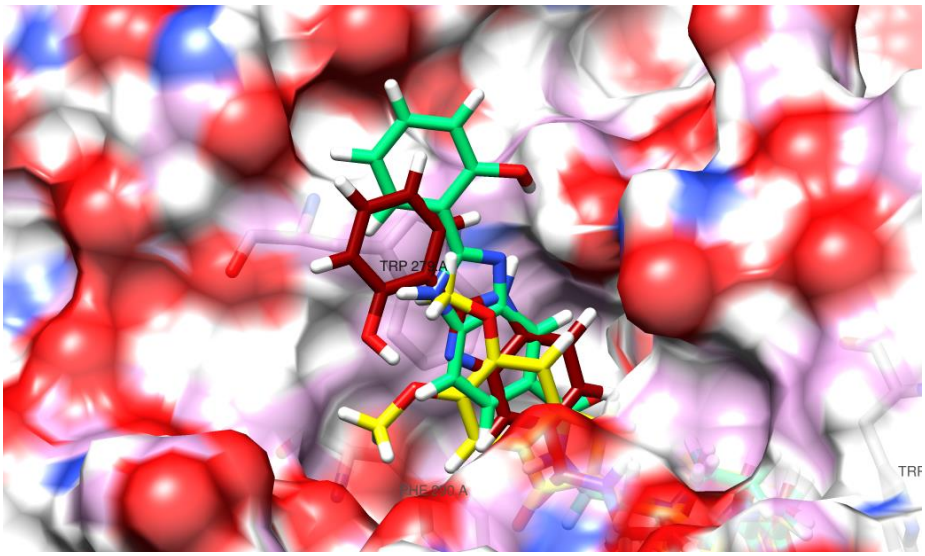

Figure II.7 – PP1 (dark red), PZ1 (green) and the original ligand E2020 (yellow) in AChE active centre (PDB code 1EVE), in a surface depiction.

Generally, compounds presenting the benzofuran motif showed a lower capacity for the inhibition of AChE as compared with those enclosing the benzimidazole motif, while **PZ3** appeared as an exception to that trend. Both **PP2** and **PZ2**, enclosing the unsubstituted benzofuran motif, presented inhibitory capacity about one-order of magnitude lower than analogues **PP1** and **PZ1**, respectively, **PP2** being the worst in all the series. The absence of any extra group in the benzofuran motif may be responsible for a lower binding with PAS, then leading to a lower interaction with the enzyme. As previously stated, **PP2** didn't show a good overlap with the original ligand in CAS (**Figure II.6**), which probably explains its bigger IC_{50} value when comparing with its counterpart **PZ2**. Also noteworthy is the fact that **PZ4** and **PZ2** present identical inhibitory capacity, thus suggesting that the presence of the hydroxyl substituent group doesn't add any extra favourable interaction with PAS.

The methoxy substituted benzofuran derivatives are a more particular case, since **PZ3** presents the lowest IC_{50} value in the series, but **PP3** presents a value like that of **PZ2** and **PZ4**. Both compounds show lower IC_{50} values, as compared with their non-substituted counterparts, probably due to favourable interactions with the active centre of the enzyme, and concomitant increase stability of the complex protein-ligand. As the above compounds, **PP3** didn't show a good overlap in CAS, thus suggesting a weaker interaction. On the contrary, **PZ3** shows a good superimposition with the original ligand in CAS,

and a good similarity between the positioning of their methoxy group in PAS, which can account for a strong binding interaction both in CAS and PAS, thus explaining the lower IC_{50} value of AChE inhibition (**Figure II.8**). Previously, it was also suggested that the methoxy group could act like the carbonyl group of donepezil and function as reinforcement for a better orientation in the PAS.

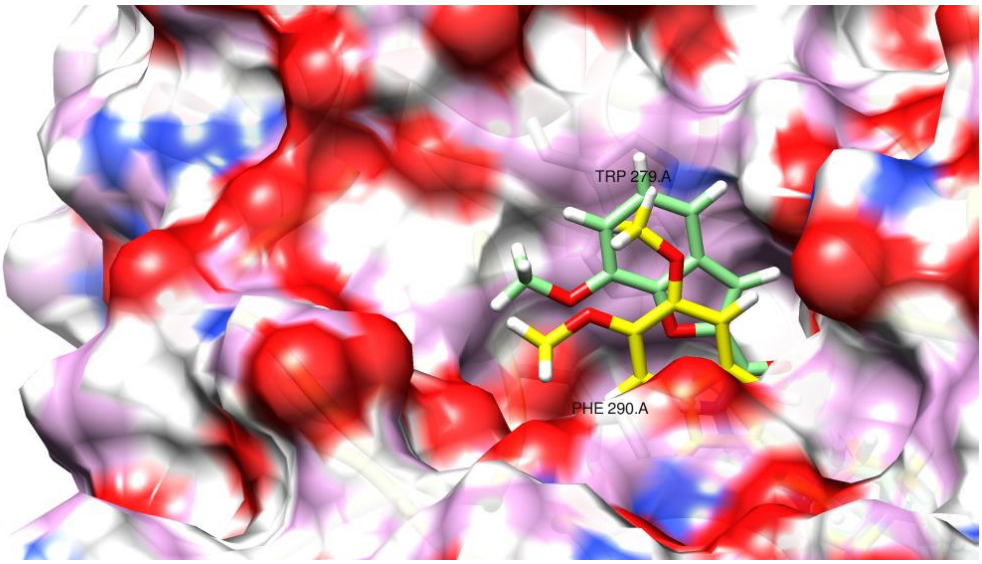

Figure II.8 – PZ3 (green) and the original ligand E2020 (yellow) in AChE active centre (PDB code 1EVE), in a surface depiction.

Globally, all compounds showed a good/moderate AChE inhibition in a low micromolar range. However, these values are not as good as those of the drugs already commercialized, neither as other tacrine-multifunctional drugs already synthesized and published, in some cases with values in a nanomolar scale[6,22,47,61]. Nevertheless, as non-tacrine hybrids, they have the advantage of being less toxic than the tacrine derivatives. In general, the compounds with benzimidazole motif showed a better AChE inhibition, due to favourable interactions in PAS, thus establishing a stronger bond with AChE and a more stable complex protein-ligand. For benzofuran substituents, compounds with piperazine ring showed better inhibition values, due to a worst overlap of **PP** compounds in CAS. An increase in chain length (adding an extra methylene group, such as in **PZ** series) could improve superimposition in CAS and a better interaction with PAS, leading to better IC_{50} values. Among the series hybrids, **PZ3** showed the best AChE inhibitory capacity, due to its structural similarity with donepezil.

II.4 Antioxidant activity

Antioxidant activity was measured by the reduction of 2,2-diphenyl-1-picrylhydrazyl (DPPH)[62]. DPPH is a stable free radical, due to the delocalisation of a spare electron on the molecule, preventing its dimerization. This delocalisation provides a strong violet colour to the solution of DPPH in methanol (MeOH), at rt, with absorption at 517 nm. A mixture of this solution with a substance that can donate hydrogen, leads to the reduction of DPPH and the loss of violet coloration, i.e. lowering absorption at 517 nm. The new molecule of diphenylpicrylhydrazine (DPPH-H) will appear with a yellow tonality, whereas the more yellow the solution greater the reduction[62,63] (**Scheme II.9**).

This DPPH assay is a rapid, simple and inexpensive method to measure the ability of hydrogen donors or free radical scavengers of new compounds. Experimentally, this method consists in the preparation of solutions with variable concentrations of compound and constant concentrations of DPPH, followed by incubation of the solutions at rt and absorbance reading at 517 nm.

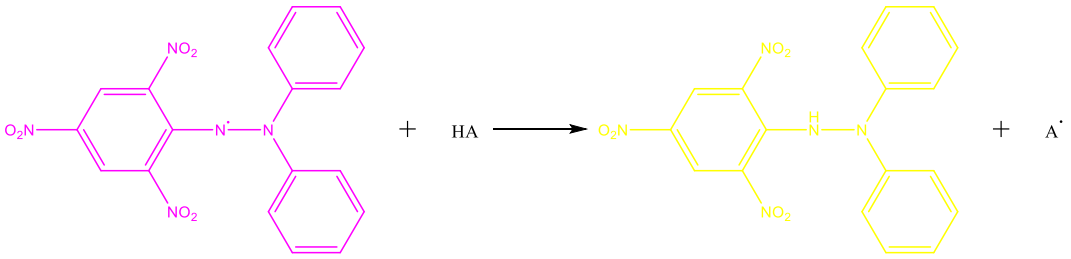

Scheme II.9 – Reduction of DPPH in the presence of an antioxidant substance.

Table II.2 – EC_{50} values for each compound, referring to antioxidant activity.

Compound	EC_{50}(μM) ± SD[a]
PP1	n.d.[b]
PP2	>10000
PP3	>10000
PZ1	594 ± 4
PZ2	>4000
PZ3	>4000
Tacrine	>1000[46]

[a]values are a mean of two independent experiments ± SD; [b]not determined

Generally, all compounds show poor or un-existing antioxidant capacity (**Table II.2**). In fact, except for **PZ1** (EC_{50} = 594 μM) and **PP1** (n.d. due to lack of solubility in MeOH), all the newly designed compounds present values in mM range. Comparison of the EC_{50} values obtained with that of a known antioxidant, such as Trolox (15 μM)[64], indicate that these compounds don't show important activity as antioxidants. Nevertheless, a wide range of compounds presenting benzofuran derivatives in their structure had already proven to have potential as antioxidants[44], which suggests that the benzofuran ring may require some extra motif to exert antioxidant activity. Despite that, future compounds **PP4** and **PZ4** could differentiate themselves from their counterparts' due to the presence of the hydroxyl group, who could act as a potential hydrogen donor.

Compound **PZ1** still presents a weak to moderate activity, with a value of 594 μM, thus being the best anti-oxidant compound in the present series. However, the hydroxyphenylbenzimidazole motif used in its design was reported to have a value of 160 μM[65]. This difference can be explained by the lack of activity of donepezil. An insertion of a radical scavenging motif in the donepezil molecular unity of the compound could result in a stronger antioxidant.

II.5 Inhibition of self-mediated $A\beta_{1-42}$ aggregation

Inhibition of $A\beta_{1-42}$ aggregation was measured using the fluorescent properties of thioflavin T (ThT)[66]. This water soluble benzothiazole salt is one of the most used dyes for visualization and quantification of amyloid aggregates. ThT alone is not an amazing fluorescent compound but, after fibril binding, fluorescence emission increases by several orders of magnitude, associated with a shift in both the excitation and emission wavelength maximum. Even more, a moderate affinity for fibrils (dissociation constant K_d in sub-μM range)[66] allows for a sensitive and efficient method for quantification of β-amyloid aggregates. It is theorized, that free rotation in the carbon-carbon bond between the benzylamine and benzathiole rings is associated with this specific property, since the immobilization of this rotation preserves the excited state, permitting high quantum yield fluorescence.

The presence of ThT-binding sites could provide for a sterically immobilization of the molecule, leading to the enhanced fluorescence (**Figure II.9**)[66].

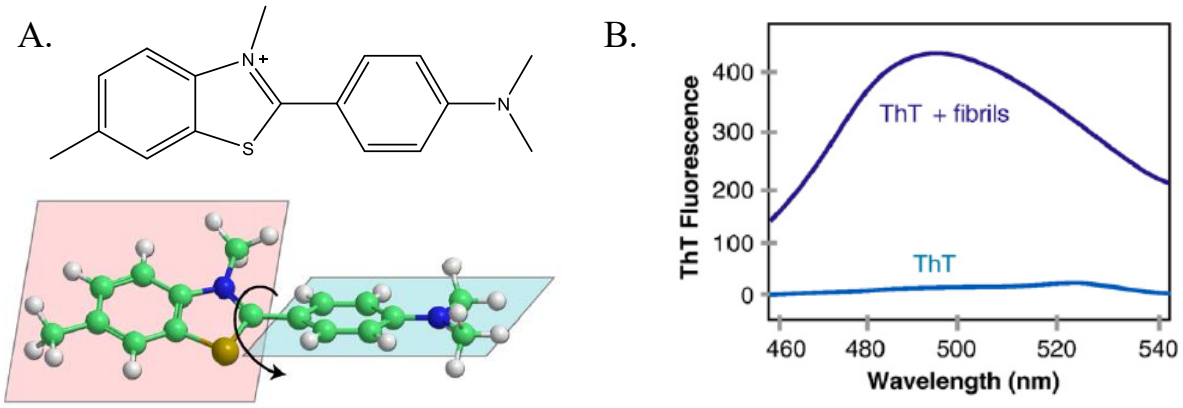

Figure II.9 – **A**. Structure of ThT (top) and 3D structure of ThT with representation of bond rotation (bottom); **B**. Graphical representation of fluorescence intensity of both ThT and ThT complexed with fibrils (λ_{exc} = 450 nm). Both images were adapted from [66].

$A\beta_{1-42}$ was left to incubate for 24 h, at 37 ºC, in the absence and presence of the new compounds. After that, ThT was added and the fluorescence was measured. In the absence of ligand, fluorescence intensity will be maximum since there is no source of inhibition of amyloid aggregation. Rationalizing the fluorescence intensity obtained for each assay with ligand, it is possible to calculate the percentage of aggregation inhibition exerted by each one of the compounds. It was also measured the fluorescence in the absence of $A\beta_{1-42}$ for the same experiments, to consider the fluorescence of the dye without binding to the fibrils.

Table II.3 – Percentage of inhibition of self-mediated $A\beta_{1-42}$ aggregation ([$A\beta_{1-42}$] = 80 μM).

Compound	$A\beta_{1-42}$ aggregation inhibition (%)[a]
PP1	36.3
PP2	14.5
PP3	26.9
PZ1	25.3
PZ2	14.4
PZ3	19.0
PZ4	27.3
Tacrine	22.8 (for $A\beta_{1-40}$)[46]

[a]values are a mean of two independent experiments.

Based on the analysis of the results presented in **Table II.3**, it is observed an inhibition of $A\beta_{1-42}$ aggregation in a weak to moderate scale. Once again, compounds with the benzimidazole motif proved to be better than their benzofuran counterparts, and in a broad sense, the **PP** series shows to have better values regarding the inhibition of the amyloid aggregation. In both series, the percentage of inhibition follows the same pattern, with compounds with benzimidazole being the most effective and compounds with the unsubstituted benzofuran being the worst ones (disregarding the compounds with hydroxybenzofuran, since the value for **PP4** is not present). Regarding the benzofuran hybrids, it is noticeable that the methoxy group affects the inhibition when comparing with the unsubstituted counterpart. Also, it is noteworthy that, despite the lack of value for inhibition of compound **PP4**, **PZ4** shows the best value in the **PZ** series, in the same range as **PZ1**, and the best value between the benzofuran compounds. Due to the better values for **PP** series, it can probably be predicted for **PP4** the

best inhibitory capacity within the series. Despite that, the mechanism of interaction between the compounds and Aβ is still not fully understood, although a disruption of the conformation in β-sheets by the benzimidazole/benzofuran moieties can be associated with this inhibition.

To rationalize these results, the best-found inhibitor (**PP1**) was tested with an independent imaging technique, transmission electron microscopy (TEM), namely to compare the aggregation in the presence and absence of the inhibitor. **Figure II.10** shows a clear differentiation for images regarding the presence of **PP1** in $A\beta_{1-42}$ aggregation. In fact, although it is still visible the presence of Aβ aggregates in the presence of **PP1**, which was expected since this compound presents a moderate percentage of Aβ aggregation inhibition (36%), the aggregates became quite sparser in the presence of the inhibitor. Regarding the morphology, in the absence of **PP1** the aggregates are dense and apparently amorphous, while in the presence of the inhibitor some elongated singular branches can be observed eventually due to ligand intercalation between β-sheets of Aβ fibrils.

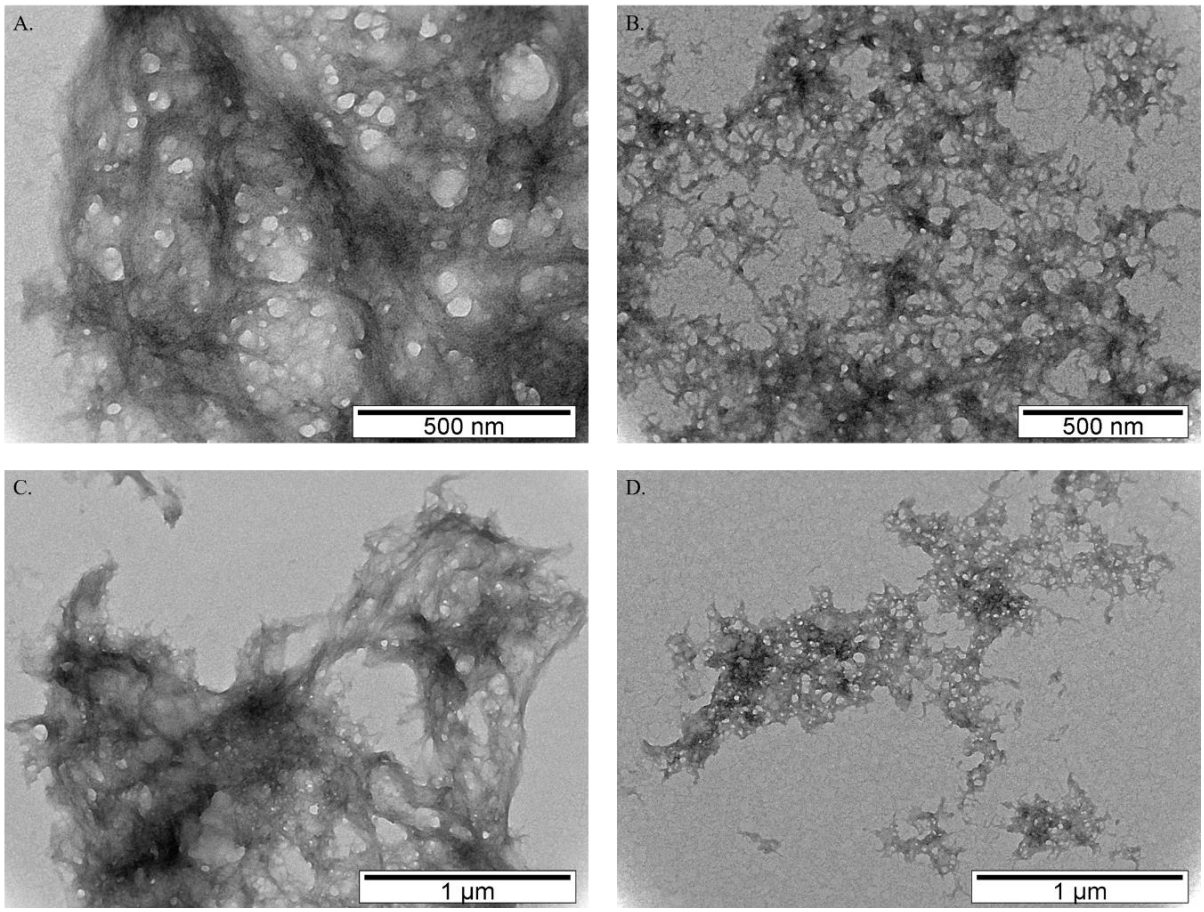

Figure II.10 – TEM images of Aβ self-aggregation inhibition experiments in the absence (A. and C.) and presence (B. and D.) of PP1, performed with samples incubated (37 ºC) for 24 h. Experimental conditions: [$A\beta_{1-42}$] = 25 µM; [PP1] = 50 µM; pH 6.6.

II.5.1 Inhibition of Cu^{2+}-induced $A\beta_{1-42}$ aggregation

As reported before, copper ion plays a prominent role in AD, due to its redox activity, as well as capacity to bind to Aβ therefore interfering with the formation of Aβ aggregates. Thus, inhibition of Aβ aggregation assays were also performed by the ThT fluorescence method in the presence of copper(II) to evaluate the role of the compounds in the Cu(II)-induced aggregation. The same procedure that was employed in self-mediated Aβ aggregation studies was used, but a solution of copper chloride was added before incubation for promoting $A\beta_{1-42}$ aggregation.

These assays were performed for compounds **PZ1** and **PZ4**, that include hydroxyphenylbenzimidazole motif and hydroxybenzofuran ring, respectively, as chelating moieties. Compound **PP1** is expected to be studied in the future.

Table II.4 – Comparison between self-mediated and Cu^{2+}-induced inhibition of $A\beta_{1-42}$ aggregation ([$A\beta_{1-42}$] = 80 μM).

Compound	$A\beta_{1-42}$ self-mediated aggregation inhibition (%)[a]	$A\beta_{1-42}$ Cu^{2+}-induced aggregation inhibition (%)[a]
PZ1	25.3	37.7
PZ4	27.3	35.5

[a]values are a mean of two independent experiments.

Table II.4 reveals that both compounds exhibit a higher inhibition of aggregation in the presence of copper(II), and once again in the same range of values. These results seem to confirm that there is competition between the chelators and the peptide for Cu(II), contributing to the disruption of the Cu(II)-mediated aggregation.

Once again, TEM assays were performed with compound **PP1** to observe, by an independent method, changes derived from the presence of copper in Aβ aggregation (**Figure II.11**). Although, **PZ1** and **PP1** contain the same chelating motif, based on the ThT assays, **PP1** proved to be the best inhibitor.

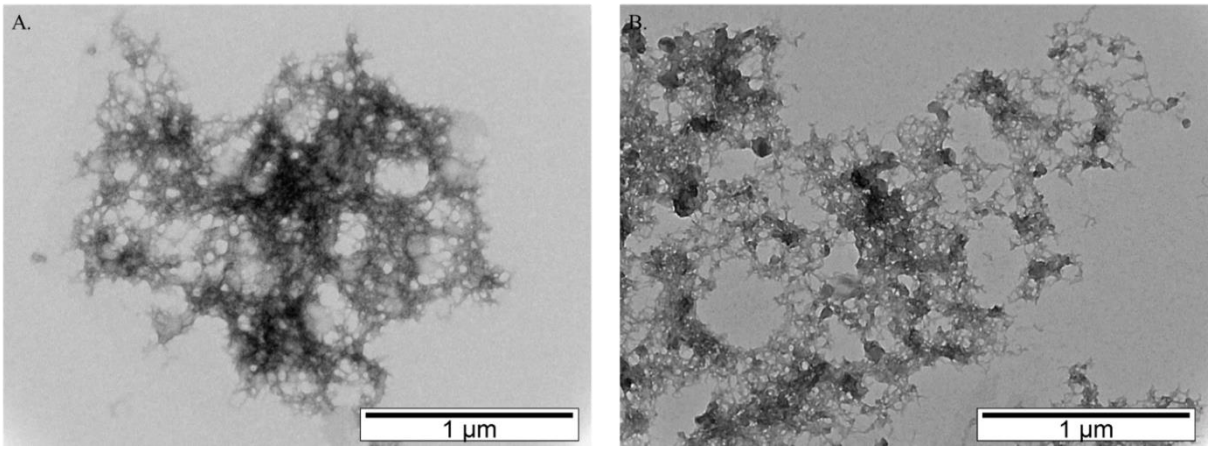

Figure II.11 – TEM images of Aβ Cu(II)-mediated aggregation inhibition experiments in the absence (A.) and presence (B.) of PP1, performed with samples incubated (37 ºC) for 24 h. Experimental conditions: [$A\beta_{1-42}$] = 25 μM; [PP1] = 50 μM; pH 6.6.

As in the case of TEM assays for self-mediated Aβ aggregation, **Figure II.11** also shows a less dense formation of agglomerates, accompanied by identifiable singular branches, in the presence of the inhibitor. This suggests that Cu(II) chelation may interfere with the aggregation process by a competition established with the inhibitor and so there is a reduction of Aβ aggregation.

II.6 Metal complexation

As already referred in the previous sub-chapter, the hydroxyphenylbenzimidazole motif can act as a metal chelating moiety, due to the presence of donor atoms, such as the phenolic hydroxyl group and the amine of the imidazole ring. Since the imidazole nitrogen can be considered a borderline base, according to the Pearson's principle of Hard and Soft Acid and Bases theory (HSAB)[67], this (*N*, *O*) core interacts with borderline acids, such as Cu(II) and Zn(II), that have already been described as intervening in AD pathology. Therefore, copper(II) and zinc(II) complexation with **PP1** and **PZ1** was studied

through pH-potentiometric assays[68,69], to evaluate the chelating affinity of these compounds due to the general recognition that chelators interfere not only in metal-induced Aβ aggregation and neurotoxicity, but also on metal homeostasis of AD brains.

An automated potentiometry apparatus was used, and titrations of the ligand only or in the presence of the metal ion (Cu(II), Zn(II)) were performed. From the obtained potentiometric data, the stability constants were calculated by fitting the experimental curves by using HYPERQUAD program[70]. Due to some solubility reasons, titrations were performed in a 50% (w/w) water/dimethyl sulfoxide (DMSO) medium, although this medium was also selected for comparison reasons with previously performed work[65].

II.6.1 Acid-base study

Prior to the metal chelation studies, the acid-base behaviour of the compound was evaluated by performing a titration of the compound alone, to determine the labile protons and calculate the protonation constants (K_i).

Both compounds were synthesized and isolated in their neutral form (HL) with the phenolic oxygen (*O*-Phe) protonated. However, in their full protonation state, they are tri-protonated (H_3L^{2+}), namely also in the imidazole ring (*N*-Im) and in the piperidine/piperazine nitrogen (*N*-Pp/*N*-Pz) (**Figure II.12**).

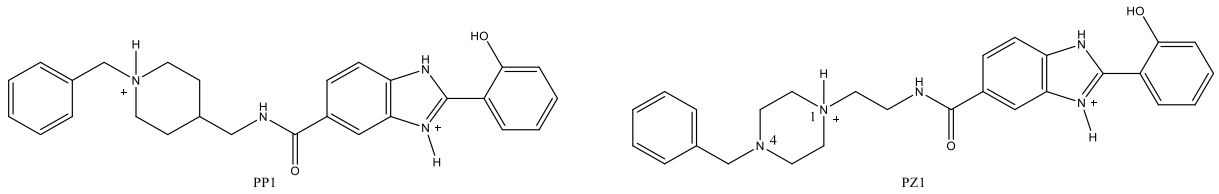

Figure II.12 – H_3L^{2+} structures of PP1 and PZ1.

The respective titration curves obtained are included in **Figure II.13** and **Figure II.14**, while the protonation constants calculated with HYPERQUAD program[70], are presented in **Table II.5**. The titration curves are the representation of pH in function of a, which corresponds to the moles of added base per mole of ligand.

Figure II.13 shows a complete titration curve, with three inflexion points, for **PZ1** compound while **Figure II.14** is incomplete and only presents points that correspond to two protonations for **PP1**. In fact, in the last case, precipitation occurs for pH ca 8.5 and above 10 the ligand **PP1** is again soluble. Due to this insolubility problem, probably related to the fact that **PP1** becomes neutral at that pH range and is more lipophilic than **PZ1**, the titration curve of compound **PP1**, was intentionally presented incomplete as shown in **Figure II.14**. Consequently, only log K_2 and log K_3 could be determined from the data treatment of the experimental curve of **PP1**, being the value of log K_1 considered equal to the respective constant obtained for **PZ1**. Nevertheless, ongoing studies of UV-vis spectrophotometric titration of **PP1** will try to determine its first protonation constant, by avoiding solubility problems, since lower concentrations of ligand are needed for performing that technique.

An identification of the protonation centres is also done for each compound in **Table II.5**, based on already obtained values for compounds with similar moieties/functional groups. Both values obtained for compounds **PP1** and **PZ1**, corresponding to *O*-Phe and *N*-Im in the benzimidazole motif, are similar to the values already reported (9.02 and 3.32, respectively, in 50% (w/w) water/DMSO medium) which were also supported by nuclear magnetic resonance (NMR) titrations[65]. Regarding the presence of two

nitrogen in the piperazine ring of **PZ1**, it is expected that the protonation atom is nitrogen 1 (**Figure II.12**), based on already published studies.

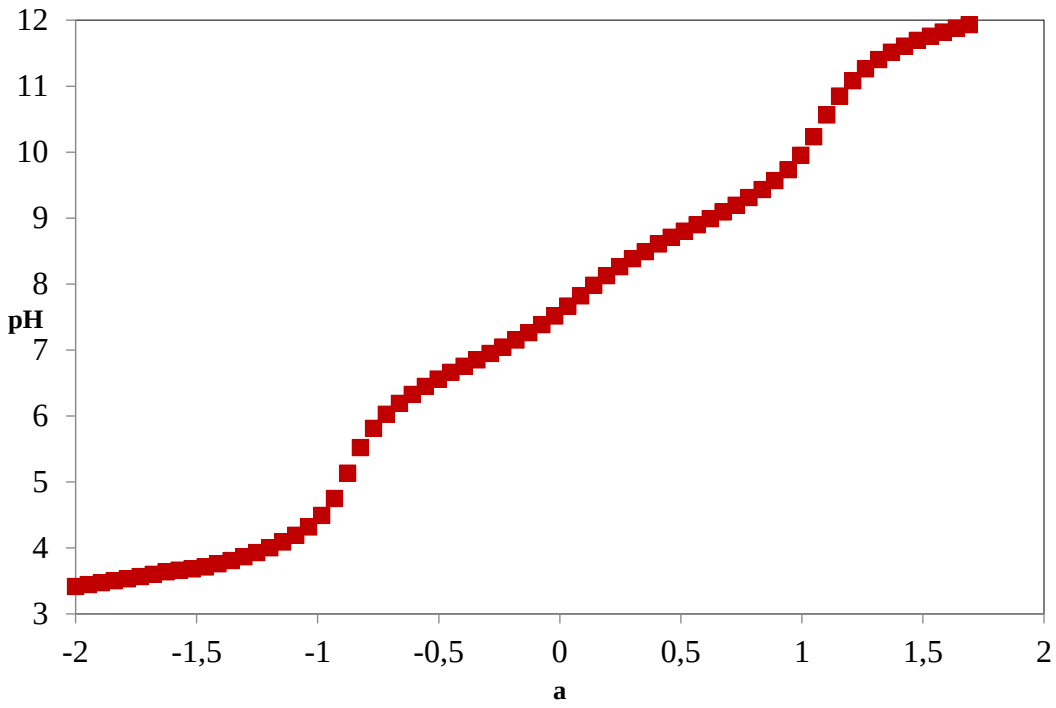

Figure II.13 – Potentiometric titration curve of PZ1 (50% w/w H_2O/DMSO, I = 0.1 M KCl, T = 25.0 ± 0.1 ºC, $C_L = 6.7\times10^{-4}$ M).

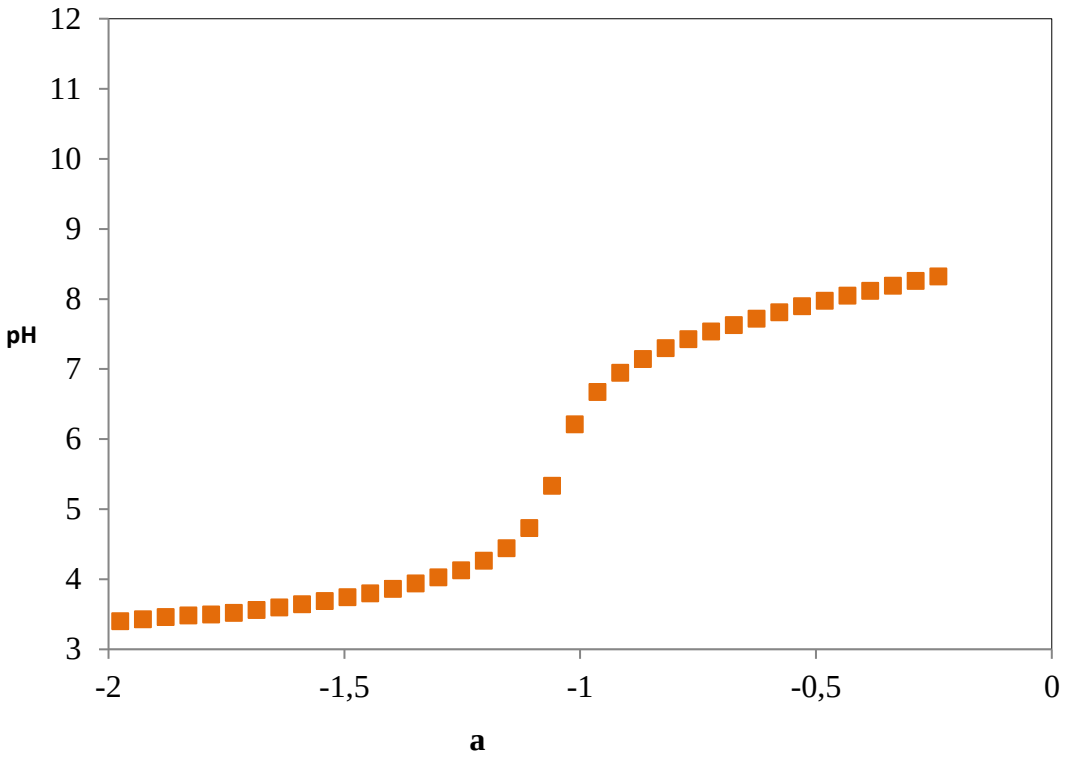

Figure II.14 – Potentiometric titration curve of PP1 (50% w/w H_2O/DMSO, I = 0.1 M KCl, T = 25.0 ± 0.1 ºC, $C_L = 6.7\times10^{-4}$ M).

Table II.5 – Stepwise protonation constants of PP1 and PZ1 (50% w/w water/DMSO, I = 0.1 M KCl, T = 25.0 ± 0.1 ºC).

Compound	$M_mH_hL_l$ (m h l)	log K_i	Protonation centre
PP1	(011)	9.04(3)*	*O*-Phe
	(021)	8.01(4)	*N*-Pp
	(031)	3.25(6)	*N*-Im
PZ1	(011)	9.04(3)	*O*-Phe
	(021)	6.76(6)	*N*-Pz
	(031)	3.37(7)	*N*-Im

In fact, a study regarding 1-(substituedphenyl)-4-propyl-piperazines[71] determined pK_a values for nitrogen 1 (7.59-8.80, in MeOH/water medium), the value depending on the substituent of the phenyl ring, while no pK_a values are presented for nitrogen 4 (**Figure II.12**). In a different report[69], a deprotonation/protonation competition process between the two piperazine nitrogen atoms is explained as an interconversion between a chair-to-boat conformation, which leads to a hydrogen bond interaction during the boat intermediate conformation, with a strong stabilization. The protonation of nitrogen 4 would happen at pH below 2, therefore only after the protonation of the imidazole nitrogen atom.

Species distribution curves were obtained through software HYSS[70], using the calculated values for the acid-base equilibrium model.

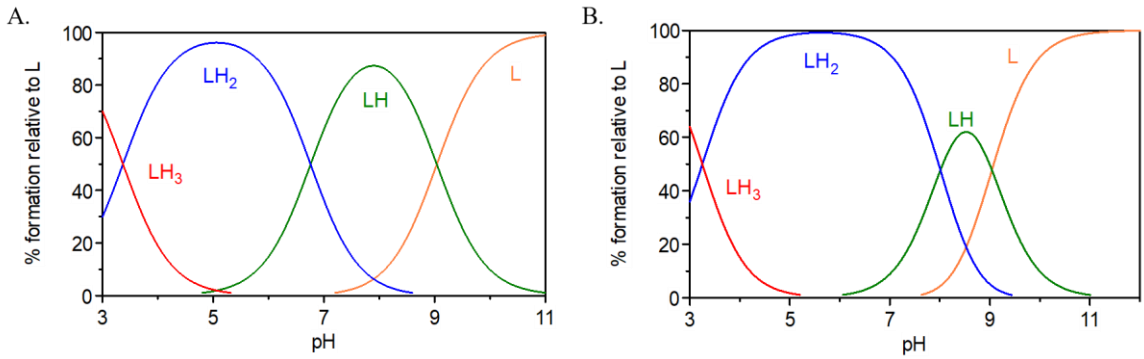

Figure II.15 – Species distribution curves for PZ1 (A.) and PP1 (B.) ($C_L = 6.7\times10^{-4}$ M).

From the species distribution curves contained in **Figure II.15**, it can be seen that, at physiological pH 7.4, the predominant species for **PZ1** is HL (neutral form), while for **PP1** is H_2L^+ (monoprotonated form). The charge of the main species present at the physiological pH will also affect the lipo-hydrophilic character of the respective compounds.

II.6.2 Copper(II) and zinc(II) complexation

The chelating capacity of the ligands towards both copper(II) and zinc(II) was also studied by potentiometric titration. Thereafter, the protonation constant previous determined, as well as the metal hydrolysis constants, were used for the calculi of the global formation constants of Cu(II) and Zn(II) complexes, by fitting the experimental curves (**Figure II.16** and **Figure II.17**) with software HYPERQUAD[70]. In **Figure II.16** and **Figure II.17** the ligand (L) titration curves previously reported (**Figure II.13** and **Figure II.14**) are superimposed with those corresponding to the systems Cu/L 1:2 and Zn/L 1:2. It is observed, in both figures, a variation of the shape of the titration curves in the presence of the metal ion comparing with the one of the ligand, which indicates the formation of the metal complexes.

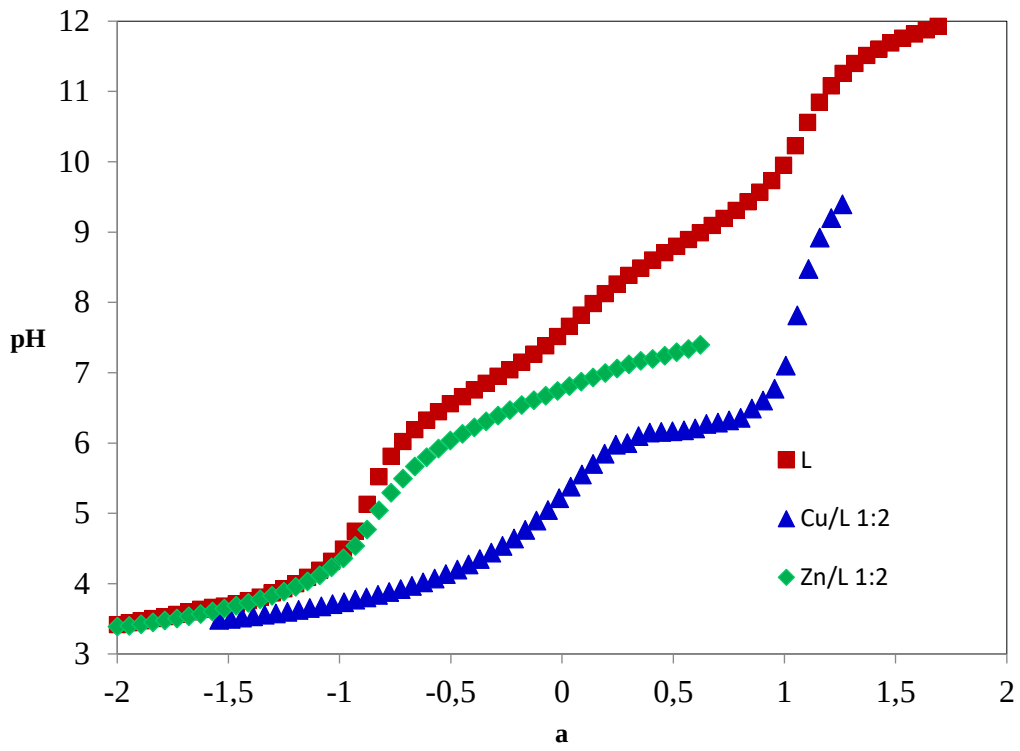

Figure II.16 – Potentiometric titration curves of PZ1 (50% w/w water/DMSO, I = 0.1 M KCl, T = 25.0 ± 0.1 ºC, C_L = 6.7×10^{-4} M).

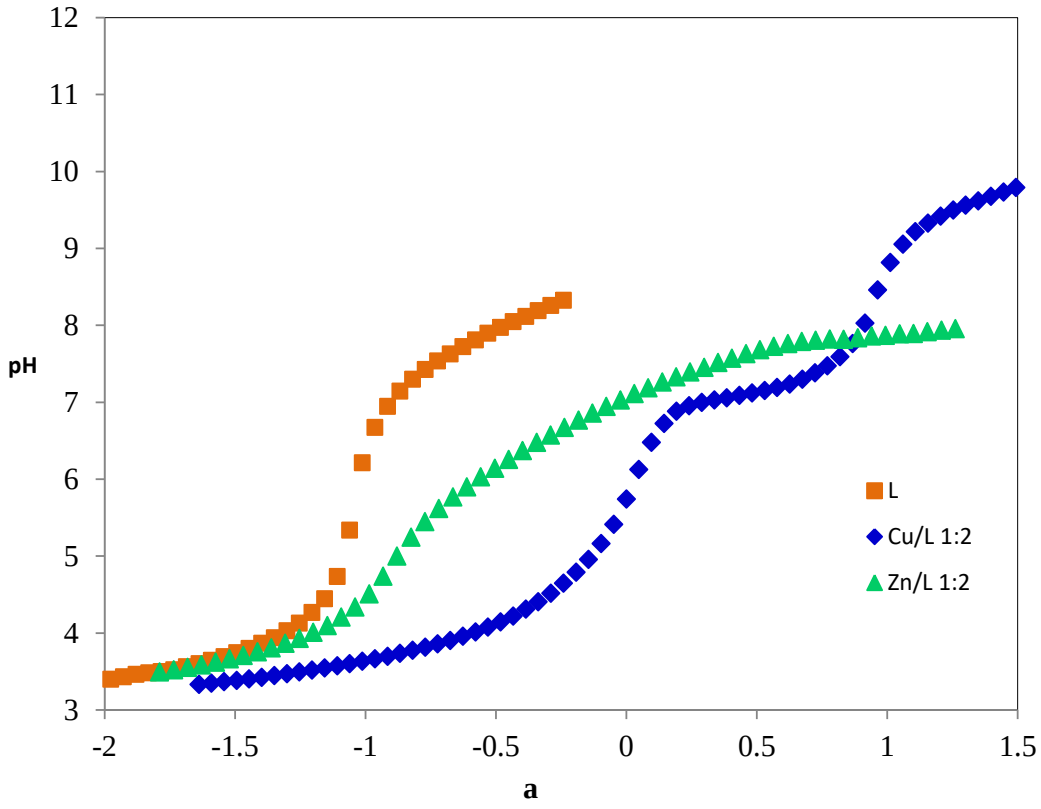

Figure II.17 – Potentiometric titration curves of PP1 (50% w/w water/DMSO, I = 0.1 M KCl, T = 25.0 ± 0.1 ºC, C_L = 6.7×10^{-4} M).

Table II.6 – Stepwise protonation constants of PP1 and PZ1, global formation constants[a] of its Cu(II) and Zn(II) complexes (T = 25.0 ± 0.1 ºC, I = 0.1 M KCl, 50% w/w water/DMSO) and pM[b] values.

Compound	$M_mH_hL_l$	log K_i	log $\beta_{Cu_mH_hL_l}$	log $\beta_{Zn_mH_hL_l}$
PP1	(011)	9.04(3)*		
	(021)	8.01(4)		
	(031)	3.25(6)		
	(111)		22.92(4)	14.08(4)
	(101)		18.75(5)	6.57(4)
	(102)		24.52(8)	11.76(4)
	pM		17.4	6.4
PZ1	(011)	9.04(3)		
	(021)	6.76(6)		
	(031)	3.37(7)		
	(111)		16.49(5)	12.98(6)
	(101)		12.88(3)	5.86(5)
	(102)		18.92(8)	10.97(8)
	pM		16.3	6.4

[a] $\beta_{M_mH_hL_l} = [M_mH_hL_l]/[M]^m[H]^h[L]^l$; [b] pM = $-\log[M_{free}]$ at pH 7.4 (C_L/C_M = 10, $C_M = 10^{-6}$ M).

The global formation constants obtained in the Cu/L and Zn/L systems are presented in **Table II.6**. It is observed the presence of three stability constants for each equilibrium model, corresponding to three different complex species: MHL, ML and ML_2 (**Figure II.18**).

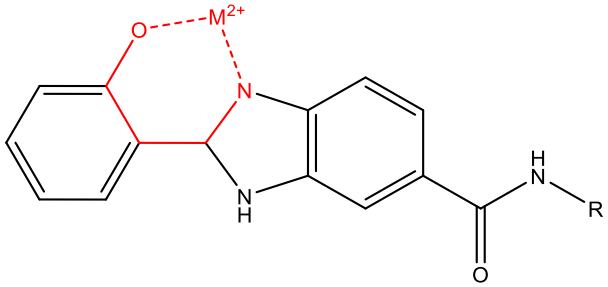

Figure II.18 – Representation of the coordination core of the metal complexes (6-member chelating ring in red); M^{2+} = Cu^{2+} or Zn^{2+} and R = PP or PZ.

Since the donor atoms *O*-Phe and *N*-Im in the benzimidazole motif are coordinated to the metal ion, the MHL complex is protonated in the *N*-Pp (**PP1**) or *N*-Pz (**PZ1**) atom, which is in accordance with the found values for the log β_{MHL} – log β_{ML} (ca 4 – 7.5). Besides the global stability constants, the pM value, a parameter that allows comparison of the relative chelating power of the chelators, was also obtained. The pM value takes different effects into account, such as the ligand basicity, denticity and the metal complex stoichiometry[8]. This value is the negative logarithm of the concentration of free metal, at pH 7.4 (physiological pH), determined for millimolar ligand concentration and ten times the concentration of metal ion. Both compounds seem to be good Cu(II) chelators (pCu = 16.3 – 17.4) and moderate Zn(II) chelators (pZn = 6.4), and this behaviour was already found for previously studies benzimidazole-tacrine hybrids, with the same benzimidazole chelating motif[65]. It can be noticed, however, that the pCu value determined for **PP1** most probably will further corrected after the ongoing spectrophotometric titration studies.

As a term of comparison clioquinol, an antifungal drug that showed a halt in the cognitive decline of AD patients due to its chelation power towards copper and zinc, appears to have quite a similar chelating capacity (pCu = 15.5 and pZn = 8.5)[8].

The species distribution curves were also obtained with the HYSS program[70] for each M/L system (**Figure II.19** and **Figure II.20**). Based on these species distribution curves, at physiological pH, the species predominant are CuL and ZnHL, while for **PZ1** the hydrolysis of copper is important (CuL_2 low concentration) and ZnL.

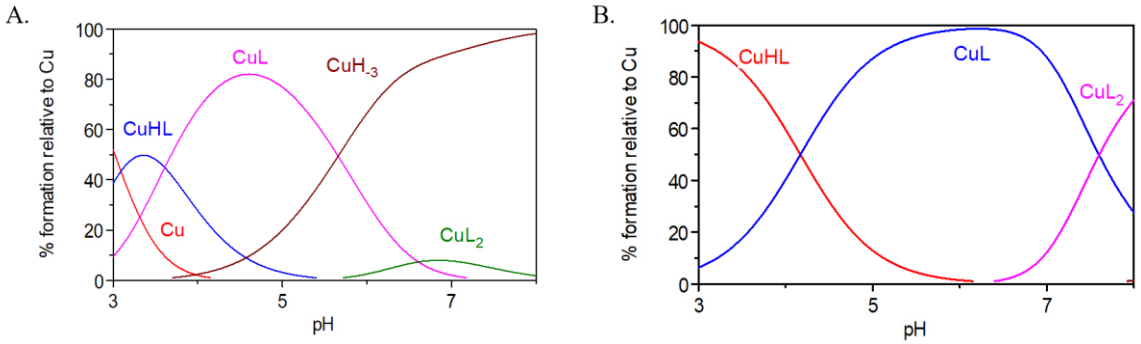

Figure II.19 – Species distribution curves for Cu^{2+}/PZ1 1:2 (A.) and Cu^{2+}/PP1 1:2 (B.) systems ($C_L = 6.7\times10^{-4}$ M).

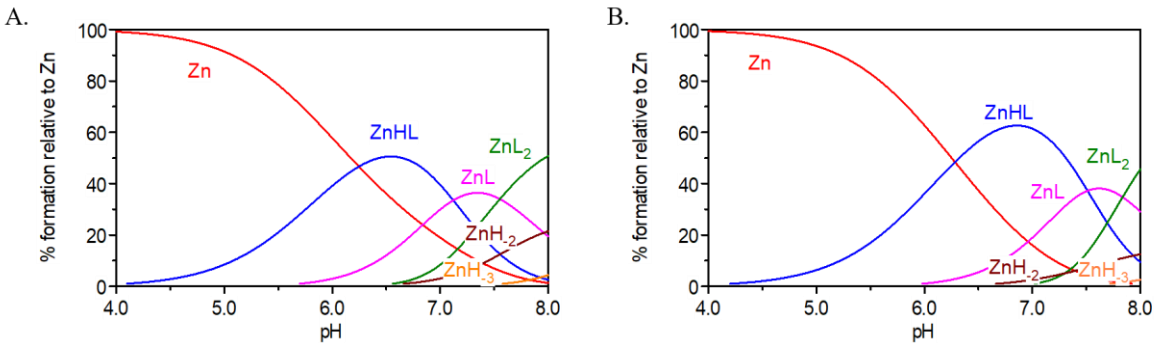

Figure II.20 – Species distribution curves for Zn^{2+}/PZ1 1:2 (A.) and Zn^{2+}/PP1 1:2 (B.) systems ($C_L = 6.7\times10^{-4}$ M).

That chelating power of the ligands seems to be a positive result regarding the aggregation of Aβ fibrils, with the possible binding and/or removal of Cu(II) from Aβ fibrils. In that way, these results support the values presented in the sub-chapter II.5.1 of this thesis, where **PZ1** presented an inhibition of 37.7% for copper(II)-induced aggregation and 25.3% for self-mediated aggregation.

In the future, these studies will also be performed for compounds **PZ4** and **PP4** to evaluate their chelation power towards Cu(II) and Zn(II), that eventually will substantiate the higher inhibition results obtained from copper(II)-induced Aβ aggregation showed by compound **PZ4** than for self-mediated aggregation.

II.7 Pharmacokinetic properties

To predict the potential of the newly designed compounds as therapeutic drugs, some pharmacokinetic properties were calculated by the software QikProp v.2.5[72]. The parameters calculated were the lipophilic character (clog *P*), the capacity to cross the blood-brain barrier (log BB), the velocity of intestinal absorption (caco-permeability), the activity on the CNS (CNS) and the number of violations of Lipinski's rule.

Table II.7 – Pharmacokinetic properties predicted *in silico* by software QikProp v.2.5[72].

Compound	molecular weight (g/mol)	clog P	log BB	caco-permeability (nm/s)	CNS	Violations of Lipinski's rule
PP1	440.554	4.386	-0.730	194	-	0
PP2	348.444	3.690	0.077	575	+	0
PP3	378.470	4.371	0.127	905	+	0
PZ1	455.558	2.587	-0.097	48	+/-	0
PZ2	363.458	3.153	0.547	243	++	0
PZ3	393.485	2.879	0.132	101	+	0

The Lipinski's rule determines if a compound has properties that allow it to be an orally active drug. The rule defines a poor absorption or permeation when: the molecular weight is bigger than 500 g/mol, the clog *P* is superior to 5, there are more than 5 hydrogen-bond donors and more than 10 hydrogen-bond acceptors[73]. From **Table II.7** it is observed that all compounds are free from violations, leading to a perfect score regarding their ability for oral administration.

The parameter clog *P* represents the lipophilic character of the compound. The software establishes the limit between -2.0 till 6.5 as acceptable, but as described, the Lipinski's rule doesn't accept values over 5. Regarding that, all values are under 5, not proposing a violation of the rule. Comparing values, the **PP** series presents higher values compared with the **PZ** series, this being an indication that the latter is more hydrophilic. Compounds **PP1** and **PP3** have clog *P* value ca 4.4, which indicates a lipophilic character that can lead to some difficulty in the bloodstream transport.

Another important value to be studied is the log BB, since it gives information about the distribution of the compound between the blood and the brain. The software defines the value -3.0 as excellent and 1.2 as bad. Only compounds with benzimidazole moiety present negative values, which turns them as the best to cross the blood-brain barrier. Compound **PZ2** presents the worst value (0.547) but it is still between the parameters defined by QikProp.

Caco-permeability was the next value to be studied, representing the capacity of absorption from the intestine into the bloodstream. Once more the software attributes a rationalization to these values, in which values lower than 25 nm/s represent a poor absorption and values superior than 500 nm/s, a great absorption. Only compounds **PP2** and **PP3** presented a great value, while all the other compounds are between the limits delimited. Compound **PZ1** presents the worst value, indicating a bad absorption in the intestine. A last value to be analysed is the compounds' activity in the CNS, being measured from – to ++. Compounds with benzimidazole derivative proved to be those with the lowest activity, while **PZ2** shows to be the one with the best activity.

Regarding these pharmacokinetic values, any compound excels in all the parameters, but any of them fails in any of the parameters neither. The lack of violations of Lipinski's rule represents a very good factor for these compounds, proposing them as potential candidates do be oral administrated drugs.

III. CONCLUSIONS AND FUTURE PERSPECTIVES

Due to the multifactorial characteristics of AD pathology, the development and study of polyfunctional compounds were the main objective of this thesis, with the ultimate aim of getting multi-targeting compounds as potential drug candidates for this disease. A set of donepezil-benzimidazole/benzofuran hybrids, donepezil mimetics, were developed and studied following a multidisciplinary approach. Thus, starting from the design of compounds by molecular modelling, they were subsequently synthesized and studied for their most important biochemical properties, including the inhibition of AChE and Aβ aggregation, metal chelation and finally analysed in terms of structure-activity relationship.

These new compounds included the benzylpiperidine (a fragment of the donepezil, a marketed AChE inhibitor drug) and the analogue benzylpiperazine motif, which were hybridized with benzimidazole and benzofuran derivatives aimed to mimic the indanone part of donepezil and potentially confer extra-properties. Regarding the AChE inhibition, the new hybrids present good capacity, in the low micromolar range (IC_{50} = 4-30 μM), but lower than that of donepezil (nanomolar range). According to the molecular modelling studies, the best inhibitory results were obtained for the hybrids which could establish a dual interaction with both binding sites, CAS and PAS, of the enzyme active site. These hybrid compounds were also evaluated for extra-properties, as compared with donepezil, namely the capacity to inhibit the Aβ aggregation. They showed moderate activity (15-36%) but, as expected, the best capacity was obtained by the hybrid with the hydroxyphenylbenzimidazole motif (PP1 with 36.3% of inhibition). The two aminophenolic derivatives, who presented the hydroxybenzimidazole molecular fragment, also demonstrated a good capacity for chelation of Cu(II) and moderate for Zn(II). The phenol group of these compounds enables also a moderate to weak radical scavenging activity (PZ1, EC_{50} = 594 μM).

Overall, among both series of donepezil mimetics, in general, the benzimidazole-containing hybrids presented better properties than their benzofuran counterparts, but all of them presented lower AChE inhibitory activity than that of the original drug. However, they present extra-properties absent in donepezil, thus providing a multi-targeting capacity. Therefore, believing that for a complex disease, a drug with a set of moderate properties may be better than one with a single good property, some of these compounds deserve to be further explored for the challenging discovery of new anti-AD therapies.

Regarding the future, a spectrophotometric titration of PP1 is ongoing, to check its protonation constants and ascertain the corresponding metal chelation models, to overcome solubility problems found by potentiometry; also assays on the inhibition of Aβ aggregation, in the presence of copper are planned. An enzymatic study of the interaction of these compounds with butyrylcholinesterase can also be a useful resource, to understand the selectivity of the compounds towards the cholinesterases. Moreover, it is expected to improve the synthesis of hydroxyl-benzofuran hybrids (PZ4 and PP4) and check the effect of this substituent group in biochemical properties, in particular the antioxidant activity and the metal-chelation properties. It will also be interesting to explore the effect of an extra methylene group in the linker of the PP series, since by modulation, that will provide the ideal linker length for a strong interaction with both CAS and PAS.

IV. MATERIALS AND METHODS

IV.1 Reagents and instrumentation

All reagents used in synthesis were purchased from Sigma-Aldrich, Alfa Aesar, Merck, Mallinckrodt, Panreac, Honeywell or Fluka, with analytical grade purity and they were used without any additional purification. The same for the solvents used in the synthesis (Sigma-Aldrich, Honeywell, or Carlo Erba). In the case of the solvents that needed to be dried, this was performed according to reported standard methods[74].

The reactions were monitored by thin-layer chromatography (TLC) with pre-coated silica gel aluminium sheets (ALUGRAM® Xtra SIL G/UV_{254}), while preparative TLCs were realized in pre-coated glass plates SIL G50 UV_{254} (MACHEREY-NAGEL). Column chromatography separations were performed on silica 60, 0,060-0,2 mm (MACHEREY-NAGEL).

A VL-6.LC UV lamp from Vilber Lourmat was used to observe the TLC sheets, at λ = 254 nm. The melting point was measured with a Leica Gallen III microscope and the values were not corrected. When needed, pH was ascertained with a pH-meter Thermo Orion, from Thermo Fischer Scientific.

The mass spectra were measured with a spectrometer Varian 500-MS equipped with a source of electrospray ionization in Instituto Superior Técnico. HPLC-HRMS analyses were performed in the National Research Council – Institute of Sciences of Food Production in Bari, Italy, by qualified technicians.

For every compound ^{1}H NMR spectrum were measured, that combined with the remaining techniques is sufficient to identify and characterize all the compounds. For the final compounds ^{13}C NMR as also measure, to complement the identification of these compounds. The spectra were obtained with a spectrophotometer Bruker Advance III 300 or Bruker Advance III 400, at rt.

IV.2 Compound synthesis

IV.2.1 Piperidine based (PP) series

IV.2.1.1 2-((1-Benzylpiperidin-4-yl)methyl)isoindoline-1,3-dione (protPP)

Phthalic acid anhydride (1 eq) and 4-(aminomethyl)piperidine (1 eq) were heated at 160 ºC for 4 h. The resulting dark brown solid (1 eq) was mixed with K_2CO_3 (6.6 eq), triethylamine (1.4 eq) and benzyl chloride (2.3 eq) and refluxed in acetonitrile for 3 h. Then, the mixture was cooled at rt, added to water, and extracted with ethyl acetate (three times). The organic layers were collected, dried over sodium sulphate anhydrous, and concentrated under reduced pressure. The crude was purified through chromatography column (eluent: DCM/MeOH/NH_4OH 92:8:0.1), affording a yellow solid (η = 34.0%). ^{1}H NMR (300 MHz, DMSO-d6), δ (ppm): 1.11-1.29, 1.52-1.91, and 3.44-3.50 (m, 9H, *piperidine*), 2.73 (d, 2H, *J* = 12.0 Hz, NC*H*$_2$CH), 3.41 (sg, 2H, NC*H*$_2$Ph), 7.15-7.40 (m, 5H, aromatics, *Ph*-CH_2), 7.79-7.91 (m, 4H, *phtalimide*); m/z (ESI-MS): 335.00 $(M+H)^+$.

IV.2.1.2 (1-Benzylpiperidin-4-yl)methanamine (PP)

2-((1-benzylpiperidin-4-yl)methyl)isoindole-1,3-dione (1 eq) and hydrazine monohydrate (6 eq) were dissolved in absolute ethanol and warmed at 60 ºC for 3 h. The reaction mixture was then filtered and concentrated under reduced pressure. The residue was dissolved in ethyl acetate, washed with brine (three times), dried over anhydrous sodium sulphate, and concentrated under reduced pressure obtaining a yellow-orange oil, purified through column chromatography (eluent: DCM/MeOH/NH_4OH 92:8:0.1) (η = 37.5%). ^{1}H NMR (300 MHz, DMSO-d6), δ (ppm): 1.00-1.25, 1.58-1.69, 1.79-1.91 and 2.36-2.41 (m, 9H, *piperidine*), 2,77 (d, 2H, *J* = 12.0 Hz, NC*H*$_2$CH) 3.42 (sg, 2H, NC*H*$_2$Ph), 7.19-7.36 (m, 5H, aromatics, *Ph*-CH_2); m/z (ESI-MS): 205.00 $(M+H)^+$.

IV.2.1.3 2-(2-Hydroxyphenyl)-1H-benzo[d]imidazole-5-carboxylic acid (1)

To a solution of salicyaldehyde (1 eq) in *N*,*N*-dimethylacetamide was added 3,4-diaminobenzoic acid (1 eq) and $Na_2S_2O_5$ (1.4 eq). The mixture was heated under reflux at 100 ºC for 12 h and then cooled at rt. The reaction mixture was diluted with ethyl acetate, dried over anhydrous sodium sulphate, and concentrated under reduced pressure. The product was dried in the vacuum line, affording a pale brown solid (η = 67.0%). ^{1}H NMR (400 MHz, DMSO-d6), δ (ppm): 7.41 (t, 1H, *J* = 8.0 Hz, BIM-H-9), 7.73 (d, 1H, *J* = 8.0 Hz, BIM-H-5), 7.91 (d, 1H, *J* = 8.0 Hz, BIM-H-4), 8.10 (d, 1H, *J* = 8.0 Hz, BIM-H-3), 8.25 (sg, 1H, BIM-H-2); m/z (ESI-MS): 253 $(M-1)^+$, 254.00 $(M)^+$, 255.00 $(M+1)^+$.

IV.2.1.4 *N*-((1-benzylpiperidin-4-yl)methyl)-2-(2-hydroxyphenyl)-1H-benzo[d]imidazole-5-carboxamide (PP1)

A mixture of 2-(2-hydroxyphenyl)-1H-benzo[d]imidazole-5-carboxylic acid (1 eq), (1-benzylpiperidin-4-yl)methanamine (1 eq), N-hydroxysuccinimide (1 eq) and DCC (1 eq) in anhydrous DMF was stirred for 40 h at rt, under a nitrogen atmosphere. Then, the mixture was filtered and the liquid phase was diluted with ethyl acetate and washed with brine (three times), dried over anhydrous sodium sulphate, concentrated under reduced pressure, and purified through column chromatography (eluent DCM/MeOH 95:5, then ethyl acetate 100%) affording a white solid (η = 71.0%). Melting point: 265-267 ºC; ^{1}H NMR (300 MHz, DMSO-d6), δ (ppm): 1.09-1.31 and 1.51-2.03 (m, 9H, *piperidine*), 2.81 (d, 2H, *J* = 12.0 Hz, 2 NHC*H*$_2$CH), 3.44 (sg, 2H, C*H*$_2$Ph), 6.97-7.07, 7.19-7.43, 7.62-7.82, and 8.06-8.20 (m, 12H, *aromatics*), 8.48 (t, 1H, *J* = 6.0 Hz, NHCO); ^{13}C NMR (300 MHz, DMSO-d6), δ (ppm): 30.3, 36.2, 45.7, 53.6, 62.8, 113.3, 117.8, 119.5, 122.8, 127.0, 127.3, 128.4, 129.3, 129.8, 132.5, 139.1, 154.3, 158.7, 167.2 ; m/z (ESI-MS): 441.36 $(M+H)^+$, 442.27 $(M+2H)^{2+}$, 443.29 $(M+3H)^{3+}$, 444.36 $(M+4H)^{4+}$; HPLC-HRMS: t_R = 4.84 min, calculated 441.2285, found 441.2266.

IV.2.1.5 Benzofuran-2-carboxylic acid (2)

To a solution of salicylaldehyde (1 eq) and anhydrous K_2CO_3 (2 eq) in DMF, ethyl chloroacetate (1.1 eq) was added. The mixture was heated under reflux at 110 ºC for 1.5 h. Then, the temperature of the reaction mixture was increased to 150 ºC for 4 h, and the reaction was monitored by TLC. After consumption of starting material, water was added to the mixture, that was left in reflux for more 1.5 h. Reaction mixture was then cooled to rt and poured into crushed ice. The basic aqueous solution was acidified with HCl to give a yellow coloured precipitate (η = 85.0%). Melting point: 193-195 ºC; ^{1}H NMR (300 MHz, DMSO-d6), δ (ppm): 7.35 (t, 1H, *J* = 7.4 Hz, O-C-C-CHC*H*), 7.50 (t, 1H, *J* = 7.3 Hz, O-C-CHC*H*), 7.67-7.71 (m, 2H, O-C-C*H*, COOH-C-C*H*), 7.80 (d, 1H, *J* = 7.7 Hz, O-C-C-C*H*); m/z (ESI-MS): 163.00 $(M+H)^+$, 164.00 $(M+2H)^{2+}$.

IV.2.1.6 *N*-((1-benzylpiperidin-4-yl)methyl)benzofuran-2-carboxamide (PP2)

Benzofuran-2-carboxylic acid (1 eq) was dissolved in dried DCM under inert conditions (N_2 atmosphere), and NMM (2.5 eq) was added. After the complete solubilization of the initial acid, T3P (1.5 eq) was added dropwise to the mixture (under inert conditions). After 30 min, (1-benzylpiperidin-4-yl)methanamine (1 eq) was added to the reaction mixture, which was stirred at rt overnight. The reaction solution was then diluted with water and ethyl acetate, and extracted. The aqueous layer was again extracted with ethyl acetate (three times), and the organic layers were combined, washed with 1N NaOH (three times) and brine (three times), dried over anhydrous sodium sulphate and concentrated under reduced pressure. The crude was purified through column chromatography (eluent: DCM/MeOH 92:8) affording a white solid (η = 30.5%). Melting point: 91-93 ºC; ^{1}H NMR (300 MHz, DMSO-d6), δ (ppm): 1.07-1.34, 1.53-1.73, 1.78-1.98 and 3.09-3.23 (m, 9H, *piperidine*), 2.77 (d, 2H, *J* = 12.0 Hz, C*H*$_2$CH), 3.43 (sg, 2H, NC*H*$_2$Ph), 7.15-7.81 (m, 10H, *aromatics*), 8.73 (t, 1H, *J* = 6.0 Hz, N*H*CO); ^{13}C NMR (300 MHz, $CDCl_3$), δ (ppm): 30.1, 36.0, 44.9, 53.0, 63.1, 110.5, 111.9, 122.8, 123.7, 126.7, 127.3,

127.7, 128.5, 128.7, 129.4, 148.7, 154.8, 159.0; m/z (ESI-MS): 349.34 $(M+H)^+$, 350.22 $(M+2H)^{2+}$, 351.29 $(M+3H)^{3+}$; HPLC-HRMS: t_R = 4.94 min, calculated 349.1911, found 349.1897.

IV.2.1.7 7-Methoxybenzofuran-2-carboxylic acid (3)

To a solution of ortho-vanillin (1 eq) and anhydrous K_2CO_3 (2 eq) in DMF, ethyl chloroacetate (1.1 eq) was added. The mixture was heated under reflux at 110 ºC for 1.5 h. Then, the temperature of the reaction mixture was increased to 150 ºC for 4 h, and the reaction was monitored by TLC. After consumption of starting material, water was added to the mixture, that was left in reflux for more 1.5 h. Reaction mixture was then cooled at rt and poured into crushed ice. The basic aqueous solution was acidified with HCl to give a yellow coloured precipitate (η = 78.0%). Melting point: 221-223 ºC; ^{1}H NMR (300 MHz, DMSO-d6), δ (ppm): 3.94 (s, 3H, OC*H*$_3$), 7.07 (d, 1H, *J* = 7.5 Hz, OCH_3-C-C*H*), 7.22-7.33 (m, 2H, O-C-C-C*H*, O-C-C-CH-C*H*), 7.63 (S, 1H, COOH-C-C*H*); m/z (ESI-MS): 193.00 $(M+H)^+$, 194.00 $(M+2H)^{2+}$.

IV.2.1.8 *N*-((1-benzylpiperidin-4-yl)methyl)-7-methoxybenzofuran-2-carboxamide (PP3)

7-methoxybenzofuran-2-carboxylic acid (1 eq) was dissolved in dried DCM under inert conditions (N_2 atmosphere), and NMM (2.5 eq) was added. After the complete solubilization of the initial acid, T3P (1.5 eq) was added dropwise to the mixture (under inert conditions). After 30 min, (1-benzylpiperidin-4-yl)methanamine (1 eq) was added to the reaction mixture which was stirred at rt overnight. The reaction solution was then diluted with water and ethyl acetate, and extracted. The aqueous layer was again extracted with ethyl acetate (three times), and the organic layers were combined, washed with 1N NaOH (three times) and brine (three times), dried over anhydrous sodium sulphate and concentrated under reduced pressure. The crude was purified through column chromatography (eluent: DCM/MeOH 92:8) affording a yellow oil (η = 26.0%). ^{1}H NMR (300 MHz, DMSO-d6), δ (ppm): 1.17-1.29, 1.48-1.73, 1.81-1.98 and 3.09-3.22 (m, 9H, *piperidine*), 2.79 (d, 2H, *J* = 12.0 Hz, C*H*$_2$CH), 3.43 (sg, 2H, NC*H*$_2$Ph), 3.96 (sg, 3H, C*H*$_3$O), 7.00-7.13, 7.19-7.38 and 7.47-7.54 (m, 9H, *aromatics*), 8.68 (t, 1H, *J* = 6.0 Hz, N*H*CO); ^{13}C NMR (300 MHz, $CDCl_3$), δ (ppm): 30.2, 31.0, 36.0, 46.7, 53.2, 56.3, 62.9, 109.0, 111.2, 114.8, 125.1, 126.9, 127.1, 128.5, 129.0, 139.3, 144.2, 145.9, 149.9, 158.7; HPLC-HRMS: t_R = 5.04 min, calculated 379.2016, found 379.2032.

IV.2.2 Piperazine based (PZ) series

IV.2.2.1 2-(2-(4-Benzylpiperazin-1-yl)ethyl)isoindoline-1,3-dione (protPZ)

Phthalic acid anhydride (1 eq) and 1-(2-aminoethyl)piperazine (1 eq) were heated at 160 ºC for 4 h. The resulting dark brown solid (1 eq) was mixed with K_2CO_3 (6.6 eq), triethylamine (1.4 eq) and benzyl chloride (2.3 eq) and refluxed in acetonitrile for 3 h, at 50 ºC. Then, the mixture was cooled at rt, added water, and extracted with ethyl acetate (three times). The organic layers were collected, dried over sodium sulphate anhydrous, and concentrated under reduced pressure. The crude was purified through chromatography column (eluent: DCM/MeOH/NH_4OH 92:8:0.1), affording a yellow solid (η = 64.4%). ^{1}H NMR (300 MHz, $CDCl_3$), δ (ppm): 2.30-2.66 (m, 8H, *piperazine*), 2.67 (t, 2H, *J* = 6.0 Hz, phtalimide-CH_2C*H*$_2$N), 3.48 (sg, 2H, NC*H*$_2$Ph) 3.83 (t, 2H, *J* = 6.0 Hz, phtalimide-C*H*$_2$$CH_2$N), 7.24-7.44 (m, 5H, aromatics, *Ph*-CH_2), 7.71-7.77 and 7.84-7.87 (m, 4H, *phtalimide*); m/z (ESI-MS): 350.00 $(M+H)^+$.

IV.2.2.2 2-(4-Benzyl-1-piperazinyl)ethanamine (PZ)

2-(2-(4-benzylpiperazin-1-yl)ethyl)isoindoline-1,3-dione (1 eq) and hydrazine monohydrate (6 eq) were dissolved in absolute ethanol and warmed at 60 ºC for 3 h. The reaction mixture was then filtered and the liquid filtrate was concentrated under reduced pressure. The residue was dissolved in ethyl acetate, washed with brine (three times), dried over anhydrous sodium sulphate, and concentrated under

reduced pressure obtaining a yellow-orange oil, purified through column chromatography (eluent: DCM/MeOH/NH_4OH 92:8:0.1) (η = 99.1%). ^{1}H NMR (400 MHz, $CDCl_3$), δ (ppm): 2.44-2.59 (m, 8H, *piperazine*), 2.43 (t, 2H, *J* = 8.0 Hz, NH_2-$CH_2C\mathit{H_2}N$), 2.79 (t, 2H, *J* = 8.0 Hz, NH_2-$C\mathit{H_2}CH_2N$), 3.53 (sg, 2H, $NC\mathit{H_2}Ph$), 7.30-7.35 (m, 5H, aromatics, *Ph*-CH_2); m/z (ESI-MS): 220.00 $(M+H)^+$.

IV.2.2.3 *N*-(2-(4-benzylpiperazin-1-yl)ethyl)-2-(2-hydroxyphenyl)-1H-benzo[d] imidazole -5-carboxamide (PZ1)

A mixture of 2-(2-hydroxyphenyl)-1H-benzo[d]imidazole-5-carboxylic acid (1 eq), 2-(4-benzyl-1-piperazinyl)ethanamine (1 eq), N-hydroxysuccinimide (1 eq) and DCC (1 eq) in anhydrous DMF was stirred for 40 h at rt, under a nitrogen atmosphere. Then, the mixture was filtered and the liquid phase was diluted with ethyl acetate and washed with brine (three times), dried over anhydrous sodium sulphate, concentrated under reduced pressure, and purified through column chromatography (eluent: DCM/MeOH 95:5) affording a white solid (η = 21.4%). Melting point: 249-252 ºC; ^{1}H NMR (400 MHz, DMSO-d6), δ (ppm): 2.25-2.52 (m, 10H, 8 *piperazine* and 2 NH_2-$CH_2C\mathit{H_2}N$), 3.20-3.61 (m, 4H, 2 $NC\mathit{H_2}Ph$ and 2 NH_2-$C\mathit{H_2}CH_2N$), 7.00-7.41, 7.67-7.83, and 8.07-8.20 (m, 12H, *aromatics*), 8.45 (t, 1H, *J* = 4.0 Hz, N*H*CO); ^{13}C NMR (400 MHz, DMSO-d6), δ (ppm): 37.5, 53.1, 53.3, 57.5, 62.6, 113.0, 117.7, 119.7, 122.8, 127.0, 127.3, 128.6, 129.3, 129.8, 132.6, 138.7, 153.8, 158.5, 166.8; m/z (ESI-MS): 456.31 $(M+H)^+$, 457.24 $(M+2H)^{2+}$, 458.26 $(M+3H)^{3+}$; HPLC-HRMS: t_R = 5.00 min, calculated 456.2394, found 456.2375.

IV.2.2.4 *N*-(2-(4-benzylpiperazin-1-yl)ethyl)benzofuran-2-carboxamide (PZ2)

Benzofuran-2-carboxylic acid (1 eq) was dissolved in dried DCM under inert conditions (N_2 atmosphere), and NMM (2.5 eq) was added. After the complete solubilization of the initial acid, T3P (1.5 eq) was added dropwise to the mixture (under inert conditions). After 30 min, 2-(4-benzyl-1-piperazinyl)ethanamine (1 eq) was added to the reaction mixture, which was stirred at rt overnight. The reaction solution was then diluted with water and ethyl acetate, and extracted. The aqueous layer was again extracted with ethyl acetate (three times), and the organic layers were combined, washed with 1N NaOH (three times) and brine (three times), dried over anhydrous sodium sulphate and concentrated under reduced pressure. The crude was purified through column chromatography (eluent: DCM/MeOH 92:8) affording a white solid (η = 40.0%). Melting point: 89-91 ºC; ^{1}H NMR (400 MHz, $CDCl_3$), δ (ppm): 2.48-2.64 (m, 8H, *piperazine*), 2.66 (t, 2H, *J* = 8.0 Hz, NH_2-$CH_2C\mathit{H_2}N$), 3.57 (sg, 2H, $NC\mathit{H_2}Ph$), 3.58-3.64 (m, 2H, NH_2-$C\mathit{H_2}CH_2N$), 7.17-7.57 and 7.67-7.72 (m, 10H, *aromatics*); ^{13}C NMR (400 MHz, $CDCl_3$), δ (ppm): 36.0, 52.9, 53.5, 56.4, 63.0, 110.0, 111.8, 122.7, 126.7, 127.1, 127.7, 128.3, 128.7, 129.2, 138.0, 149.0, 154.8, 158.9; m/z (ESI-MS): 364.30 $(M+H)^+$, 365.25 $(M+2H)^{2+}$, 366.29 $(M+3H)^{3+}$, 367.31 $(M+4H)^{4+}$, 386.28 $(M+Na)^+$; HPLC-HRMS: t_R = 4.97 min, calculated 364.2020, found 364.2003.

IV.2.2.5 *N*-(2-(4-benzylpiperazin-1-yl)ethyl)-7-methoxybenzofuran-2-carboxamide (PZ3)

7-methoxybenzofuran-2-carboxylic acid (1 eq) was dissolved in dried DCM under inert conditions (N_2 atmosphere), and NMM (2.5 eq) was added. After the complete solubilization of the initial acid, T3P (1.5 eq) was added dropwise to the mixture (under inert conditions). After 30 min, 2-(4-benzyl-1-piperazinyl)ethanamine (1 eq) was added to the reaction mixture, which was stirred at rt overnight. The reaction solution was then diluted with water and ethyl acetate, and extracted. The aqueous layer was again extracted with ethyl acetate (three times), and the organic layers were combined, washed with 1N NaOH (three times) and brine (three times), dried over anhydrous sodium sulphate and concentrated under reduced pressure. The crude was purified through column chromatography (eluent: DCM/MeOH 92:8) affording a yellow oil (η = 52.0%). ^{1}H NMR (300 MHz, $CDCl_3$), δ (ppm): 2.57-3.21 (bs, 10H, 8 *piperazine* + $CH_2C\mathit{H_2}N$), 3.72 (bs, 2H, $C\mathit{H_2}NHCO$), 3.80 (sg, 2H, $NC\mathit{H_2}Ph$), 4.05 (sg, 3H, CH_3O), 6.88-6.98 and 7.17-7.73 (m, 9H, *aromatics*); ^{13}C NMR (300 MHz, $CDCl_3$), δ (ppm): 35.7, 51.3, 51.6, 56.3,

56.6, 63.4, 108.4, 111.0, 114.8, 124.6, 126.9, 127.2, 127.7, 128.5, 129.2, 144.4, 145.6, 148.6, 159.1; m/z (ESI-MS): 394.29 $(M+H)^+$, 395.23 $(M+2H)^{2+}$, 396.26 $(M+3H)^{3+}$, 397.31 $(M+4H)^{4+}$; HPLC-HRMS: t_R = 4.97 min, calculated 394.2125, found 394.2121.

IV.2.2.6 7-Hydroxybenzofuran-2-carboxylic acid (4)

BCl_3 (5 eq) in anhydrous DCM was added dropwise at -78 ºC to a solution of 7-methoxybenzofuran-2-carboxylic acid (1 eq) and TBAI (3 eq) in anhydrous DCM under nitrogen atmosphere. Then, the solution was poured on ice and DCM was concentrated under reduced pressure. The aqueous phase was extracted with ethyl acetate (three times), washed with brine (three times), dried over anhydrous sodium sulphate and concentrated under reduced pressure, affording a dark brown solid (η = 67.4%). ^{1}H NMR (300 MHz, DMSO-d6), δ (ppm): 6.92 (dd, 1H, *J* = 3.0 Hz, *aromatic*), 7.09-7.20 (m, 2H, *aromatics*), 7.60 (sg, 1H, *aromatic*), 10.32 (sg, 1H, O*H*); m/z (ESI-MS): 179.00 $(M+H)^+$.

IV.2.2.7 *N*-(2-(4-benzylpiperazin-1-yl)ethyl)-7-hydroxybenzofuran-2-carboxamide (PZ4)

A mixture of 2-(2-hydroxyphenyl)-1H-benzo[d]imidazole-5-carboxylic acid (1 eq), 7-hydroxybenzofuran-2-carboxylic acid (1 eq), N-hydroxysuccinimide (1 eq) and DCC (1 eq) in anhydrous DMF was stirred for 40 h at rt, under a nitrogen atmosphere. Then, the mixture was filtered and the liquid phase was diluted with ethyl acetate and washed with brine (three times), dried over anhydrous sodium sulphate, concentrated under reduced pressure, and purified through column chromatography (eluent: DCM/MeOH 95:5, then acetonitrile/water 19:1) affording a white solid (η = 14.2%). Melting point: 84-85 ºC; ^{1}H NMR (300 MHz, DMSO-d6), δ (ppm): 2.26-2.61 (m, 10H, 8 *piperidine* and CH_2CH), 3.45 (sg, 2H, NCH_2Ph), 6.73-7.10 and 7.18-7.43 (m, 9H), 8.38 (bs, 1H, CON*H*); ^{13}C NMR (300 MHz, DMSO-d6), δ (ppm): 36.3, 52.6, 52.8, 56.9, 62.1, 109.7, 112.2, 112.4, 124.4, 126.9, 128.2, 128.9, 129.0, 138.3, 143.8, 148.8, 158.2; m/z (ESI-MS): 394.00 $(M+H)^+$; HPLC-HRMS: t_R = 4.76 min, calculated 380.1969, found 380.1950.

IV.3 Antioxidant activity

The DPPH method was used to determine antioxidant activity[63] consisting in the addition of different volumes of stock solution of compound to a solution of 2.5 mL of DPPH. The final volume of the assay was 3.5 mL, corrected with MeOH, which provided different concentrations of our compound in each assay. The control solution includes only MeOH and DPPH (**Table IV.1**).

Table IV.1 – Sample preparation for antioxidant assay.

Solution	1	2	3	4	5	6
DPPH (mL)	2.5	2.5	2.5	2.5	2.5	2.5
MeOH (µL)	1000	800	600	400	200	-
Inhibitor (µL)	-	200	400	600	800	1000

The samples were left to incubate for 30 min, at rt, protected from the light, where the absorbance was measured at 517 nm, against a blank solution (MeOH). The percentage of antioxidant activity is calculated through the equation:

$$\%AA = \frac{A_{DPPH} - A_{sol}}{A_{DPPH}} \times 100$$

Equation IV.1

The assays were realized in duplicate, in which the EC_{50} was obtained through the graphical representation of the %AA vs. the inhibitor concentration,

$$EC_{50} = \left(\frac{50 - b}{m}\right),$$

Equation IV.2

where, b is the interception in the y axis and m is the slope. The parameters for statistical analysis were calculated with Microsoft Office Excel®.

IV.4 Enzymatic inhibition

Enzymatic activity was measured using an adaptation of Ellman's method[59]. The readings were performed in a spectrophotometer Perkin-Elmer Lambda 35 UV-Vis.

HEPES buffer was used for the enzymatic assays, with a molar concentration of 50 mM in pH 8.0. DTNB solution was obtained dissolving the reagent in HEPES buffer with salts, namely NaCl (50 mM) and $MgCl_2$ (20 mM), obtaining a solution with 3 mM. The enzyme AChE of *Electrophorus electricus* (electric eel) stock (500 U) was dissolved in TRIS 50 mM, pH 8.0, being posteriorly diluted to assay concentrations (5 U), obtaining an aliquot of 1 mL. The enzyme substrate used was AChI 16 mM, which was prepared with deionized water. The compounds tested were diluted in MeOH (1 mg/mL), with further dilution, and five different concentrations were used for each compound, obtaining different percentages of AChE inhibition.

The assay consists in the addition of 374 µL of HEPES, 10-50 µL of inhibitor, 25 µL of AChE and MeOH to make up for 0.449 mL of mixture in a 1 mL cuvette. The mixture was left to incubate for 15 min, and afterwards was added 75 µL of AChI and 476 µL of DTNB (**Table IV.2**).

Table IV.2 – Sample preparation for enzymatic assay.

Solution	**Control (100% activity)**		**50 µL inhibitor**		**40 µL inhibitor**		**30 µL inhibitor**		**20 µL inhibitor**		**10 µL inhibitor**	
	Assay	**Blank**	**Assay**	**Blank**	**Assay**	**Blank**	**Assay**	**Blank**	**Assay**	**Blank**	**Assay**	**Blank**
HEPES (µL)	374	399	374	399	374	399	374	399	374	399	374	399
MeOH (µL)	50		-		10		20		30		40	
Inhibitor (µL)	-		50		40		30		20		10	
AChE (µL)	25	-	25	-	25	-	25	-	25	-	25	-
	After 15 minutes											
AChI (µL)	75											
DTNB (µL)	476											

The enzymatic reaction was followed through the measurements of absorbencies at 405 nm during 5 min. The assays were measured against a blank solution containing all the components except the enzyme that was substituted for an equal volume of HEPES, which allows considering the non-enzymatic reaction. A control reaction was used using MeOH instead the new compounds, and was considered the reaction corresponding to 100% enzymatic activity. Each assay was performed in quintuplet.

The percentage of inhibition of enzyme activity, for each concentration of inhibitor, was calculated through the following formula:

$$\%I = 100 - \frac{v_i}{v_{control}} \times 100$$

Equation IV.3

The inhibition curves were obtained through graphical representation of the percentage of enzymatic inhibition vs. inhibitor. The IC_{50} was obtained from each graphical representation from the equation:

$$IC_{50} = \frac{50 - b}{m},$$

Equation IV.4

where, b is the interception in the y axis and m is the slope. The statistical analysis was performed in Microsoft Office Excel®.

IV.5 Inhibition of Aβ$_{1-42}$ aggregation

Aβ$_{1-42}$ aggregation was measured based on the fluorescence properties of ThT. The readings were performed in a Varian Cary Eclipse spectrofluorimeter.

IV.5.1 Preparation of Aβ$_{1-42}$ films

Lyophilised Aβ$_{1-42}$ (1 mg) was dissolved in 1,1,1,3,3,3-hexafluoro-2-propanol (HFIP) (1.5 mL) by brief sonication, to a concentration of 149 μM, and kept overnight at 25 ºC. In the next day, the resulting clean solution was partitioned in ice, into 6 Eppendorf tubes (250 μL each). HFIP was left to evaporate overnight at 25 ºC. The resulting films can then be stored at -20 ºC for months.

IV.5.2 Preparation of samples for aggregation study

One film of Aβ$_{1-42}$ was dissolved in a fresh mixture of 69.5 μL CH_3CN/Na_2CO_3 (300 μM)/NaOH (250 mM) (48.3/48.3/3.4 μL v/v/v) by brief sonication. To the resulting alkaline Aβ$_{1-42}$ solution (531.24 μM) was added 392.5 μL of phosphate buffer 215 mM, pH 8.0, affording a concentration of Aβ$_{1-42}$ of 80 μM. The compounds tested were diluted in MeOH (1 mg/mL), being further diluted in phosphate buffer to a concentration of 480 μM. For copper-induced aggregation studies was used a solution of $CuCl_2$ 240 μM.

Four different types of experiments were prepared in a final volume of 60 μL (**Table IV.3**).

Table IV.3 – Sample preparation for Aβ aggregation studies.

Solution	**Control - Ligand**		**Ligand**		**Control - Ligand + Metal**		**Ligand + Metal**	
	Assay	**Blank**	**Assay**	**Blank**	**Assay**	**Blank**	**Assay**	**Blank**
Phosphate buffer (μL)	30	60	20	50	20	50	10	40
Aβ$_{1-42}$ (μL)	30	-	30	-	30	-	30	-
Ligand (μL)	-		10		-		10	
$CuCl_2$ (μL)	-				10			

Control ligand assay consists in 30 µL of phosphate buffer and 30 µL of $A\beta_{1-42}$, to observe the aggregation without any inhibition, while the ligand assay is composed of 20 µL of phosphate buffer, 30 µL of $A\beta_{1-42}$ and 10 µL of ligand, to observe the effect of the ligand in the aggregation. The same can be applied to the metal studies, with the difference that 10 µL of $CuCl_2$ were present to induce the fibril aggregation. Each experiment is composed of an assay and a blank sample, where the blank sample doesn't present $A\beta_{1-42}$, to monitor the effect of the compounds in the fluorescence. These samples were left to incubate in a water bath CERTOMAT WR, for 24 h, at 37 ºC with gentle shaking.

After 24 h, the samples were removed from the bath. The fluorimeter was calibrated with a solution of rhodamine B. After calibration, add 180 µL of Glycine-NaOH buffer (50 mM, pH 8.5) containing ThT (5 µM) were added to each sample. Samples were placed in a microplate and the fluorescence signal was monitored at 446 nm (λ_{exc}) and 490 nm (λ_{em}), with a slit of 10 nm.

The percentage of inhibition for each compound was obtained from the graphical representation of the fluorescence intensity vs. the wavelength, where the maximum of absorbance was defined for each assay. From that, the percentage of inhibition was obtained, following the formula:

$$\%I = 100 - \left(\frac{F_i}{F_0}\right) * 100,$$

Equation IV.4

where, F_i and F_0 are the fluorescence intensities in the presence and absence of the test compound, respectively, minus the fluorescence intensities of the respective blanks. Statistical analysis was performed in Microsoft Office Excel®.

IV.6 TEM samples preparation

One film of $A\beta_{1-42}$ (prepared as in IV.5.1 Preparation of Aβ1-42 films) was dissolved in a fresh mixture of 106.6 µL of CH_3CN/NaCl (300 µM)/NH_4OH (2 %) (48.3/48.3/10.0 µL v/v/v) by brief sonication. To the resulting alkaline $A\beta_{1-42}$ solution (346.35 µM) was added 631.80 µL of HEPES buffer 50 mM, pH 6.6, affording a concentration of $A\beta_{1-42}$ of 50 µM. The compounds tested were diluted in MeOH (1 mg/mL), being further diluted in HEPES buffer to a concentration of 240 µM. For copper-induced aggregation studies was used a solution of $CuCl_2$ 120 µM.

Four different types of experiments were prepared in a final volume of 60 µL (**Table IV.4**).

Table IV.4 – Sample preparation for TEM assays.

Solution	Control - Ligand	Ligand	Control - Ligand + Metal	Ligand + Metal
HEPES buffer (µL)	30	17,5	17,5	5
$A\beta_{1-42}$ (µL)	30			
Ligand (µL)	-	12,5	-	12,5
$CuCl_2$ (µL)	-		12,5	

According to **Table IV.4**, compounds (50 μM final concentration) were added to the sample of Aβ (25 μM final concentration) in the absence or in the presence of copper chloride (25 μM final concentration) followed by incubation in a water bath CERTOMAT WR for 24 h at 37 ºC with gentle shaking.

Formvar/Carbon 200-mesh Cu grids (Ted Pella) were treated with Aβ peptide aggregated samples (10 μL) for 2 min at rt. Excess samples were removed using filter paper followed by washing twice with deionized water. Each grid incubated with uranyl acetate (1%, 10 μL, 1 min) was stained and dried for 15 min at rt. Images from each sample were taken by a Hitachi H8100 TEM with a LaB6 filament (200kV, 10000-20000x magnification). The samples were analysed in MICROLAB, Electron Microscopy Laboratory in Instituto Superior Técnico, and the microscope was operated by a specialized technician.

IV.7 Potentiometric studies

Potentiometric titrations were performed by an automated potentiometry system, with a Crison MicropH 2002 pH meter, together with a Metrohm 6.1033.500 glass electrode and an Orion 900100 Ag-AgCl reference electrode. pH-potentiometric titrations were accomplished in 50% w/w DMSO/water medium, at temperature 25.0 ± 0.1 ºC and ionic strength 0.1 M KCl. The temperature was controlled with a thermostatic bath HAAKE G Fisons while ionic strength was achieved with KCl 1 M. Atmospheric CO_2 was excluded from the cell during titration by passing purified N_2 across the top of the experimental solution in the reaction cell.

Both glass and Ag/AgCl reference electrodes were previously conditioned in different DMSO/water mediums of increasing percentage of DMSO composition, and the response of the glass electrode was evaluated by strong acid – strong base (HCl/KOH) calibrations, with the determination of the Nernst parameters by Gran's method[75].

HCl 0.1 M solution was prepared from a Titrisol ampoule. KOH 0.1 M solution was also prepared from a Titrisol ampoule carbonate free, and was added in the titrations with a Crison microBU 2031 burette. The KOH solution was standardized by titration with a solution of potassium hydrogen phthalate 2 mM, being the percentage of carbonate determined by Gran's method[75].

The measurements were performed in a final volume of 30 mL, with a ligand concentration of 667 μM. The titrations were accomplished in the presence of metal ions (zinc(II) and copper(II)) in different C_M/C_L ratios: 0:1, 1:1 and 1:2. The aqueous zinc stock solution (0.0156 M) and aqueous copper stock solution (0.0150 M) were prepared from 1000 ppm standards (Titrisol) and its metal content was evaluated by atomic absorption.

The stepwise protonation constants of the ligands,

$$K_i = \frac{[H_iL]}{[H_{i-1}L][H]},$$

Equation IV.5

and the overall metal-complex stability constants,

$$\beta_{M_mH_hL_l} = \frac{[M_mH_hL_l]}{[M]^m[H]^h[L]^l},$$

Equation IV.6

were calculated by fitting the pH-potentiometric data with Hyperquad program[70]. The metal hydrolysis constants (log $\beta_{Cu_2H_{-3}}$ = -11.92; log $\beta_{ZnH_{-2}}$ = -14.79, log $\beta_{ZnH_{-3}}$ = -23.48) were determined under the defined experimental conditions (I = 0.1 M, 50% w/w DMSO/water, T = 25.0 ± 0.1 ºC) and were included in the fitting of the experimental data towards the equilibrium models concerned with the M/L systems.

The species distribution curves were obtained with Hyss program[70].

IV.8 Molecular modulation

The x-ray structure of AChE was downloaded from the database RCSB PDB[76]. The structure chosen for enzyme model has the code 1EVE, corresponding to the complex of the enzyme, from the species *Torpedo californica*, with E2020 (Aricept®), the marketed trade name of donepezil. After the obtainment of the structure, it was treated with the program Maestro v.9.3[77] to remove molecules of solvent, molecules from co-crystallization and the original ligand and then adding hydrogen atoms[61].

The construction of the new ligand was realized with the software Maestro v.9.3[77] and then, using the software Ghemical v.3.0[78], the new compounds were submitted to a geometry optimization and a random conformational search of 1000 cycles and 2500 steps of optimization using a force field Tripos 5.2[79].

For each ligand, it was determined the conformation with the lowest energy, to be used in the docking studies. These studies were performed with the software GOLD v.5.1[56], that after the selection of the protein structure and its ligands, defined a zone of interest with the residues that will be found within a radius of 10 Å from the original ligand position in the x-ray structure (defining the binding site). The parameters of the GOLD software were indicated automatically[80], except the option for "allow early termination" that was deactivated. The minimized ligands were submitted to a 100 genetic algorithm cycle, which mean that 100 conformations of the ligand were generated and evaluated in iterative calculations using a genetic algorithm. The method needs a fitness function to evaluate the result of each conformation generated by the calculi and the function chosen was the ASP function, since it was proved before to obtain the best prediction for AChEI[64]. The docking results used for this work were the ones with the best score, based on the function used.

The docking results were then compared in Chimera v.1.11[81], through a superimposition with the original ligand, which allowed checking for potential interactions between the studied compounds and AChE.

IV.9 Pharmacokinetic properties

Pharmacokinetic properties were calculated using the software QikProp v.2.5[72], for parameters clog *P*, log BB, caco-2 permeability, the activity in the CNS and the verification of the Lipinski's rule. To calculate these parameters, the docking structures obtained in the molecular modulation were submitted to the software QikProp v.2.5, which calculated the value for each parameter.

REFERENCES

1.Alzheimer's Association. 2017 Alzheimer's disease facts and figures. *Alzheimer's Dement.* **13,** 325–373 (2017).

2.Lau, L.-F. & Brodney, M. A. Therapeutic approaches for the treatment of Alzheimer's disease: an overview. *Top. Med. Chem.* **2,** 1–24 (2008).

3.Berchtold, N. C. & Cotman, C. W. Evolution in the conceptualization of dementia and Alzheimer's disease: Greco-Roman period to the 1960s. *Neurobiol. Aging* **19,** 173–189 (1998).

4.Cipriani, G., Dolciotti, C., Picchi, L. & Bonuccelli, U. Alzheimer and his disease: a brief history. *Neurol. Sci.* **32,** 275–279 (2011).

5.Esiri, M. M. The basis for behavioural disturbances in dementia. *J. Neurol. Neurosurg. Psychiatry* **61,** 127–130 (1996).

6.Quintanova, C., Keri, R. S., Marques, S. M., G-Fernandes, M., Cardoso, S. M., Serralheiro, M. L. & Santos, M. A. Design, synthesis and bioevaluation of tacrine hybrids with cinnamate and cinnamylideneacetate derivatives as potential anti-Alzheimer drugs. *Medchemcomm* **6,** 1969–1977 (2015).

7.Jakob-Roetne, R. & Jacobsen, H. Alzheimer's disease: from pathology to therapeutic approaches. *Angew. Chemie Int. Ed.* **48,** 3030–3059 (2009).

8.Santos, M. A., Chand, K. & Chaves, S. Recent progress in multifunctional metal chelators as potential drugs for Alzheimer's disease. *Coord. Chem. Rev.* **327–328,** 287–303 (2016).

9.Reitz, C. & Mayeux, R. Alzheimer disease: Epidemiology, diagnostic criteria, risk factors and biomarkers. *Biochem. Pharmacol.* **88,** 640–651 (2014).

10.Mohandas, E., Rajmohan, V. & Raghunath, B. Neurobiology of Alzheimer's disease. *Indiana J. Psychiatry* **51,** 55–61 (2009).

11.Francis, P. T., Palmer, A. M., Snape, M. & Wilcock, G. K. The cholinergic hypothesis of Alzheimer's disease : a review of progress. *J Neurol Neurosurg Psychiatry* **66,** 137–147 (1999).

12.Contestabile, A. The history of the cholinergic hypothesis. *Behav. Brain Res.* **221,** 334–340 (2011).

13.Shen, Z. X. Brain cholinesterases: II. The molecular and cellular basis of Alzheimer's disease. *Med. Hypotheses* **63,** 308–321 (2004).

14.DeKosky, S. T. & Scheff, S. W. Synapse loss in frontal cortex biopsies in Alzheimer's disease: correlation with cognitve severity. *Ann. Neurol.* **27,** 457–464 (1990).

15.Chan, S., Kantham, S., Rao, V. M., Kumar, M., Pham, H. L., Shaw, P. N., Mcgeary, R. P. & Ross, B. P. Metal chelation, radical scavenging and inhibition of Aβ42 fibrillation by food constituents in relation to Alzheimer's disease. *Food Chem.* **199,** 185–194 (2016).

16.Xu, P., Zhang, M., Sheng, R. & Ma, Y. Synthesis and biological evaluation of deferiprone-resveratrol hybrids as antioxidants , Aβ1-42 aggregation inhibitors and metal-chelating agents for Alzheimer's disease. *Eur. J. Med. Chem.* **127,** 174–186 (2017).

17.O'Brien, R. J. & Wong, P. C. Amyloid percursor protein processing and Alzheimer's disease. *Annu. Rev. Neurosci.* **34,** 185–204 (2011).

18.Nunes, A., Marques, S. M., Quintanova, C., Silva, D. F., Cardoso, S. M., Chaves, S. & Santos, M. A. Multifunctional iron-chelators with protective roles against neurodegenerative diseases. *Dalt. Trans.* **42,** 6058–6073 (2013).

19.Šimić, G., Babić Leko, M., Wray, S., Harrington, C., Delalle, I., Jovanov-Milošević, N., Bažadona, D., Buée, L., de Silva, R., Giovanni, G. Di, Wischik, C. & Hof, P. R. Tau protein hyperphosphorylation and aggregation in alzheimer's disease and other tauopathies, and possible neuroprotective strategies. *Biomolecules* **6,** 2–28 (2016).

20.Zhao, L. N., Long, H., Mu, Y. & Chew, L. Y. The toxicity of amyloid β oligomers. *Int. J. Mol. Sci.* **13,** 7303–7327 (2012).

21.Gandy, S., Simon, A. J., Steele, J. W., Lublin, A. L., Lah, J. J., Walker, L. C., Levey, A. I., Krafft, G. A., Levy, E., Checler, F., Glabe, C., Bilker, W. B., Abel, T., Schmeidler, J. & Ehrlich, M. E. Days to criterion as an indicator of toxicity associated with human Alzheimer amyloid-β oligomers. *Ann. Neurol.* **68,** 220–230 (2010).

22.Santos, M. A., Chand, K. & Chaves, S. Recent progress in repositioning Alzheimer's disease drugs based on a multitarget strategy. *Future Med. Chem.* **8,** 2113–2142 (2016).

23.Barnham, K. J. & Bush, A. I. Metals in Alzheimer's and Parkinson's diseases. *Curr. Opin. Chem. Biol.* **12,** 222–228 (2008).

24.Winterbourn, C. C. Toxicity of iron and hydrogen peroxide: the Fenton reaction. *Toxicol. Lett.* **82–83,** 969–974 (1995).

25.Conte-Daban, A., Day, A., Faller, P. & Hureau, C. How Zn can impede Cu detoxification by chelating agents in Alzheimer's disease: a proof-of-concept study. *Dalt. Trans.* **45,** 15671–15678 (2016).

26.Cuajungco, M. P., Goldstein, L. E., Nunomura, A., Smith, M. A., Lim, J. T., Atwood, C. S., Huang, X., Farrag, Y. W., Perry, G. & Bush, A. I. Evidence that the β-amyloid plaques of Alzheimer's disease represent the redox-silencing and entombment of Aβ by zinc. *J. Biol. Chem.* **275,** 19439–19442 (2000).

27.Garai, K., Sahoo, B., Kaushalya, S. K., Desai, R. & Maiti, S. Zinc lowers amyloid-β toxicity by selectively precipitating aggregation intermediates. *Biochemistry* **46,** 10655–10663 (2007).

28.González-Domínguez, R., García-Barrera, T. & Gómez-Ariza, J. L. Homeostasis of metals in the progression of Alzheimer's disease. *Biometals* **27,** 539–549 (2014).

29.IUBMB Enzyme Nomenclature. EC 3.1.1.7. Available at: http://www.chem.qmul.ac.uk/iubmb/enzyme/EC3/1/1/7.html.

30.Rosenberry, T. L. *Acetylcholinesterase*. *Advances in enzymology and related areas of moleular biology* **43,** (John Wiley & Sons, 1975).

31.Singh, M., Kaur, M., Kukreja, H., Chugh, R., Silakari, O. & Singh, D. Acetylcholinesterase inhibitors as Alzheimer therapy: From nerve toxins to neuroprotection. *Eur. J. Med. Chem.* **70,** 165–188 (2013).

32.Dvir, H., Silman, I., Harel, M., Rosenberry, T. L. & Sussman, J. L. Acetylcholinesterase: From 3D structure to function. *Chem. Biol. Interact.* **187,** 10–22 (2010).

33.Gupta, S., Fallarero, A., Järvinen, P., Karlsson, D., Johnson, M. S., Vuorela, P. M. & Mohan, C. G. Discovery of dual binding site acetylcholinesterase inhibitors identified by pharmacophore modeling and sequential virtual screening techniques. *Bioorganic Med. Chem. Lett.* **21,** 1105–1112 (2011).

34.Xu, Y., Colletier, J.-P., Weik, M., Jiang, H., Moult, J., Silman, I. & Sussman, J. L. Flexibility of aromatic residues in the active-site gorge of acetylcholinesterase: X-ray versus molecular dynamics. *Biophys. J.* **95,** 2500–2511 (2008).

35.Cavalli, A., Bolognesi, M. L., Mînarini, A., Rosini, M., Tumiatti, V., Recanatini, M. & Melchiorre, C. Multi-target-directed ligands to combat neurodegenerative diseases. *J. Med. Chem.* **51,** 347–372 (2008).

36.Galimberti, D. & Scarpini, E. Old and new acetylcholinesterase inhibitors for Alzheimer's Disease. *Expert Opin. Investig. Drugs* 1–26 (2016).

37.Crismon, M. L. Tacrine: First drug approved for Alzheimer's disease. *Ann. Pharmacother.* **28,** 744–751 (1994).

38.Zeb, M. W., Riaz, A. & Szigeti, K. Donepezil: a review of pharmacological characteristics and role in the management of Alzheimer disease. *Clin. Med. Insights Geriatr.* **10,** 1–14 (2017).

39.Polinsky, R. J. Clinical pharmacology of rivastigmine: a new-generation acetylcholinesterase inhibitor for the treatment of Alzheimer's disease. *Clin. Ther.* **20,** 634–647 (1998).

40.Scott, L. J. & Goa, K. L. Galantamine: a review of its use in Alzheimer's disease. *Drugs* **60,** 1095–1122 (2000).

41.R.G., I. & D.D., M. Heterocyclic chemistry of benzimidazoles and potential activities of derivatives. *Int. J. Drug Res. Technol.* **1,** 26–32 (2011).

42.Karthikeyan, C., Solomon, V. R., Lee, H. & Trivedi, P. Synthesis and biological evaluation of 2-(phenyl)-3H-benzo[d]imidazole-5-carboxylic acids and its methyl esters as potent anti-breast cancer agents. *Arab. J. Chem.* **10,** 1–7 (2013).

43.Salahuddin, Shaharyar, M. & Mazumder, A. Benzimidazoles: a biologically active compounds. *Arab. J. Chem.* **10,** S157–S173 (2017).

44.Chand, K., Rajeshwari, Hiremathad, A., Singh, M., Santos, M. A. & Keri, R. S. A review on antioxidant potential of bioactive heterocycle benzofuran: natural and synthetic derivatives. *Pharmacol. Reports* **69,** 281–295 (2017).

45.Khanam, H. & Shamsuzzaman. Bioactive benzofuran derivatives: a review. *Eur. J. Med. Chem.* **97,** 483–504 (2015).

46.Chao, X., He, X., Yang, Y., Zhou, X., Jin, M., Liu, S., Cheng, Z., Liu, P., Wang, Y., Yu, J., Tan, Y., Huang, Y., Qin, J.,

Rapposelli, S. & Pi, R. Design, synthesis and pharmacological evaluation of novel tacrine-caffeic acid hybrids as multi-targeted compounds against Alzheimer's disease. *Bioorganic Med. Chem. Lett.* **22,** 6498–6502 (2012).

47.Hiremathad, A., Chand, K., Esteves, A. R., Cardoso, S. M., Ramsay, R. R., Chaves, S., Keri, R. S. & Santos, M. A. Tacrine-allyl/propargylcysteine–benzothiazole trihybrids as potential anti-Alzheimer's drug candidates. *RSC Adv.* **6,** 53519–53532 (2016).

48.Dias, K. S. T., de Paula, C. T., dos Santos, T., Souza, I. N. O., Boni, M. S., Guimarães, M. J. R., da Silva, F. M. R., Castro, N. G., Neves, G. A., Veloso, C. C., Coelho, M. M., de Melo, I. S. F., Giusti, F. C. V., Giusti-Paiva, A., da Silva, M. L., Dardenne, L. E., Guedes, I. A., Pruccoli, L., Morroni, F., Tarozzi, A. & Viegas, C. Design, synthesis and evaluation of novel feruloyl-donepezil hybrids as potential multitarget drugs for the treatment of Alzheimer's disease. *Eur. J. Med. Chem.* **130,** 440–457 (2017).

49.Bautista-Aguilera, O. M., Esteban, G., Bolea, I., Nikolic, K., Agbaba, D., Moraleda, I., Iriepa, I., Samadi, A., Soriano, E., Unzeta, M. & Marco-Contelles, J. Design, synthesis, pharmacological evaluation, QSAR analysis, molecular modeling and ADMET of novel donepezil-indolyl hybrids as multipotent cholinesterase/monoamine oxidase inhibitors for the potential treatment of Alzheimer's disease. *Eur. J. Med. Chem.* **75,** 82–95 (2014).

50.Alonso, D., Dorronsoro, I., Rubio, L., Muñoz, P., García-Palomero, E., Del Monte, M., Bidon-Chanal, A., Orozco, M., Luque, F. J., Castro, A., Medina, M. & Martínez, A. Donepezil-tacrine hybrid related derivatives as new dual binding site inhibitors of AChE. *Bioorganic Med. Chem.* **13,** 6588–6597 (2005).

51.Zagidullin, R. N. Reactions of N-(β-aminoethyl)piperazine and its derivatives. *Chem. Heterocycl. Compd.* **27,** 309–312 (1991).

52.Bai, H., Zhao, X., Zhong, J., Gong, Y., Zhu, Q., Liu, X., Zheng, X. & Liu, L. Benzodioxole derivative and preparation method and use thereof. 1–29 (2015).

53.Porcelli, L., Gilardi, F., Laghezza, A., Piemontese, L., Mitro, N., Azzariti, A., Altieri, F., Paradiso, A., Pochetti, G., Simone, G. M., Tortorella, P., Crestani, M. & Loiodice, F. Synthesis, characterization and biological evaluation of ureidofibrate-like derivatives endowed with peroxisome proliferator-activated receptor activity. *J. Med. Chem.* **55,** 37–54 (2012).

54.Brooks, P. R., Wirtz, M. C., Vetelino, M. G., Rescek, D. M., Woodworth, G. F., Morgan, B. P. & Coe, J. W. Boron trichloride/tetra-n-butylammonium iodide: a mild, selective combination reagent for the cleavage of primary alkyl aryl ethers. *J. Org. Chem.* **64,** 9719–9721 (1999).

55.CommonOrganicChemistry.com. Amine to amide (T3P). Available at: http://www.commonorganicchemistry.com/Rxn_Pages/Amine_to_Amide_Coupling/Amine_to_Amide_Coupling_T3P_Mech.htm.

56.Jones, G., Willett, P., Glen, R. C., Leach, A. R. & Taylor, R. Development and validation of a genetic algorithm for flexible docking. *J. Mol. Biol.* **267,** 727–748 (1997).

57.Kryger, G., Silman, I. & Sussman, J. L. Structure of acetylcholinesterase complexed with E2020 (Aricept): implications for the design of new anti-Alzheimer drugs. *Structure* **7,** 297–307 (1999).

58.Cardozo, M. G., Iimura, Y., Sugimoto, H., Yamanishi, Y. & Hopfinger, A. J. QSAR analyses of the substituted indanone and benzylpiperidine rings of a series of indanone-benzylpiperidine inhibitors of acetylcholinesterase. *J. Med. Chem.* **35,** 584–589 (1992).

59.Ellman, G. L., Courtney, K. D., Andres, V. J. & Featherstone, R. M. A new and rapid colorimetric determination of acetylcholinesterase activity. *Biochem. Pharmacol.* **7,** 88–95 (1961).

60.Worek, F., Eyer, P. & Thiermann, H. Determination of acetylcholinesterase activity by the Ellman assay: a versatile tool for in vitro research on medical countermeasures against organophosphate poisoning. *Drug Test. Anal.* **4,** 282–291 (2012).

61.Keri, R. S., Quintanova, C., Marques, S. M., Esteves, A. R., Cardoso, S. M. & Santos, M. A. Design, synthesis and neuroprotective evaluation of novel tacrine-benzothiazole hybrids as multi-targeted compounds against Alzheimer's disease. *Bioorg. Med. Chem.* **21,** 4559–4569 (2013).

62.Kedare, S. B. & Singh, R. P. Genesis and development of DPPH method of antioxidant assay. *J. Food Sci. Technol.* **48,** 412–422 (2011).

63.Sharma, O. P. & Bhat, T. K. DPPH antioxidant assay revisited. *Food Chem.* **113,** 1202–1205 (2009).

64.Šebestík, J., Marques, S. M., Falé, P. L., Santos, S., Arduíno, D. M., Cardoso, S. M., Oliveira, C. R., Serralheiro, M. L. M. & Santos, M. A. Bifunctional phenolic-choline conjugates as anti-oxidants and acetylcholinesterase inhibitors. *J. Enzyme*

Inhib. Med. Chem. **26,** 485–497 (2011).

65.Hiremathad, A., Keri, R. S., Chaves, S. & Santos, M. A. Novel tacrine hydroxyphenylbenzimidazole hybrids as potential drug candidates for Alzheimer's disease, 11th Inorganic Chemistry Conference (ICC 11), Sintra, Portugal. (2016).

66.Biancalana, M. & Koide, S. Molecular mechanism of thioflavin-T binding to amyloid fibrils. *Biochim. Biophys. Acta* **1804,** 1405–1412 (2010).

67.Pearson, G. Hard and Soft Acids and Bases. *J. Am. Chem. Soc.* **85,** 3533–3539 (1963).

68.Quintanova, C., Keri, R. S., Chaves, S. & Santos, M. A. Copper(II) complexation of tacrine hybrids with potential anti-neurodegenerative roles. *J. Inorg. Biochem.* **151,** 58–66 (2015).

69.Chaves, S., Gil, M., Marques, S., Gano, L. & Santos, M. A. Alkylaryl-amino derivatives of 3-hydroxy-4-pyridinones as aluminium chelating agents with potential clinical application. *J. Inorg. Biochem.* **97,** 161–172 (2003).

70.Gans, P., Sabatini, A. & Vacca, A. Investigation of equilibria in solution. Determination of equilibrium constants with the HYPERQUAD suite of programs. *Talanta* **43,** 1739–1753 (1996).

71.Lacivita, E., Leopoldo, M., Giorgio, P. De, Berardi, F. & Perrone, R. Determination of 1-aryl-4-propylpiperazine pKa values: the substituent on aryl modulates basicity. *Bioorganic Med. Chem.* **17,** 1339–1344 (2009).

72.Schrödinger, L. QikProp version 2.5. (2005).

73.Lipinski, C. A., Lombardo, F., Dominy, B. W. & Feeney, P. J. Experimental and computational approaches to estimate solubility and permeability in drug discovery and development settings. *Adv. Drug Deliv. Rev.* **64,** 4–17 (2012).

74.Armarego, W. L. F. & Perrin, D. D. *Purification of laboratory chemicals*. (Butterworth-Heinemann, 1999).

75.Rossotti, F. J. C. & Rossotti, H. Potentiometric titrations using Gran plots. *J. Chem. Educ.* **42,** 375–378 (1965).

76.RCSB PDB. Available at: http://www.rcsb.org/pdb/home/home.do.

77.Schrödinger Inc. Maestro version 9.3. (2012).

78.Acton, A., Banck, M., Bréfort, J., Cruz, M., Curtis, D., Hassinen, T., Heikkilä, V., Hutchison, G., Huuskonen, J., Jensen, J., Liboska, R. & Rowley, C. Ghemical version 3.0. (2011).

79.Clark, M., Cramer III, R. D. & Opdenbosch, N. Van. Validation of the general purpose Tripos 5.2 force field. *J. Comput. Chem.* **10,** 982–1012 (1989).

80.Haq, Z., Halim, S. A., Uddin, R. & Madura, J. D. Benchmarking docking and scoring protocol for the identification of potential acetylcholinesterase inhibitors. *J. Mol. Graph. Model.* **28,** 870–882 (2010).

81.University of California. UCSF Chimera version 1.11. (2016).

ANNEX I – 14th Internation Symposium on Applied Bioinorganic Chemistry – ISABC (Abstract for oral communication)

Exploiting hydroxyphenylbenzimidazol-based hybrids for metal-modulation in potential anti-Alzheimer´s drugs

Asha Hiremathad,[a,b] Luca Piemontese,[a,c] Daniel Tomás,[a] Rangappa S. Keri,[b] Sílvia Chaves,[a] M. Amélia Santos[a]

[a] Centro de Química Estrutural, Instituto Superior Técnico, Universidade Técnica de Lisboa, Av. Rovisco Pais 1, 1049-001 Lisboa, Portugal;[b] Centre for Nano and Material Sciences, Jain University, Jain Global Campus, Jakkasandra post, Kanakapura Road, Ramanagara District, Bangalore 562112, India;[c] Dipartimento di Farmacia–Scienze del Farmaco, Università degli Studi di Bari "Aldo Moro", Via E. Orabona 4, 70125 Bari, Italy; masantos@ist.utl.pt.

Alzheimer´s Disease (AD) is the most serious age dependent degenerative disorder characterized by progressive loss of memory and cognitive deficits, and with no cure so far [1]. The main brain hallmarks of the AD patients are the senile plaques, the neurofibrilary tangles and the deficit of acetylcholine in the brain. However, other pathological features play important roles in the disease process, namely in upstream events, including enhanced brain oxidative stress and disruption of metal homeostasis [2]. Many targets have been explored aimed to control AD process or effects, such as the extracellular β-amyloid (Aβ), the intracellular τ-protein and acetylcholinesterase (AChE). AChE inhibitors have been the most explored targets as, among the five FDA approved drugs four are AChE inhibitors. However, the available drugs only improve symptoms but do not have really disease modifying effects [3].

The evidenced multi-factorial nature of AD has been considered one of the main reasons for the absence of cure so far. Thereby, we have assisted to the development of multi-target candidate drugs, aimed at interfering with multiple disease pathways. Many multipotent compounds have been designed and studied based on repositioning well known AChEi classical anti-AD drugs, such as tacrine and donepezil [4].

On the continuation of our interest on the development of multifunctional compounds as potential anti-AD drugs with capacity for the metal modulation [5], we present herein the results of the study of a series of compounds which include a hydroxyphenyl benzimidazole (HOBIM) moiety attached to a molecular moiety able to inhibit AChE, namely a tacrine or a donepezil mimic. The enclosed HOBIM moiety, besides improving the AChE inhibitory activity of the "old" drugs, because of the bimodal interaction within the active site of the enzyme, provides the new hybrid compounds with metal (Cu, Zn) chelation ability, anti-oxidant activity and capacity for anti-Aβ aggregation. Thereby these new hybrids appear as potential anti-AD drugs.

References

[1] A. Wimo, M. Guerchet, G.-C. Ali, Y.-T. Wu, A.M. Prina, B. Winblad, L. Jönsson, Z. Liu, M. Prince, *Alzheimer's & Dementia* **2017**, *13*, 1-7.

[2] C.L. Masters, R. Cappai, K.J. Barnham, V.L. Villemagne, *J. Neurochem.* **2006,** *97*, 1700.

[3] M.L. Crismon, *Ann. Pharmacother*, **1994**, *28*, 744–751.

[4] M.A. Santos, K. Chand, S. Chaves, *Fut. Med. Chem*. **2016**, *8*, 2113-2142.

[5] M.A. Santos, K. Chand S. Chaves, *Coord. Chem. Rev.* **2016**, *327-328*, 287-303.

ANNEX II – XXVI Congresso Nazionale della Società Chimica Italiana (Abstract for poster)

Metal chelators for the multi-target therapy of Alzheimer´s Disease: isolation/synthesis and preliminary biological evaluation of new natural and synthetic compounds

Luca Piemontese[a,b], Daniel Tomás[c], Asha Hiremathad[d], Marco Catto[a], Antonio Laghezza[a], Sílvia Chaves[c], Filippo Maria Perna[a], Fulvio Loiodice[a], Maria Amélia Santos[c], Michele Solfrizzo[b], Vito Capriati[a]

[a]Dipartimento di Farmacia–Scienze del Farmaco, Università degli Studi di Bari "Aldo Moro", Consortium C.I.N.M.P.I.S., Via E. Orabona 4, I-70125 Bari, Italy; [b]CNR-Istituto di Scienze delle Produzioni Alimentari, via Amendola, 122/O, I-70125 Bari, Italy; [c]Centro de Química Estrutural, Instituto Superior Técnico, Universidade de Lisboa, Av. Rovisco Pais 1, 1049-001 Lisboa, Portugal; [d]Centre for Nano and Material Sciences, Jain University, Jain Global Campus, Jakkasandra post, Kanakapura Road, Ramanagara District, Bangalore 562112, India; e-mail: luca.piemontese@uniba.it.

Alzheimer's Disease (AD) is widely recognized as a social problem. Nowadays, only five drugs are FDA approved for the therapy of this widespread neurodegenerative disease, however, with poor results. Four of them (Tacrine, Donepezil, Rivastigmine, Galantamine) are acetylcholinesterase (AChE) inhibitors, whereas Memantine is a NMDA receptor antagonist (1). Because of the multiple origin of this pathology, a multi-target strategy is currently strongly pursued by physicians. This approach is based on the identification of multifunctional molecules designed in order to act simultaneously on at least two disease targets with the aim of achieving synergistic actions and of improving the therapeutic efficacy (1,2). Currently, inhibition of AChE and monoaminoxidase, NMDA receptor antagonism, antioxidant activity, inhibition of Abeta amyloid plaques (Aβ) aggregation, and chelation of copper, iron and/or zinc cations are among the most heavily investigated drug targets (1). Recent evidence, in particular, have shown that the removal and/or redistribution of metal ions at the level of the nervous system can significantly reduce the formation of Aβ and thus of reactive oxygen species, which are typical of the first stages of AD and other neurodegenerative diseases (3).

Considering that many synthetic and natural compounds possess anti-oxidant, anticholinesterase and/or metal chelation activity (4), several scaffolds have been selected in order to design new derivatives. A list of secondary metabolites of fungi, in particular, have been isolated and preliminarily tested with the aim of finding new hit compounds for future Structure-Activity Relationship studies. In addition, starting from the structure of Donepezil and two selected synthetic scaffolds, new hybrid derivatives have been synthesized aimed at obtaining a better AChE inhibitory activity, an anti-oxidant activity, and the inhibition of Aβ aggregation. In this communication, the results of the preliminary biological studies will be discussed.

Intervento cofinanziato dal Fondo di Sviluppo e Coesione 2007-2013 –APQ Ricerca Regione Puglia "Programma regionale a sostegno della specializzazione intelligente e della sostenibilità sociale ed ambientale - Future In Research". Project ID: I2PCTF6.

References: 1. Piemontese L. Neu. Regen. Res. 2017, 405-6. 2. Chaves S., Piemontese L., Hirematad A., Santos M.A. Curr. Med. Chem., 2017, 10.2174/0929867324666170330092304. 3. M.A. Santos, K. Chand S. Chaves, Coord. Chem. Rev. 2016, 287-303. 4. Habtemariam S. Curr. Med. Chem. 2016, 860-873.

ANNEX III – Graphical representation of antioxidant activity (PZ1 as example)

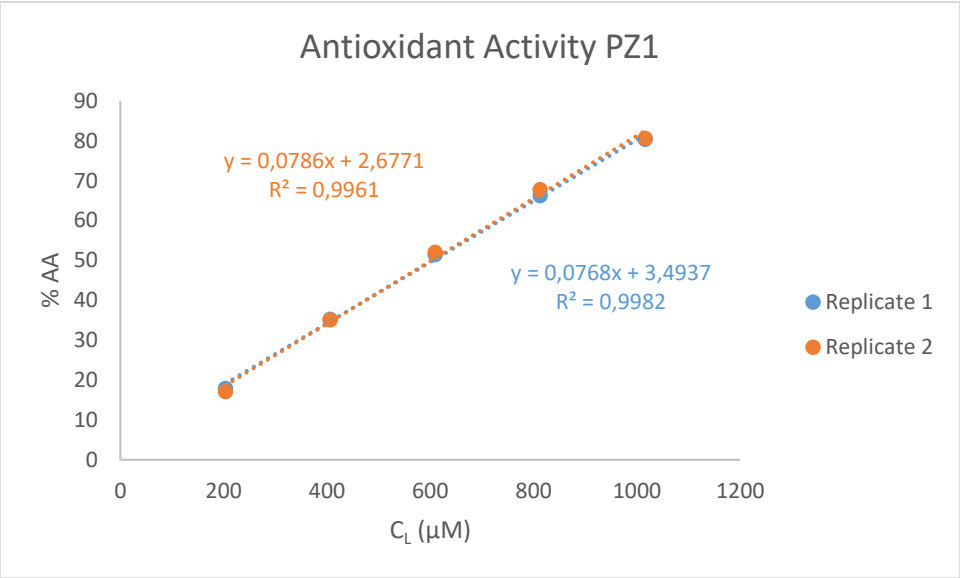

ANNEX IV – Graphical representation of AChE inhibition (PZ3 as example)